DEVELOPMENT OF ZrO_2-CeO_2-Nb_2O_5 AND ZrO_2-CeO_2-Sm_2O_3 CERAMICS FOR BIOMEDICAL APPLICATIONS

A dissertation work
submitted in partial fulfillment of the requirements
for the award of the degree of

DOCTOR OF PHILOSOPHY

in

METALLURGICAL AND MATERIALS ENGINEERING

by

SHIVA BEJUGAMA
(Roll No.716035)

Under the guidance of

Dr. AJOY KUMAR PANDEY

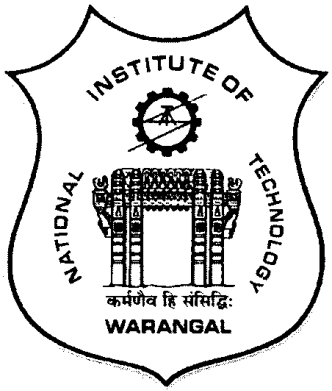

DEPARTMENT OF METALLURGICAL AND MATERIALS ENGINEERING
NATIONAL INSTITUTE OF TECHNOLOGYWARANGAL
DECEMBER – 2020

Dedicated to
My Family and Friends

Thesis Approval for Ph.D.

The thesis entitled **"Development of ZrO_2-CeO_2-Nb_2O_5 and ZrO_2-CeO_2-Sm_2O_3 ceramics for biomedical applications"** which is submitted by **Mr. Shiva Bejugama (Roll No.716035)** is approved for the degree of **Doctor of Philosophy** in Metallurgical and Materials Engineering.

Examiner

_____

Supervisor

_____

Chairman

_____

Date: _____

DEPARTMENT OF METALLURGICAL AND MATERIALS ENGINEERING

NATIONAL INSTITUTE OF TECHNOLOGY

WARANGAL - 506 004 (T.S) INDIA

CERTIFICATE

This is to certify that the work presented in the thesis entitled **"Development of ZrO_2-CeO_2-Nb_2O_5 and ZrO_2-CeO_2-Sm_2O_3 ceramics for biomedical applications"** which is being submitted by **Mr. Shiva Bejugama (Roll No.716035)**to National Institute of Technology Warangal in partial fulfilment of the requirements for the award of the degree of **Doctor of Philosophy** in **Metallurgical and Materials Engineering**is a bonafide work carried out under my supervision**.** To the best of our knowledge, the work incorporated in this thesis has not been submitted to any other university or institute for the award of any other degree or diploma.

Dr. Ajoy Kumar Pandey

Assistant Professor and Thesis Supervisor
Department of Metallurgical and Materials Engineering
National Institute of Technology Warangal
Warangal-506 004

DECLARATION

This is to certify that the work presented in the thesis entitled **"Development of ZrO_2-CeO_2-Nb_2O_5 and ZrO_2-CeO_2-Sm_2O_3 ceramics for biomedical applications"** is abonafide work done by me under the supervision of **Dr. Ajoy Kumar Pandey**and was not submitted elsewhere for the award of any degree.I declare that this written submission represents my ideas in my ownwords and where others' ideas or words have been included, I haveadequately cited and referenced the original sources. I also declare thatI have adhered to all principles of academic honesty and integrity andhave not misrepresented or fabricated or falsified any idea / data / fact /source in my submission. I understand that any violation of the abovewill be a cause for disciplinary action by the Institute and can also evokepenal action from the sources which have thus not been properly citedor from whom proper permission has not been taken when needed.

(Shiva Bejugama)

Acknowledgements

I take this opportunity to express my deep sense of gratitude and heartfelt thanks to my research supervisor **Dr. Ajoy Kumar Pandey**, Assistant Professor, Department of Metallurgical and Materials Engineering, National Institute of Technology, Warangal for his wholehearted support, encouragement, guidance and patience during the research work. Without his untiring mentorship, constant inspiration, valuable discussions and suggestions, this thesis wouldn't have been possible. It was indeed a great honour and privilege to work underhis supervision.

I am grateful to **Prof. N.V. Ramana Rao**, Director, NIT Warangal; **Prof. T. Srinivasa Rao,** former Director, NIT Warangal for giving me an opportunity to carry out research work in the institute.

My sincere thanks and appreciation to the Doctoral Scrutiny Committee members, **Dr. AsitKumar Khanra** (Chairman & Head of the Department), **Dr. BontaSrinivasa Rao** (Assistant professor),**Dr. Brahma Raju Golla** (Assistant professor), Department ofMetallurgical and Materials Engineering, and **Dr. Asim BikasDas** (Assistant professor), Department of Biotechnology, NIT Warangal for their helpful suggestions, remarks andperiodical review of my research progress.

I am thankful to **Prof. N. Narasaiah**, former Head of the Department, for his continuousencouragement, valuable advice and support. I would also like to express mygratefulness to**Prof. M. K. Mohan**, **Dr. R. ArockiaKumar**, **Dr. C. Vanitha,** for their help in various ways during the research work. Isincerely acknowledge the financial support provided by the institute during the entireperiod of doctoral research study.

It is my privilege to express a sense of gratitude to**Dr. Falguni Pati**, Assistant Professor Department of Biomedical Engineering, IIT Hyderabad for allowing me to conduct cell culture studies in his lab and **Mr. Shibu Chameettachal**, Research scholar IIT Hyderabad for helping me to carry out experiments.

I thank technical staff **Miss. G. Ramya**, **Mr. G. Srinivasulu**for helping me to carryout X-ray diffraction and Scanning Electron Microscopy analysis**.** I also thank**Mr. G. Savvaiah**, Mechanic A grade (Retired) and **Mr. K. Balaswamy**, Mechanic A grade (Retired), **Mr. Fayaz**, **Mr. Prasad**and other technical and office staff of Metallurgical and Materials Engineering Department, NIT Warangal for their help during this research work.

I extend my sincere thanks to present and past lab mates, **Mr. E. Obulapathi**, **Mr. Giridhar Gudivada**, **Mr. Narendra Kumar Gadwal**, **Mr. V. Ganesh** and **Mr. Ashok Allamula** for their assistance in experiments.

I also wish to thank all my friends, especially to **Dr. Prakash**, **Dr. Sai Mahesh Kaku**, **Dr. Bheekya Naik**, **Mr. Raju Vemoori**, **Mr. Katti Bharath**, **Mr. C. Ravikanth Reddy**, **Mr. Venkateswara Reddy**, **Mr. K. Venkata Ashish Srivatsav**,**Mr. Siva Kumar Reddy**, **Mr. Shaik Mahammad Ali**, **Mr. T. Sravan** and **Miss. Shaik Mubina** for their valuable assistance and support.

Finally, I express my profound gratitude to my grandparents, my father **Sri.B. Prabhakar,**mother **Smt. Padma, brother Mr. Srikanth** and other family members for their patience,understanding, love,support and encouragement.

(SHIVA BEJUGAMA)

December 2020

List of Abbreviations

CSZ – Ceria Stabilized Zirconia

12Ce-TZP – 12 mol.% Ceria stabilized Tetragonal Zirconia Polycrystal

YSZ – Yttria Stabilized Zirconia

3Y-TZP – 3 mol.% Yttria stabilized Tetragonal Zirconia Polycrystal

mol.% - Mole percent

wt.% - Weight percent

vol.% - Volume percent

XRD – X-ray Diffraction

ICSD – Inorganic Crystal Structure Database

SEM – Scanning Electron Microscope

EDS – Energy Dispersion Spectroscopy

SE – Secondary Electrons

BSE – Back Scattered Electrons

nm – Nano meters

NbCSZ – Niobia doped Ceria Stabilized Zirconia

SmCSZ – Samaria doped Ceria Stabilized Zirconia

MTT – 3-(4, 5-dimethylthiazol-2-yl)-2, 5-diphenyltetrazolium bromide

PBS – Phosphate buffered saline

DMEM – Dulbecco's modified eagle's medium

RPM – Rotations per minute

LVDT – Linear Variable Differential Transducer

HV – Vickers Hardness

IFT – Indentation Fracture Toughness

PSZ – Partially Stabilized Zirconia

FSZ – Fully Stabilized Zirconia

TZP – Tetragonal Zirconia Polycrystals

TCP- Tri Calcium Phosphate

LTD – Low Temperature Degradation

CSS – Conventional Single-step Sintering

TSS – Two-step Sintering

MPa – Mega Pascal

Mg-PSZ – Magnesia doped Partially Stabilized Zirconia

Ca-CSZ – Calcia doped Cubic Stabilized Zirconia

ATP – Adenosine Triphosphate

PVA – Polyvinyl alcohol

GOF – Goodness of fit

a.u. – Arbitrary units

KV – Kilo volts

mA – Milli amps

ASTM – American Society for Testing and Materials

ISO – International Organization for Standardization

NCCS – National Centre for Cell Sciences

List of Symbols

T – Tetragonal zirconia

M – Monoclinic zirconia

μ – Coefficient of friction

θ – Diffraction angle

d – Interplanar spacing

λ – Wave length

Å – Angstrom

°C – Degree celsius

ρ - Density

ϕ – Diameter

E – Youngs Modulus

P – Load

N – Newton

μm – Micro meter

μl – Micro liter

B – Full width half maxima

Abstract

The catastrophic failure of yttria-stabilized zirconia implants due to low-temperature degradation (LTD) left incredulity on the use of YSZ in biomedical applications. It is reported that replacing yttria with ceria as a stabilizer in zirconia (ceria stabilized zirconia) prevents the LTD. However, ceria stabilized tetragonal zirconia (CSZ) possess poor mechanical properties like hardness and strength compared to yttria-stabilized tetragonal zirconia (3YSZ). The poor mechanical properties of CSZ are due to its large grain size. The grain growth of CSZ is due to the need for high temperature and longer times for sintering, and lack of proper grain growth restriction mechanism (segregation) like in 3YSZ.

Present work deals with the study of the effect of Nb_2O_5 and Sm_2O_3 co-doping on the grain growth behaviour, mechanical properties, and tribological behaviour of CSZ. The low-temperature degradation and biocompatibility of the developed systems are also studied. Nanopowders of Nb_2O_5 doped CSZ (NbCSZ) and Sm_2O_3 doped CSZ (SmCSZ) are synthesized using co-precipitation synthesis, and obtained powders are compacted using a uniaxial hydraulic press. The compacted samples are sintered in air atmosphere using a conventional single-step and two-step sintering schedules. The amount of Nb_2O_5 or Sm_2O_3 in CSZ, calcination temperature of powders and sintering schedules are optimized based on the phases present, density, microstructure and mechanical properties of the sintered sample.

It is observed that Nb_2O_5 helped in decreasing the sintering temperature of CSZ, and Sm_2O_3 suppressed the grain growth by segregating at the grain boundaries of CSZ. The two-step sintering process refined the microstructure in both the systems. The improved grain size of 1.57 µm along with a hardness of 1175 HV10 and optimum fracture toughness of 6.2 MPa $m^{1/2}$achieved for 1 mol % niobia doped ceria stabilized zirconia. The fine grain size of 0.64 µm with a high hardness of 1288 HV10 along with an optimum fracture toughness of 5.37 MPa $m^{1/2}$is observed for Samaria doped ceria stabilized zirconia.

The tribological properties of optimized NbCSZ, SmCSZ samples are evaluated using a pin on disc wear machine. The surface analysis of worn surfaces shown evidence of grain pull-outs, grain fracture and abrasion. The SmCSZ samples shown better wear resistance than NbCSZ and CSZ samples.

The accelerated aging study revealed no phase transformation in NbCSZ and SmCSZ even after 200 hours of treatment, indicating high resistance to low-temperature degradation. The *in vitro* cell culture study on NbCSZ and SmCSZ using human osteoblast-like cells (MG-63) shown active proliferation and attachment of cells on samples indicating biocompatibility of the developed materials.

Keywords: Ceria stabilized zirconia, Nb_2O_5, Sm_2O_3, Grain refinement, Tribological properties, Low-temperature degradation, *In vitro* study

Index

LIST OF FIGURES

LIST OF TABLES

Chapter-1

Introduction

Ceramics are non-metallic inorganic materials with a broad range of composition; they have many applications in all engineering disciplines (Hamadouche and Sedel, 2000). The word ceramic is derived from the Greek word keramos, meaning 'pottery', which intern derived from an ancient Sanskrit root, meaning 'to burn'. Traditional ceramics are clay-based; domestic wares, art objects and building parts are examples of clay-based ceramics. Ceramics are usually prepared by the following process: mixing of constituent powders with water or binder, pressing of the powders to form the desired shape, pre-firing for binder removal and sintering at elevated temperature for full densification. Nowadays, ceramic has a broader meaning and includes glass, cement and advanced ceramics. Advanced ceramics are different from traditional ceramics, and they are not generally clay-based; instead, they are made up of various oxides or non-oxides (Metal oxides, borides, nitrides, carbides and silicates). A simple classification of advanced ceramics is shown in **Fig. 1.1**.

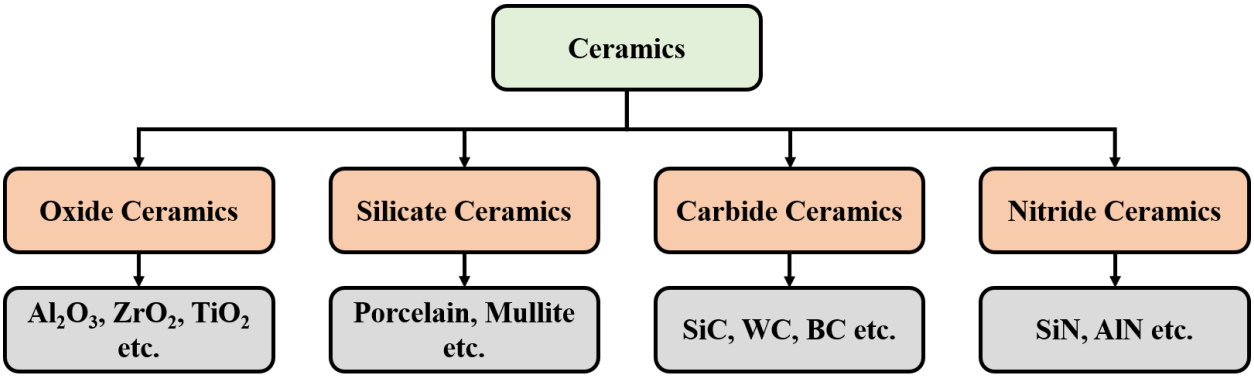

Fig. 1.1: *Classification of advanced ceramics* (Kopeliovich, 2000).

To be precise, a ceramic is defined as "a solid material comprising an inorganic compound of metal, non-metal or metalloid atoms held with ionic and covalent bonds" (Sabu et al., 2018). In general, ceramics possess high melting points, low electrical and thermal conductivity, high

compressive strength, high hardness, excellent thermal and chemical stability (M. N. Rahaman, 2007).

Nowadays, ceramics have found wide applications from domestic tiles to advanced microchips. Ceramics are also playing a vital role in biomedical applications because of their properties like corrosion resistance, wear-resistance and biocompatibility (Abd El-Ghany and Sherief, 2016; Hamadouche and Sedel, 2000; Piconi et al., 2003; Piconi and Maccauro, 1999; Ramesh et al., 2012).

1.1 Ceramics as biomaterials:

Biomaterials are defined as "Non-viable materials, which are intended to interact with biological systems" (Williams, 1987), a class of ceramic materials that satisfies the requirements of biomaterial are known as bioceramics. The use of bioceramics in clinical practice as an implant material for dental started in 18^{th} century with the use of porcelain for dental crowns, and as bone filling material for orthopaedics in late 19^{th} century with the use of calcium sulfate dihydrate (gypsum). From the beginning of the 20^{th} century, rapid developmentin ceramic technology introduced several advanced ceramics for biomedical applications as represented in **Fig. 1.2**. In 1920 tricalcium phosphate (TCP) was proposed as a bioresorbable material to fill bone gaps and in 1970, alumina was used in load-bearing orthopedics. Later TCP and alumina were replaced by synthetic calcium phosphate and zirconia respectively because of their improved properties.

In 1970, alumina was introduced as an alternative to metallic implants in loadbearing orthopaedics due to its high hardness, wear resistance, low coefficient of friction, excellent corrosion resistance, and high chemical stability (Piconi et al., 2003). However, intrinsic brittleness and higher fracture rate of alumina ceramic have a limited range of applications, and it is only suitable where mechanical load-bearing capabilities are less stringent (Higuchi et al., 1995). Zirconia-based ceramics were introduced to overcome the problem of alumina's brittleness and the consequent limitations in its use as a biomaterial. A unique combination of wear and frictional properties, crack resistance, biocompatibility and *in vivo* stability made zirconia an excellent choice as biomaterial (Piconi et al., 2006, 1998; Richter and Willmann, 1999).

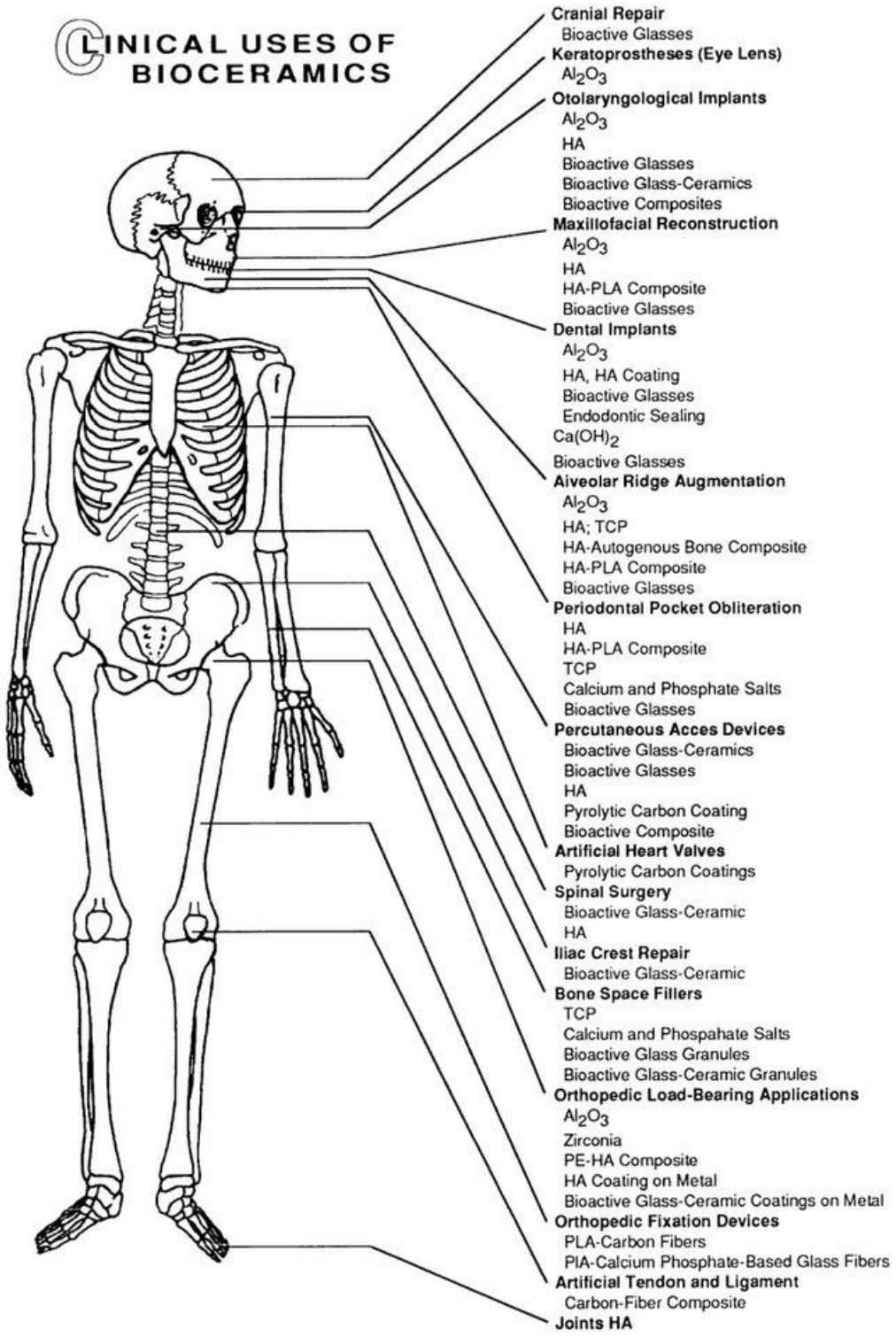

Fig. 1.2: *Clinical uses of bioceramics(Dorozhkin, 2018).*

1.2 Zirconia as bioceramic:

Ceramic steel is the name given to the zirconia because of its high strength and toughness, unlike traditional ceramics that are hard and brittle (Garvie et al., 1975). Zirconia exists in the monoclinic phase at room temperature and can form tetragonal and cubic phases at high temperatures (Garvie and Nicholson, 1972). Volume change associated with phase transformation during cooling (results in crack generation) makes the sintering of pure zirconia difficult (Fabris et al., 2002). High-temperature phases (Tetragonal or Cubic) of zirconia can be stabilized at room temperature using suitable stabilizers like calcia, magnesia, yttria, ceria, etc.(Pereira et al., 2015; Pyda and Haberko, 1987; Vleugels et al., 2004). These stabilized zirconia ceramics show high toughness as they undergo transformation toughening. When a crack tries to propagate through stabilized zirconia, the grains in the vicinity of the crack undergo a stress-induced transformation from metastable tetragonal phase to stable monoclinic phase (Subbarao et al., 1974). This transformation is a diffusionless martensitic type, which is accompanied by a volume change (expansion) of about ~ 4% results in compressive stress around the crack tip, thereby preventing crack propagation.

Among all zirconia ceramics, yttria-stabilized zirconia (YSZ) ceramics were popular and widely used in biomedical applications because of their superior mechanical properties and biocompatibility. However, the orthopaedic implants' catastrophic failure events in-service condition reported in the year 2001 left incredulity on using YSZ as an implant material (Chevalier, 2006; Kohorst et al., 2012; Pereira et al., 2015). The fracture surfaces of failed zirconia implants have been studied by many researchers across the world (Haraguchi et al., 2001; Hernigou and Bahrami, 2003) and found a remarkable increase of monoclinic content. Further investigations revealed that YSZ ceramics are sensitive to the moisture environment. Since then, aging resistance became a major priority for zirconia-based materials to use in biomedical applications (Chevalier, 2006).

1.3 Catastrophic failure of YSZ implants:

It is understood that, in the presence of moisture, YSZ can transform from the tetragonal phase to a stable monoclinic phase. The phase transformation involves volume expansion leading stresses developed, resulting in micro and macro cracks formation along the grain boundaries. The developed cracks allow water to penetrate inside. Moreover, with the time of aging,

cracktransformationproceeded from the surface of the sample to the inside and causes implant failure; this phenomenon is known as Low-Temperature Degradation (LTD).

1.4 Advantage of ceria as stabilizer over yttria:

The susceptibility of zirconia ceramics to LTD majorly depends on grain size, stabilizer type and its concentration. Tsukuma et al. (Tsukuma et al., 1983), Watanabe et al. (Watanabe et al., 1983) reported that the decrease in grain size, increase in stabilizer content in YSZ improved the resistance to LTD but did not completely prevent the transformation. It is reported that replacing yttria with ceria as a stabilizer in zirconia (ceria stabilized zirconia) completely prevents the LTD and also improves fracture toughness (Matsumoto, 1988).

1.5 Limitations of ceria stabilized zirconia:

Though the ceria stabilized zirconia is highly resistant to low temperature degradation, it posses poor mechanical properties like hardness and strength compared to YSZ due to its larger grain size (Duh et al., 1988; Pandey and Biswas, 2011; Tsukuma, 1986; Tsukuma and Shimada, 1985). The grain growth of CSZ is related to its poorsinterability due to a lack of defects in its lattice (Pandey and Biswas, 2011). Hence, it requires a high temperature for successful sintering, which leads to large grain growth.

The material used for load-bearing orthopaedic implants need to be wear-resistant, biocompatible, chemically stable, should possess good strength, hardness and toughness. It is known that the wear resistance of material majorly depends on its hardness, and hardness intern depends on composition, grain size, porosity etc. (Rainforth, 2004). To improve wear resistance and hardness of a specific ceramic material, one should control its grain size and minimize porosity.

1.6 Improving the mechanical properties of ceria stabilized zirconia:

It is understood that achieving full density with fine grain size is vital for ceria stabilized zirconia (CSZ) ceramics to improve mechanical properties. The Grain boundary migration and grain boundary diffusion are two major mechanisms during sintering of ceramics. Grain boundary migration mainly contributes to grain growth, and grain boundary diffusion contributes to the densification (Ferreira et al., 2012). To produce a dense and fine-grainedmicrostructure, one has

to suppress grain boundary migration and enhance the grain boundary diffusion. In principle, this can be achieved by the following two methods:

First, the addition of suitable dopants which can inhibit grain boundary migration by changing boundary, lattice and surface diffusivities thereby decreasing the mobility of grain boundaries, and/or added dopant ions could segregate to the boundary and produces a drag force on boundary motion. Sometimes, if there is an excess amount of dopant (more than the solubility limit), it might form precipitates, and that can pin down the boundary and restricts its movement (Powers and Glaeser, 1998).Second, changing or altering the sintering schedule where grain boundary diffusion is active, but grain boundary migration is restricted, which helps to continue densification without significant grain growth, this can be done effectively by two-step sintering process (Lóh et al., 2016).

1.7 Proposed work:

Considering above discussed points, two different zirconia ceramics, i.e. Niobia doped ceria stabilized zirconia (NbCSZ), Samaria doped ceria stabilized zirconia (SmCSZ) were proposed and two types of sintering schedules were adopted for sintering, i.e., conventional single step (CSS) and Two-step sintering (TSS). In due course of material development, the mechanical properties like hardness, fracture toughness, tribological properties were also evaluated.

As mentioned in earlier sections, the tetragonal stabilized zirconia is susceptible to ageing. Hence, the prior testing of newly developed zirconia ceramics for ageing behaviour is highly essential. It is challenging to test ageing behaviour at actual conditions as it is a slow and time-consuming process. Researchers developed an accelerated aging method which precisely estimates the aging behaviour of zirconia in-service condition (*In-vivo*). It is reported that one-hour hydrothermal treatment at 134°C under 0.2 MPa in the presence of water can be extrapolated to 3−4 years *in vivo* (Chevalier et al., 1999; Gremillard et al., 2004).

Bioceramics used for implant applications also require a favourable cellular response (biocompatibility) in terms of cell proliferation, differentiation, adhesion and cell attachment (Anselme, 2000; Ko et al., 2007). The implant material should not show any toxic effects in the host. Cell culture and cellular metabolic activity assays are the most commonly used tests to evaluate the cellular response of biomaterial in *In-vitro*.

1.8 Organization of the thesis:

The thesis has been divided into the following seven chapters:

Chapter 1: Introduction

Chapter 2: Literature Review

Chapter 3: Experimental procedure

Chapter 4: Development of Niobia doped ceria stabilized zirconia ceramics

Chapter 5: Development of Samaria doped ceria stabilized zirconia ceramics

Chapter 6: Tribological properties, Low-temperature degradation and *In vitro* cytotoxicity of developed materials.

Chapter 7: Conclusions and scope for future work.

A brief discussion of these chapters is given below:

Chapter 1 presents the background of ceramics and its applications in various fields, the use of different ceramic materials, especially zirconia-based ceramics in biomedical applications and organization of the thesis.

Chapter 2 outlines a detailed review of literature available on zirconia, the effects of dopants on stabilization of its high-temperature phases, transformation toughening, and low-temperature degradation. It also includes the scope of work, objectives and work plan of the thesis.

Chapter 3 deals with the details of the raw materials used in this study and powder synthesis methods followed, consolidation of powders, sintering methods used, equipment and techniques used for physical, mechanical and bio-functional characterization.

Chapter 4 describes the effect of Nb_2O_5 on densification, physical and mechanical properties of ceria stabilized zirconia. The Nb_2O_5 content and sintering schedules are optimized based on the density, phase, microstructure and mechanical properties of the sintered products.

Chapter 5 explains the effect of Sm_2O_3 on densification, physical and mechanical properties of ceria stabilized zirconia. The Sm_2O_3 content and sintering schedules are optimized based on the density, phase, microstructure and mechanical properties of the sintered products.

Chapter 6 devoted to the evaluation of tribological properties, low-temperature degradation behaviour and cytocompatibility of Niobia doped ceria stabilized zirconia (NbCSZ), and Samaria

doped ceria stabilized zirconia (SmCSZ) through a pin on disc wear test, accelerated aging and *Invitro* cell culture studies respectively.

Chapter 7 bring out the significant findings and concludes the outcomes of the research work carried out and also presents the scope for future work.

Chapter-2

Literature Review

This chapter presents the detailed review of literature available on zirconia, the effects of dopants on stabilization of its high-temperature phases, transformation toughening, and low-temperature degradation. It also includes the scope of work, objectives and work plan of the thesis.

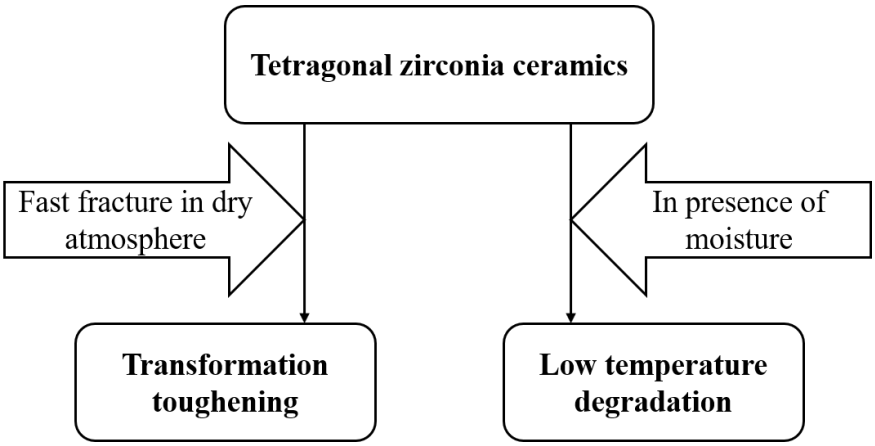

Fig. 2.5*: Effect of tetragonal to monoclinic transformation in zirconia* (Chevalier et al., 2009).

2.5Negative consequences of T to M transformation in zirconia:

Low-temperature degradation (LTD) is a negative consequence of T – M martensitic transformation in zirconia. It was first observed in zirconia cutting tools when subjected to steam sterilization. Kobayashi et al.(Kobayashi et al., 1981) in 1981 were the first ones to report an unusual degradation phenomenon in Zirconia-Yttria ceramics during aging at low temperatures (50 to 350 °C) in a humid atmosphere. They explained that the aging of Zirconia-Yttria ceramics at 300 °C for prolonged time resulted in the partial transformation of tetragonal to monoclinic structure accompanied by severe microcracking in the sample.

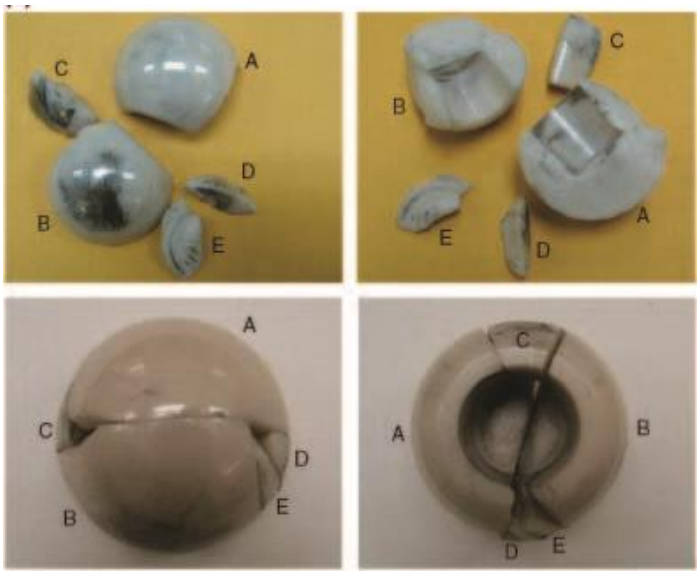

Fig. 2.6: *Photograph indicating failure of femoral head implant*(Masonis et al., 2004)

This low-temperature degradation behaviour was considered important only above room temperature until the year 2001 (Chevalier, 2006), but the catastrophic failure events of the implants made up of YSZ (**Fig. 2.6**) in the year 2001 due to LTD, left incredulity on using YSZ as implant material (Chevalier, 2006; Kohorst et al., 2012; Pereira et al., 2015). Investigations on this phenomenon revealed that; aging (T $\rightarrow$ M transformation) occurs at the surface by slow transformation to stable monoclinic phase in the presence of water. Transformation starts at an isolated grain on the surface, which causes stress on the neighbouring grains and forms microcracks and surface roughening because of the volume expansion of monoclinic grain (**Fig. 2.7**). The surface roughening causes increased wear of the component, and the microcracks offer a path to the water to penetrate deep in to sample and transforms other grains, as shown in **Fig. 2.8.** The initial transformation of the specific isolated grain can be related to its size, stabilizer content, or presence of residual stresses.

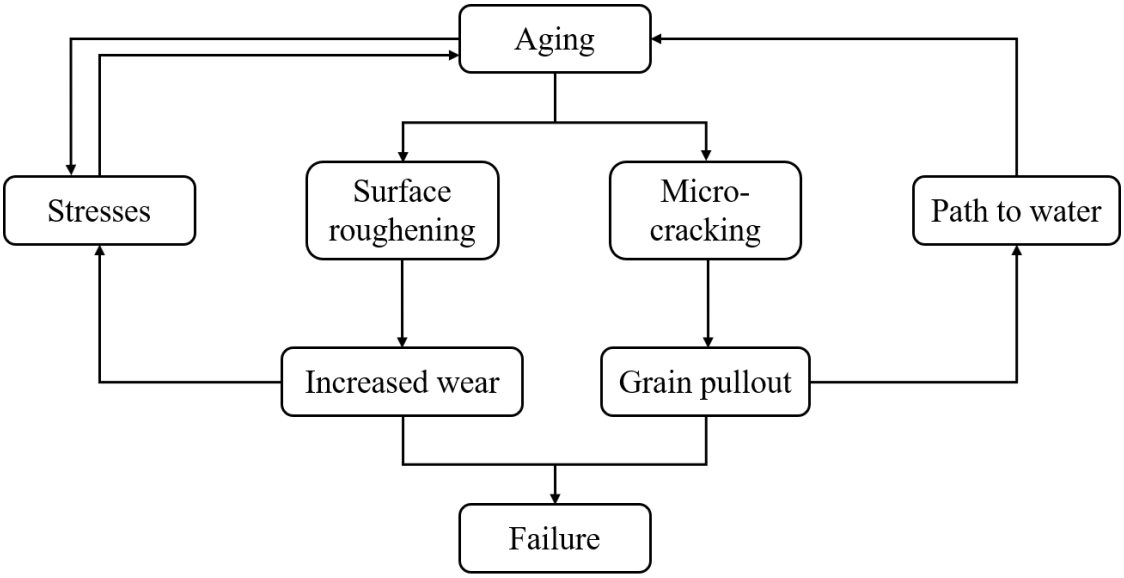

***Fig. 2.7**: Effect of aging in zirconia ceramics* (Chevalier et al., 2009).

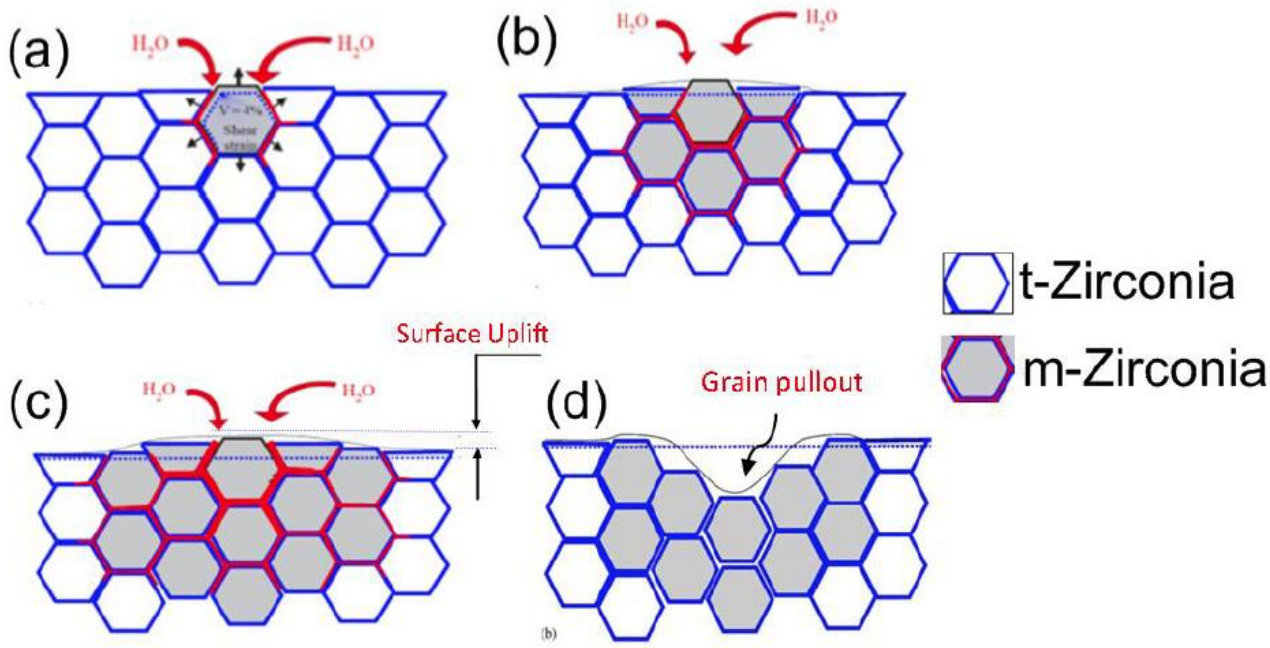

***Fig. 2.8**: Schematic representation of the Low-temperature degradation process in zirconia. a) Transformation of surface grain. b) Penetration of water molecules through the micro cracks. c) Surface uplift caused due to transformation. d) Pull out of transformed surface grains* (Chevalier, 2006).

2.6 Mechanism of Aging:

Though the exact mechanism of LTD is unclear till date, it may be explained by 3 possible reasons. First, the water molecules react with Y_2O_3 to form $Y(OH)_3$ clusters, which depletes the amount of stabilizer in zirconia grains which are then free to transform to stable monoclinic phase (Lange et al., 1986). Second, the destabilization of tetragonal zirconia is due to the dissociation of water molecules into O^{2-} and OH^- causes the filling up of oxygen vacancies responsible for the tetragonal stabilization around Zr (Chevalier et al., 2009). Third,chemical adsorption of water vapour (H_2O) on the surface of stabilized zirconia, which leads to the formation of Zr-OH and/or Y-OH bonds by breaking Zr-O and/or Y-O at the surface (**Fig. 2.9**). Which creates stress accumulation and generates lattice defects; these lattice defects act as a nucleating agent for monoclinic transformation (Yoshimura et al., 1987).

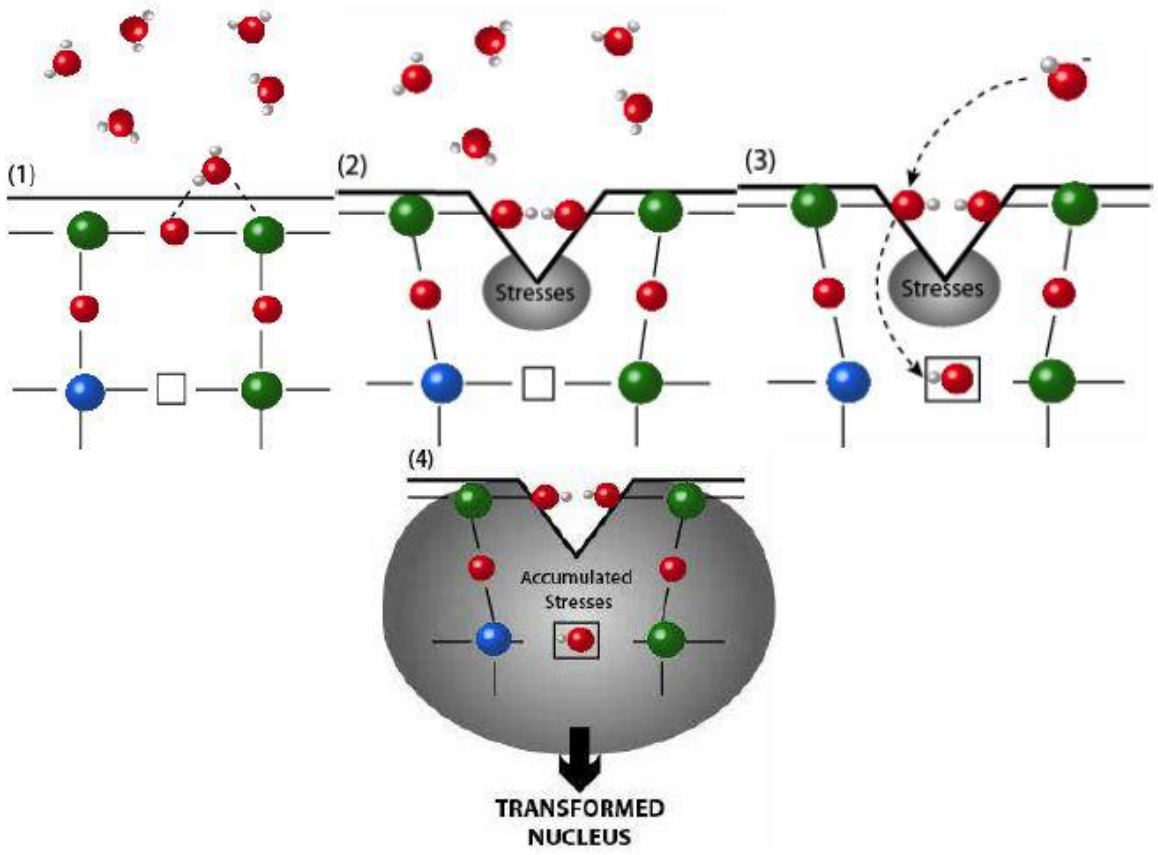

***Fig. 2.9**: Schematic of water adsorption during aging* (Yoshimura et al., 1987).

2.7Aging resistant zirconia ceramics:

Transformation of tetragonal to the monoclinic structure is responsible for aging, and this transformation depends on threemajor factors; grain size, stabilizer type, and content.

2.7.1 Grain size effect:

Grain size is the principal factor in the aging resistance of zirconia. It is observed that the stability of the tetragonal phase is increasing with a decrease in grain size. There is a critical grain below which no monoclinic transformation occurs, and this critical grain size depends on the stabilizer content. When the grain size exceeds this critical value, the transformation to the monoclinic phase increases with aging time, as shown in **Fig. 2.10.**

Tsukuma et al. reported that yttria-stabilized samples with more than 1μm grain size shown a high amount of transformation when subjected to hydrothermal aging, whereas the samples with below 0.4 μm shown no significant transformation(Tsukuma et al., 1983).

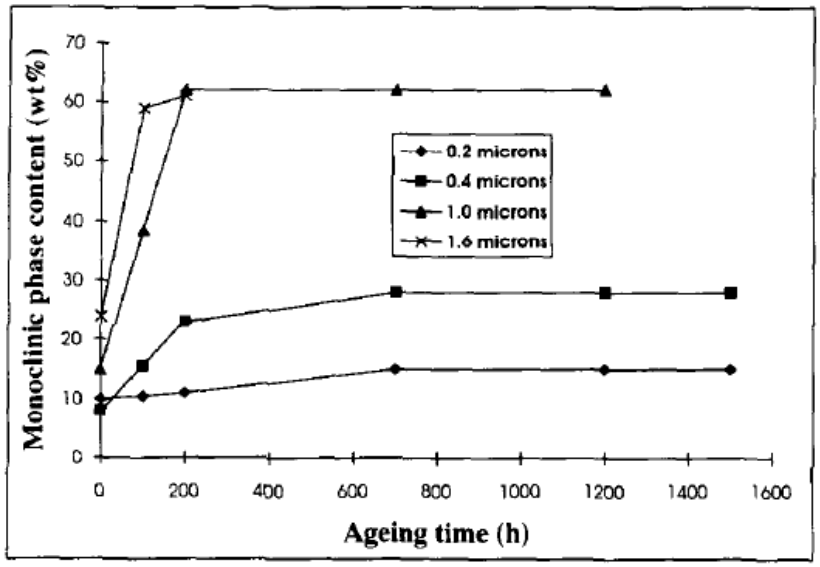

***Fig. 2.10**: Grain-size dependence of phase transformation in 3Y-TZP aging* (Tsukuma et al., 1983).

This critical grain size depends on the stabilizer content, Watanabe et al., in his research on yttria-stabilized zirconia system, found that critical grain size is varied from 0.2 to 0.6 μm when yttria content increased from 2 to 5 mol.% (**Fig. 2.11**) (Watanabe et al., 1983).

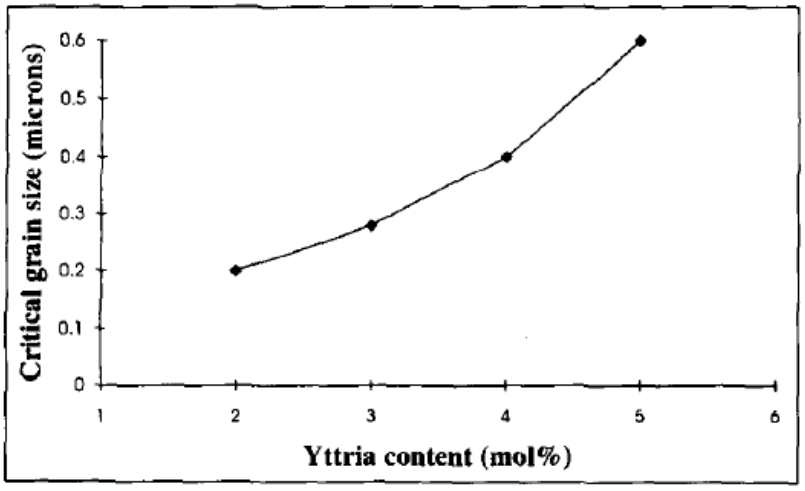

Fig. 2.11*: Critical grain size as a function of yttria content when aged* (Watanabe et al., 1983).

2.7.2 Effect of stabilizer type:

The stabilization mechanism is different for a differentkind of stabilizing oxides, the stabilization of Y-TZP, Mg-PSZ, and Ca-CSZ is due to the presence of oxygen vacancies in the lattice. The annihilation of these vacancies in the presence of moisture leading to the degradation of these systems.

The absence of these vacancies in tetravalent doped zirconia systems (Ex: Ce-TZP), makes them highly resistant to low-temperature degradation. The use of more than one stabilizer also improves the LTD resistance in some cases; forexample, the addition of CeO_2 to the Y-TZP significantly improved the aging resistance(Boutz et al., 1995; Sato et al., 1986). This topic is elaborately explained in section 2.9.1.2.

2.7.3 Effect of stabilizer content:

An increase in stabilizer content increases the free energy required to transform from tetragonal to monoclinic phase, as discussed in section 2.2, thereby improving the stability of the tetragonal phase. Being less transformable to the monoclinic phase, it is less prone to aging, as shown in **Fig. 2.12**, Tsukuma et al. found that the amount of monoclinic transformation is decreasing with an increase in yttria content in the samples with the same tetragonal grain size.

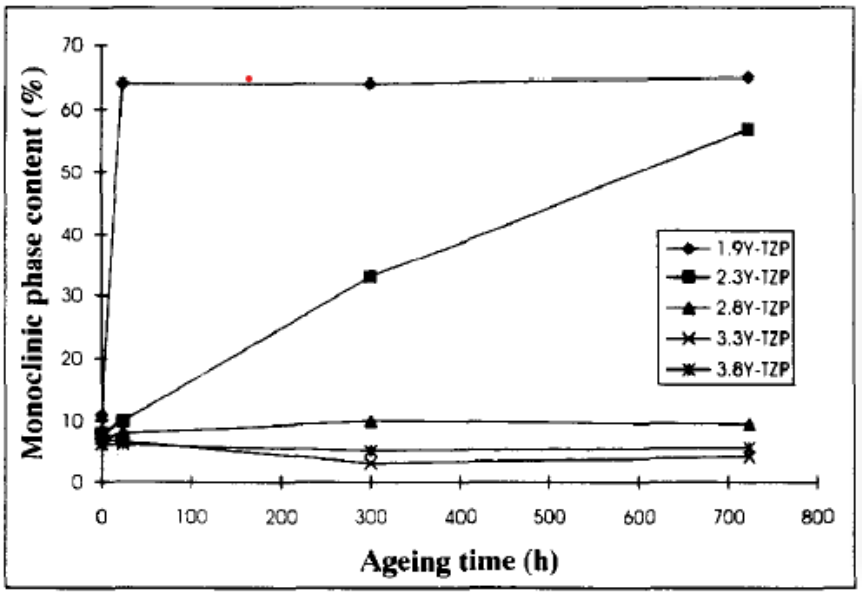

***Fig. 2.12**: Phase transformation with respect to the yttria content in yttria TZPs (grain size of all samples ~0.4 μm)* (Tsukuma et al., 1983).

But the increase in stabilizer content also increases the quantity of cubic phase, though the cubic phase considered to be more resistant to aging; it leads to the decrease in mechanical properties such as fracture toughness, as transformation toughening occurs only on metastable tetragonal phase.

2.8 Benefit of ceria stabilized zirconia over yttria stabilized zirconia:

The stabilization mechanism of the ceria stabilized zirconia system is different from yttria, magnesia, and calciastabilized zirconia systems, as discussed in the section. 2.2. The addition of ceria to the zirconia will not create any oxygen vacancies like yttria but causes dilation of the lattice and decreases the oxygen overcrowding around the zirconium atoms to stabilize metastable tetragonal phase (Li et al., 1994b).

As the mechanism of LTD mainly related to oxygen vacancy annihilation, as discussed in sec. 2.6, ceria stabilized zirconia is less susceptible to LTD because of the absence of oxygen vacancies in its lattice. However, some reports showed that ceria stabilized zirconia also susceptible to LTD but relatively much slower kinetics (Matsumoto, 1988; Sato and Shimada, 1985). Though the exact mechanism of LTD in ceria is not fully understood, one of the possible reasons might be the reduction of Ce^{4+} to Ce^{3+} and subsequent formation of oxygen vacancies

(Zhao et al., 2000). The reduction of Ce^{4+} to Ce^{3+} generally takes place when sintered in a non-oxidizing environment; this reduction is accompanied by a colour change (Heussner and Claussen, 1989; Vleugels et al., 2004; Zhao et al., 2000).

Combined with the high resistance to LTD, ceria stabilized zirconia also offers high fracture toughness. But ceria stabilized zirconia ceramics show lower hardness and strength due to its larger grain size (Duh et al., 1988; Tsukuma, 1986; Tsukuma and Shimada, 1985). Ceria stabilized zirconia ceramics require a higher temperature and longer times for successful sintering compared to YSZ because of lack of defects in its structure, which leads to the substantial growth in grain size. It is known that reducing the grain size improves the mechanical properties of ceramics, such as hardness, strength, and wear resistance. Substantial research has been done on reducing the grain size of zirconia ceramics to pursue these desirable mechanical properties.

The grain growth of CSZ can be controlled by the addition of suitable dopantsand/or using an alternative sintering process.

2.9 Improving mechanical properties of zirconia:

For load-bearing orthopaedics and dental applications, a material needs to be corrosion protected, wear-resistant and should possess good hardness and toughness. The wear resistivity of materials mainly depends upon their hardness, and hardness intern depends on composition, grain size, porosity etc. To improve wear resistance and hardness of ceramics, one should control its grain size and minimize porosity (improve sinterability), this can be carried out by the following methods.

2.9.1 Addition of dopants:

Grain boundary migration and grain boundary diffusion are two mainmechanisms during the sintering of ceramics. Grain boundary migration mainly contributes to grain growth, and grain boundary diffusion contributes to the densification (Ferreira et al., 2012). The addition of suitable dopants can inhibit grain boundary migration by changing boundary, lattice and surface diffusivities thereby decreasing the mobility of grain boundaries and/or added dopant ions could segregate to the boundary and produces a drag force on boundary motion. Sometimes, if there is

an excess amount of dopant (more than the solubility limit), it might form precipitates, and that can pin down the boundary and restricts its movement (Powers and Glaeser, 1998).

Dopants can also act as sintering aids/additives, the addition of suitable dopant either promote liquid state sintering or creates defects in the lattice. The presence of defects enhances the diffusional mass transport, which further helps in improving sintering kinetics and lowers the sintering temperature (M. N. . Rahaman, 2007).

2.9.1.2 Effect of co-doping on stabilized zirconia:

The effect of different dopants on stabilized zirconia ceramics was first studied by Sato et al. (Sato et al., 1986). They co-doped 3 mol.% yttria-stabilized zirconia with varying amounts of either CeO_2, MgO, TiO_2 or CaO and studied their effect on phase transformation, densification, and grain growth. The addition of CaOsuppressed the grain growth, and TiO_2 accelerated the grain growth, but CeO_2 and MgO caused no change, they also concluded that the addition of CeO_2, TiO_2, and decrease in zirconia grain size improved the resistance of tetragonal to monoclinic transformation.

J.G Duh et al. (Duh et al., 1988) reported that the addition of Y_2O_3 and/or MgO to 10 mol.% CeO_2 stabilized zirconia suppressed grain size and improved the tetragonal stability. Dae-Joon Kim(Kim, 1990) found that co-doping 3YSZ with TiO_2, Nb_2O_5,and HfO_2 enhanced the fracture toughness and increased the tetragonal distortion without much-effecting grain size.

Shyh-Lung Hwang et al. (Hwang and Chen, 1990) studied the effect of several dopants (of different ionic radii and valency) on grain growth and segregation behaviour in 12Ce-TZP and other TZP materials. They found that the dopants of lower cation valency and larger ionic radius are effective in suppressing the grain growth, they also concluded that the suppression of grain growth is related to the segregation of dopant ions at the grain boundary. As the grain boundary in TZPs is positively charged, the added lower valency cations attract towards the grain boundary and form a negative space charge layer (Boutz et al., 1994; Hwang and Chen, 1990; Theunissen et al., 1989). The drag force caused by these dopant ions present at boundaries retards the grain boundary mobility and restricts its growth.

Jeong-HyunPark et al (Park and Moon, 1992) found that the addition of small amounts of CaO, MgO improved the sinterability, decreased grain growth of 12Ce-TZP. They reported that the

improvement in sinterability is due to the reason that the addition of lower valency oxides than zirconia, which induces oxygen vacancies in the lattice, and it is known that the oxygen vacancy diffusion is much faster than the cation diffusion.

Deuk Yong Lee (Lee et al., 1998), Dae-Joon Kim (Kim et al., 2005) found that doping with pentavalent dopants like Nb_2O_5 can improve the fracture toughness of 3Y-TZP by increasing internal strain in lattice through annihilation of oxygen vacancies, which enhances the transformability of tetragonal phase.

Fangwei Guo (Guo and Xiao, 2012), A.M. Hassan (Hassan et al., 2015), Pei-Chia Chen (Chen et al., 2016), and In-Jin Shon (Shon et al., 2009) reported that addition of trivalent or pentavalent dopants of a smaller ionic radius than zirconia promoted the densification behaviour of TZPs. The defects created by the doping trivalent and pentavalent oxides improved the diffusion rate of Zr^{4+} ions, which is responsible for the densification.

2.9.2 Two-step sintering method:

Conventional pressure less sintering process requires high temperatures and long processing time to densify the ceramic components, which substantially increases the grain size. Most of the efforts were undergone to restrict the grain growth of ceramics by using advanced sintering processes like hot pressing, spark plasma sintering, and microwave sintering. But all these sintering techniques require sophisticated instruments, and these methods are expensive.

Chen and wang developed a simple, novel, andcost-effective method to restrict the grain growth of ceramics known as “two-step sintering” by modifying the conventional sintering process (Chen and Wang, 2000).

Two-step sintering is a method, which inhibits the grain growth by restricting grain boundary migration in the final stage of sintering. In two-step sintering (**Fig. 2.13**), samples were first heated to a high-temperature T_1 (first stage temperature) for shorter dwell time, where more than 70% of densification (known as critical density) will be achieved through grain boundary migration and grain boundary diffusion. Then samples were cooled to a lower temperature T_2

(second stage temperature) for a long dwell time, where Grain boundary migration will be restricted, and the rest of the densification will be done through only grain boundary diffusion.

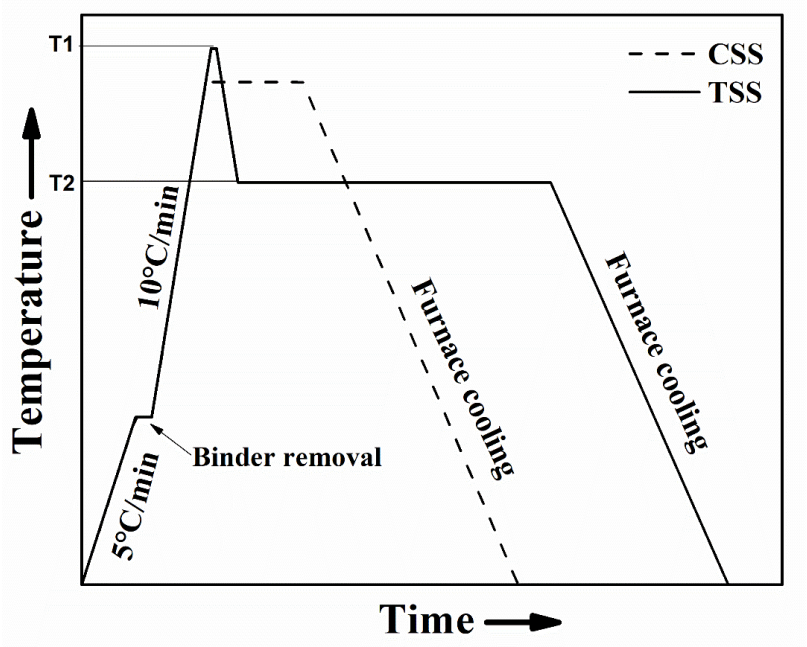

Fig. 2.13*: Sintering profiles representing a conventional single-step and two-step sintering.*

One can achieve a near full density (>98%) using a two-step sintering process by exploiting the "kinetic window", which separates the grain boundary migration and grain boundary diffusion (Ferreira et al., 2012). If sintering condition falls down the kinetic window, full density cannot be achieved and above the kinetic window grain growth will take place. Hence it is vital to exploit proper kinetic window (i.e., T_1 and T_2 temperatures) to get a dense body with fine grains.

2.10Making zirconia bioactive:

Zirconia ceramics are bioinert; they cannot form a bond with living bone directly (Ferraris et al., 2000; Uchida et al., 2001). To use zirconia in applications like bone substitute material under load-bearing conditions, it needs to be bioactive and should form a bond with the host's living bone via formation of a bonelike apatite layer on its surface (Uchida et al., 2001). Several chemical treatment methods are reported in the literature to make the surface of zirconia bioinert (Ke et al., 2017; Uchida et al., 2002a, 2002b, 2001). Masaki Uchida et al. (Uchida et al., 2002a) and Miho Nakamura et al. (Nakamura and Inuzuka, 2011) induced the bioactivity in tetragonal zirconia polycrystals through chemical treatment with H_3PO_4, H_2SO_4 and HCl etc., these

chemical treatments were found to produce surface OH groups, which later acted as nucleation sites for apatite formation.**Fig. 2.14** illustrates the chemical treatment process described by the Miho nakamura et. al. to make surface of zirconia bioactive by inducing Zr-OH bonds.

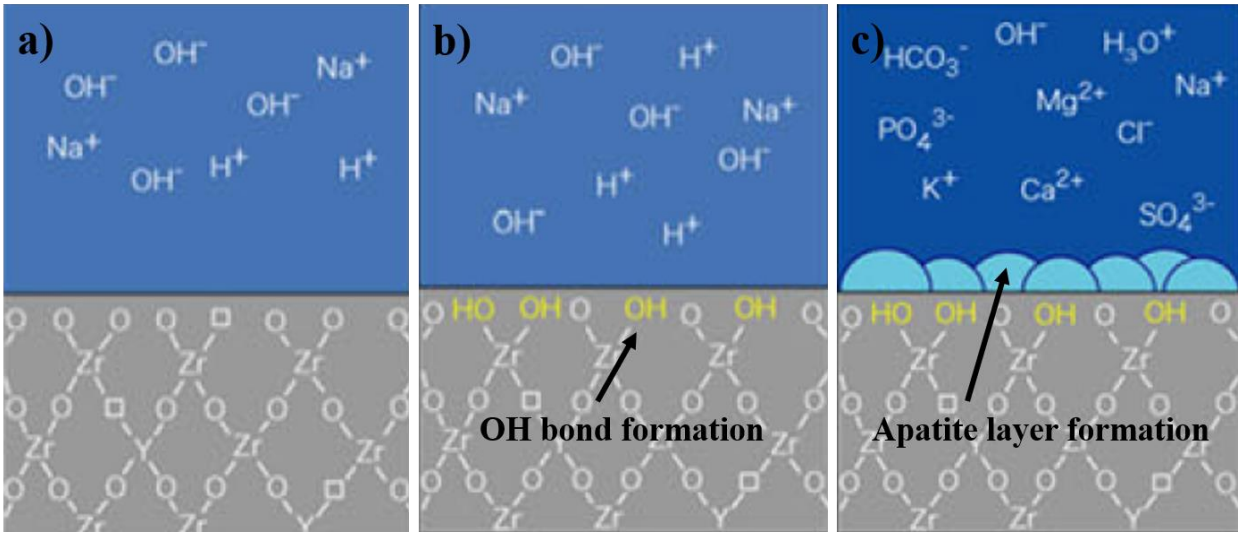

Fig. 2.14:*The process of formation of Zr–OH functional groups on the chemical treated zirconia surfaces to induce apatite layer formation*(Nakamura and Inuzuka, 2011).

2.11 Biocompatibility:

The definition of biocompatibility is "The ability of a material to perform with an appropriate host response in a specific application" (Williams, 1987). Appropriate host response implies that the material should show resistance to blood clotting, resistance to bacterial colonization, and should not show any adverse effect co-existing living organisms. ISO standard 10993 "Biological evaluation of medical devices" provides the requirements of implant material and series of biological tests to evaluate the biocompatibility depending on the intended use of material. Part 1 of the standard provides the guidance for the selection of suitable tests, part 2 covers the animal welfare requirements, and part 3 to 19 covers the guidelines for specific test procedures and testing related issues.

As per ISO 10993 the selection of tests to evaluate biocompatibility depends on the composition of material, conditions of exposure and duration of exposure of material with the host. **Table 2.1** categorizes the materials and provides the required tests for biological evaluation.

A series of tests are suggested to evaluate the biocompatibility of materials as shown in **Table. 2.1**, depending on the application one can choose one or more tests to assess the biocompatibility.

Table 2.1*: Biological evaluation of biomaterials*(ISO 10993, 2009).

Nature of body contact		Contact duration A – (<24h) B – 24h to 30 days C – (>30 days)	Cytocompatibility evaluation	Sensitization	Irritation or Intracutaneous reactivity	Systemic toxicity (Acute)	Subacute and sub chronic toxicity	Genotoxicity	Implantation	Hemocompatibility
Category	**Contact**									
Surface Device	Skin	A	√	√	√					
		B	√	√	√					
		C	√	√	√					
	Mucosal membrane	A	√	√	√					
		B	√	√	√					
		C	√	√	√		√	√		
	Breached or compromised surface	A	√	√	√					
		B	√	√	√					
		C	√	√	√		√	√		
External Communicating device	Blood path, indirect	A	√	√	√					√
		B	√	√	√					√
		C	√	√		√	√	√		√
	Tissue/bone/ dentin	A	√	√	√					
		B	√	√	√	√	√	√	√	
		C	√	√	√	√	√	√	√	
	Circulating blood	A	√	√	√	√				√
		B	√	√	√	√	√	√	√	√
		C	√	√	√	√	√	√	√	√
Implant device	Tissue/bone	A	√	√	√					
		B	√	√	√	√	√	√	√	
		C	√	√	√	√	√	√	√	
	Blood	A	√	√	√	√	√		√	√
		B	√	√	√	√	√	√	√	√
		C	√	√	√	√	√	√	√	√

2.11.1 Cytocompatibility:

Cytocompatibility tests involves the exposure of test material to the suitable cell culture lines. Cell cultures are very sensitive and readily display signs of toxicity in the presence of harmful substances leached from test material. The following section describes the most widely used methods to test the cytocompatibility.

2.11.1.1 Cell culture and cellular metabolic activity assay:

Cell culture and cellular metabolic activity assays are the most commonly used tests to evaluate the cytocompatibility of biomaterial in *Invitro*. These tests are simple, rapid, inexpensive, easily reproducible, and do not require animals. Cellular metabolic activity assays are based on various cell functions such as cell membrane permeability, cell adhesion, cell proliferation, adenosine triphosphate (ATP) production (Ishiyama et al., 1996). In cell culture studies, isolated animal or human cells are grown in a tissue flask. The cells are then seeded on to the surface of the material and incubated at standard conditions. The cell viability or the cytotoxicity of the materials assayed through the activity of the mitochondrial enzyme. The activity of mitochondrial enzymesis often determined through 3-(4, 5- dimethylthiazol-2-yl)-2, 5-diphenyltetrazolium bromide assay, or MTT assay (Stockert et al., 2018).

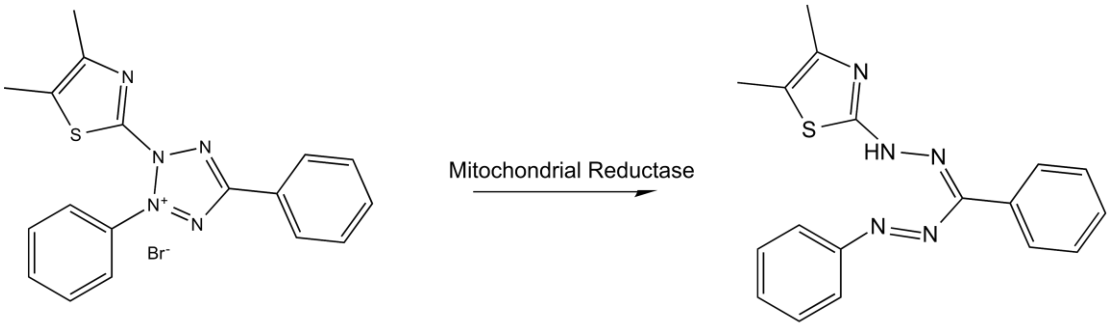

***Fig. 2.15**: Enzymatic reduction of MTT to formazan* (Kuete et al., 2017).

MTT assay is a colorimetric assay; this yellow tetrazolium dye (MTT) is reduced to an insoluble purple formazan in the presence of mitochondrial enzyme present in the cytosolic compartment of the cell as shown in **Fig. 2.15**(Mosmann, 1983). Then the purple formazan is dissolved in a soluble solution, and absorbance of this solution is measured, the degree of absorbance indicates the viability of cells.

2.12 Scope of work:

As discussed earlier, poor mechanical properties of ceria stabilized zirconia are due to its larger grain size. In general, achieving high density with fine grain size are vital for zirconia ceramics to enhance the stability of the tetragonal phase with improved mechanical properties. It is known that grain growth of ceria stabilized zirconia is due to its poor sinterabilityand/or lack of proper grain growth restriction mechanism (segregation/solute drag) like in yttria-stabilized zirconia. Improved sinterability requires efficient transportation of matter, which in crystallite solids occurs by the process of diffusion involving atoms, ions, and molecules. Crystallite solids are not ideal in the structure; they contain various defects. It is the presence of defects that allow diffusional mass transport to take place. As the defects control the rate of mass transportation, they contribute to the sintering rate and grain growth. The addition of aliovalent dopants may improve the sinterability of CSZ by increasing defect density in its lattice, as observed in the literature discussed in section 2.9.1.2. Two dopants with different valency are chosen in the present study; they are pentavalent Nb_2O_5 and tetravalent Sm_2O_3. Addition of Nb^{5+} of the ionic radius (0.64 Å) smaller than Zr^{4+} and O^{2-} can promote the sintering of CSZ by creating point defects (substitutional/Interstitial) (Guo and Xiao, 2012) and also Nb^{5+} addition increases the tetragonality (c/a ratio), which decreases the tetragonal stability of CSZ and improves the fracture toughness (Kim et al., 2005). Being low valency cation with larger ionic radius (1.08 Å) Sm^{3+} ions expected to suppress the grain growth by segregating at the grain boundary (Hwang and Chen, 1990).

Another way to control grain growth in CSZ is to use a two-step sintering method. Two-step sintering can effectively control the grain boundary migration, which is responsible for grain growth and allows densification through grain boundary diffusion, as discussed in section 2.9.2.1.

2.13 Objectives of the work:

- Synthesis of ceria stabilized zirconia co-doped with Nb_2O_5 and Sm_2O_3nanopowders through the co-precipitation method.
- Study of the effect of co-dopants on sinterability and grain growth of CSZ.
- Optimization of the calcination temperature and sintering schedule based on density, microstructure, and mechanical properties of samples.
- Evaluation of mechanical properties, such as hardness and fracture toughness.
- Evaluation of Low-temperature degradation of samples through accelerated aging studies.
- Biocompatibility study of developed systems.

2.14 Plan of Work:

The work plan of the present research is represented in **Fig. 2.16**. Nanopowders of niobia doped ceria stabilized zirconia, and samaria doped ceria stabilized zirconia with varying amounts (0-2 mol. %) of niobia and samaria will be synthesized through co-precipitation synthesis.

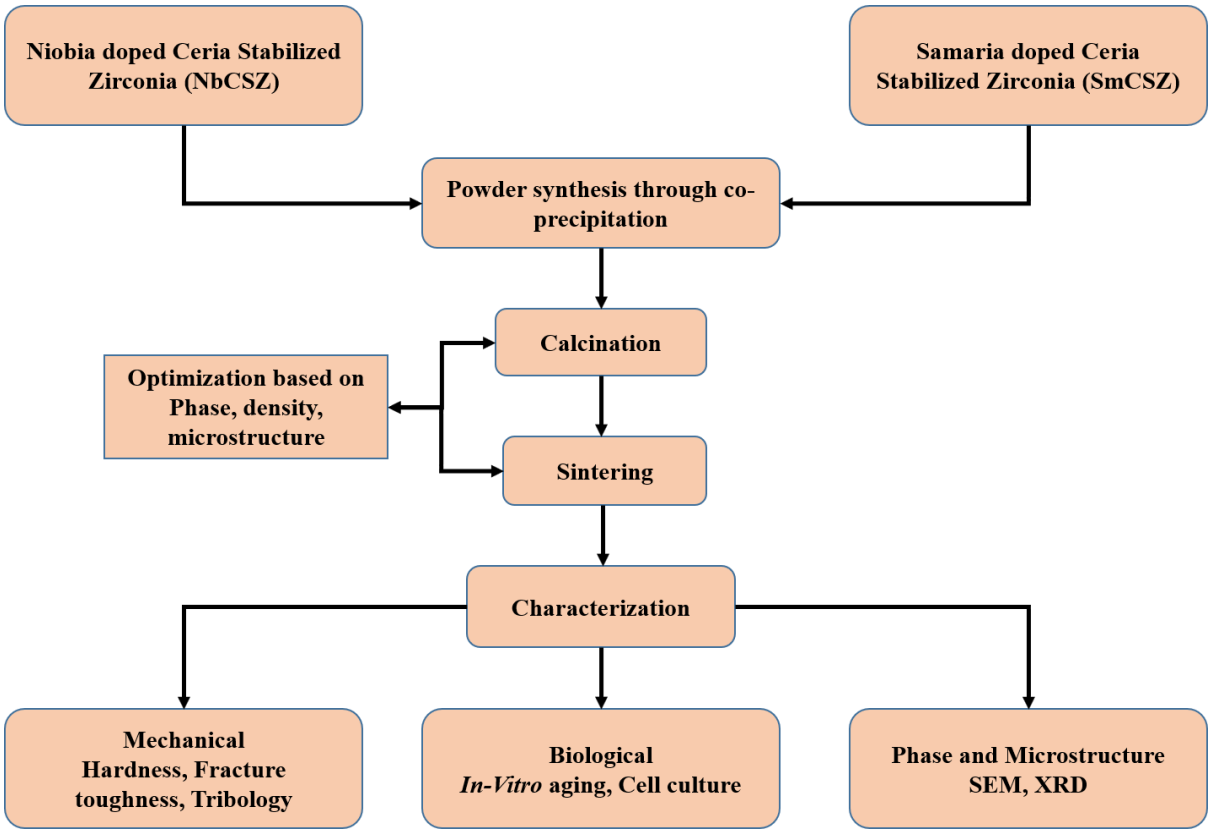

***Fig. 2.16**: Schematic of the plan of work.*

Dopant concentration and sintering schedule will be optimized based on density, microstructure, phases present, and mechanical properties of the sintered component. Phase and microstructure, Mechanical behaviour (hardness, fracture toughness, compressive strength), tribological properties, *in vitro* aging (hydrothermal treatment), and biological response (biocompatibility) will be evaluated.

Chapter-3

Materials and Experimental Methods

This chapter deals with the details of the raw materials used in this study and powder synthesis methods followed, consolidation of powders, sintering methods used, equipment and techniques followed for physical, mechanical and bio-functional characterization.

3.1 Raw materials used:

Raw materials used for the preparation of desired powders were zirconyl nitrate, cerous nitrate, samarium nitrate and niobium oxalate hydrate. The source and purity of raw materials are mentioned in **Table 3.1**. The raw materials of the required quantities were measured using an electronic balance with a 0.1mg precision.

***Table 3.1**: Source and purity of raw materials used for powder synthesis.*

Raw material	Chemical formula	Purity	Source
Zirconyl nitrate	$ZrO(NO_3)_2.xH_2O$	99.5%	LobaChemie, India
Cerous nitrate	$Ce(NO_3)_3 \cdot 6H_2O$	99.5%	LobaChemie, India
Samarium nitrate	$Sm(NO_3)_3.6H_2O$	99.99%	Alfa Aesar, Russia
Niobium oxalate hydrate	$Nb(HC_2O_4)_5.xH_2O$	99.9%	Alfa Aesar, USA

3.2 Wet chemical synthesis of powders:

Three kinds of powders, i.e., Ceria Stabilized Zirconia (CSZ), Niobia doped Ceria Stabilized Zirconia (NbCSZ) and Samaria doped Ceria Stabilized Zirconia (SmCSZ), were prepared with different stoichiometry. The compositional variation and their nomenclatures are listed in **Table 3.2.**

***Table 3.2**: Different samples used in this study, along with their chemical composition.*

System	Sample ID	mol.% Niobia	mol.% of Samaria	mol.% of Ceria	mol.% of Zirconia
CSZ	CSZ	0	0	12	88
NbCSZ	0.5NbCSZ	0.5	0	12	87.5
	1NbCSZ	1	0	12	87
	1.5NbCSZ	1.5	0	12	86.5
	2NbCSZ	2	0	12	86
SmCSZ	0.5SmCSZ	0	0.5	12	87.5
	1SmCSZ	0	1	12	87
	1.5SmCSZ	0	1.5	12	86.5
	2SmCSZ	0	2	12	86

The powders of different compositions were synthesized through co-precipitation method. The respective amounts of precursor salts were dissolved in distilled water in proper ratios and then co-precipitated by dropwise addition of ammonia solution as represented in **Fig. 3.1**. A pH level of 9-10 was maintained for total precipitation to occur.

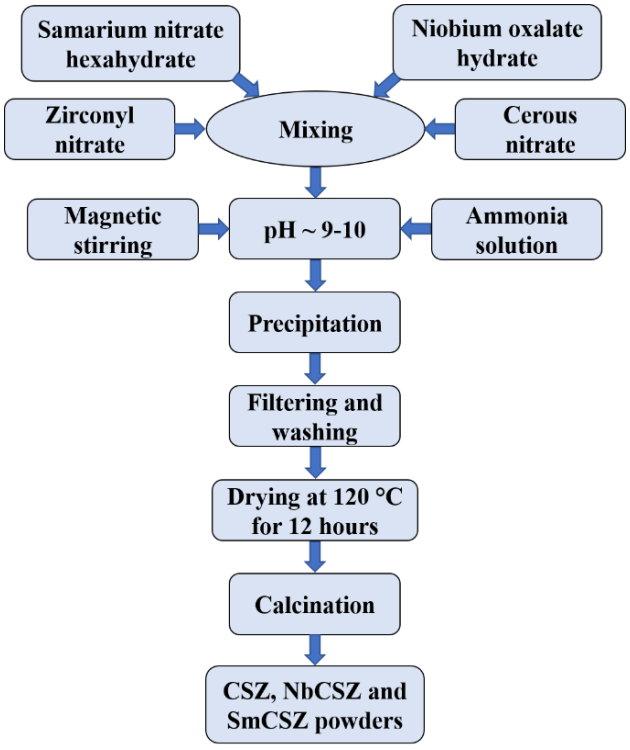

***Fig. 3.1**: Schematic representation of powder synthesis process.*

The precipitates were filtered and washed with distilled water for several times to ensure ammonia is completely removed from precipitates, **Fig.3.2**shows the complete experimental setup used for the powder synthesis. The filtered precipitates were dried in a hot air oven at 110 °C for 12 hours to remove moisture.

The reaction kinetics are as shown below:

$$ZrO(NO_3)_2.H_2O + 3NH_4OH \rightarrow Zr(OH)_4 + 2NH_4NO_3 \qquad \text{(Eq. 3.1)}$$

Fig. 3.2*: Experimental setup used for the co-precipitation process.*

3.3 Calcination of synthesized powders:

The synthesized powders were calcined at different temperatures (600-1000 °C) for 2 hours in air atmosphere using a resistance heating furnace. The calcination process removes volatile materials present in powders and converts amorphous hydroxide to crystalline oxides. The reaction kinetics of powders during calcination can be represented as follows:

$$Zr(OH)_4 \xrightarrow{heat} ZrO_2 + H_2O \qquad \text{(Eq. 3.2)}$$

3.4 Uniaxial compaction of powders:

After calcination, the powders were compacted to cylindrical pellets of different diameters (6mm to 10mm) at a pressure of 600 MPa using compaction dies and a uniaxial hydraulic press (**Fig.3.3**). Zinc stearate was applied to the die walls as a lubricant to reduce the die wall friction and 1 wt. % PVA (Poly Vinyl Alcohol) solution was added to the powder before compaction as a binder to increase the green strength of pellet.

Fig. 3.3*: Uniaxial hydraulic press used for compaction of powders.*

3.5 Sintering of compacts:

Compacted pellets were sintered in a box-type electric resistance furnace equipped with $MoSi_2$ heating elements (OKAY, Bysakh& Co., India) shown in **Fig.3.4.**Initially, pellets were heated to 500 °C with a slow heating rate of 5 °C/min and 30 min holding was provided to remove binder added during compaction, then the remaining schedule was carried out at a heating rate of 10 °C/min. In present work, two different types of sintering schedules were used, i.e., conventional single step, two-step sintering. The representative sintering profiles of a conventional single-step and two-step sintering process are represented in **Fig.3.5**.

***Fig. 3.4**: Box type electric resistance furnace used for sintering of compacted samples.*

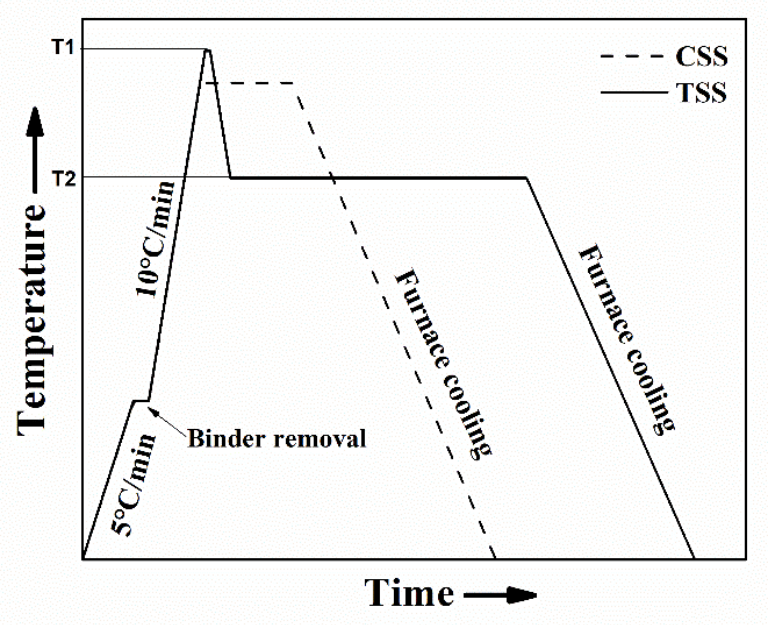

***Fig. 3.5**: Representative sintering schedules indicating a conventional single-step and two-step sintering.*

3.6 Characterization methods used:

After sintering, samples were subjected to physical, phase, microstructural, mechanical and biological characterization. The details of the characterization techniques and equipment used were discussed below.

3.6.1 Physical characterization:

3.6.1.1 Density measurement:

The green density (ρ_g) of the compacted pellets was calculated by measuring the weight and estimating volume through the dimensions of the compact.

$$\rho_g = \frac{Mass}{Volume} \qquad \text{(Eq. 3.3)}$$

The density measurement setup, as shown in the **Fig.3.6**, was used to measure the density of sintered samples. The density of the sintered samples was measured using the Archimedes principle following ASTM B 962-15 standard (ASTM International, 2017a). The sintered density (ρ_s) is given as:

$$\rho_s = \frac{m_s \rho_w}{m_s - m_w} \qquad \text{(Eq. 3.4)}$$

where, ρ_s = sintered density, ρ_w =density of water at room temperature, m_s = mass of the sintered body in the air, m_w =mass of the sintered body in water.

Relative density can be calculated as:

$$\% \ \rho_{rel} = \frac{\rho_s}{\rho_{th}} \text{ x } 100 \qquad \text{(Eq. 3.5)}$$

Where ρ_{th} is theoretical density.

3.6.2 Phase and microstructural analysis:

Phase and microstructure of powders and sintered samples were analysed using X-Ray Diffractometer and Scanning Electron Microscope (SEM) as discussed in the following sections.

3.6.2.1 X-ray diffraction analysis:

Phase and crystallite sizes of powders and sintered specimens were characterized using X-Ray Diffractometer (XRD: X'Pert PRO, PANalytical, The Netherlands) shown in **Fig. 3.7**. Diffraction peaks were obtained using CuK_{α} radiation (wavelength $\lambda = 0.15406$ nm) operated at 45 kV, 30 mA, taking step size of 0.02°. The patterns were then analyzed using X'Pert Highscore Plus (PANalytical, The Netherlands) software for phase identification and quantification equipped with ICDD (International Center for Diffraction Data) and ICSD (Inorganic Crystal Structure Database). Rietveld refinement method was used for quantification of phases.

***Fig. 3.7**: X-ray diffractometer used for phase analysis.*

3.6.2.2 Measurement of crystallite size from XRD:

Crystallite sizes were calculated from XRD patterns using Debye Scherrer's formula. In order to eliminate the effect of instrument broadening, standard coarse-grained samples were prepared using similar composition, and XRD patterns were obtained.

Crystallite size according to Debye Scherrer's formula

$$t = \frac{0.94.\lambda}{B_c.COS\theta} \qquad \text{(Eq. 3.6)}$$

Where t is crystallite size, λ is X-ray wavelength, θ is the diffraction angle and B_c is the peak broadening due to crystallite size

In general broadening (Full width half maxima) is a combined effect of crystallite size, lattice strain and instrument broadening. Broadening due to instrument B_i can be calculated from the standard sample. Now by subtracting B_i from observed broadening B_o, we can obtain broadening due to crystallite size and lattice strain B_r ($B_r = B_c + B_s$),

$$B_r = \sqrt{(B_o^2 - B_i^2)} \quad \text{(Eq. 3.7)}$$

Where B_o is the broadening of the actual sample, B_i is the broadening of the standard sample.

Broadening due to only crystallite size can be obtained from the equation 3.6,

$$B_c = \frac{k\lambda}{t\ cos\theta} \quad \text{(Eq. 3.8)}$$

Broadening due to only lattice strain can be calculated from the below formula

$$B_s = \eta\ tan\theta \quad \text{(Eq. 3.9)}$$

As Br is the combined effect of crystallite size and lattice strain it can be written as follows

$$B_r = B_c + B_s \quad \text{(Eq. 3.10)}$$

$$B_r = \frac{k\lambda}{t\ cos\theta} + \eta\ tan\theta \quad \text{(Eq. 3.11)}$$

$$B_r\ cos\theta = \frac{k\lambda}{t} + \eta\ sin\theta \quad \text{(Eq. 3.12)}$$

Now if we plot a graph by considering sinθ as X-axis and B_r cosθ asY-axis as shown in the **Fig. 3.8**, the slope of the graph will give us the lattice strain (η) value. The crystallite size can be calculated from the intercept.

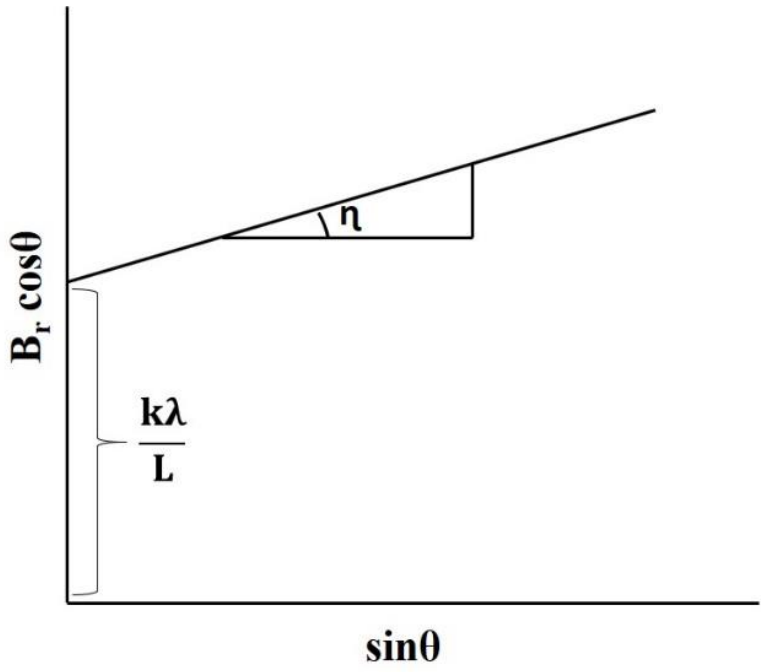

***Fig. 3.8**: Williamson-Hall plot indicating the intercept (kλ/L) and slope.*

3.6.2.3 Microstructural analysis:

The Microstructure of the samples was examined with a Scanning Electron Microscope (**Fig. 3.9**)with tungsten filament electron source (SEM: VEGA 3LMV, TESCAN, Czech Republic) using Secondary Electron (SE) and Back Scattered Electron (BSE) imaging modes. Chemical composition of the samples was qualitatively measured using Energy Dispersive X-ray Spectroscopy (EDS: Oxford Technologies, UK) attached to the SEM. The SEM was operated at an accelerated voltage of 15 kV for imaging and 20 kV for EDS analysis. Before observing in SEM, the samples were metallographically polished and thermal etched at 1200 °C for 1hr, and samples surface was sputter-coated with an ultra-thin coating (2 - 10 nm) of electrically conducting gold/palladium (80/20). Sputter coating makes the sample surface conductive and prevents the charging effect.

***Fig. 3.9**: Scanning Electron Microscope used for microstructural analysis of samples.*

3.6.3 Mechanical property evaluation:

Mechanical properties such as Hardness, Fracture toughness and Wear properties of sintered samples were analysed as described in the following sections.

3.6.3.1 Hardness measurement:

Vickers indentation hardness was measured on the polished specimen at a test load of 98 N using Vickers hardness tester (Via-S, Matsuzawa, Japan) shown in **Fig. 3.10** following ASTM C 1327-15 (ASTM International, 2019). The indentation was observed with an attached optical microscope, and diagonal lengths were measured. An average of 5-10 readings was taken at random positions on the samples. Vickers hardness(HV) was calculated using the formula.

$$HV = 1.854 \frac{F}{d^2} \qquad \text{(Eq. 3.8)}$$

Where F= applied a load (Kgf), d=average length of the diagonals (mm).

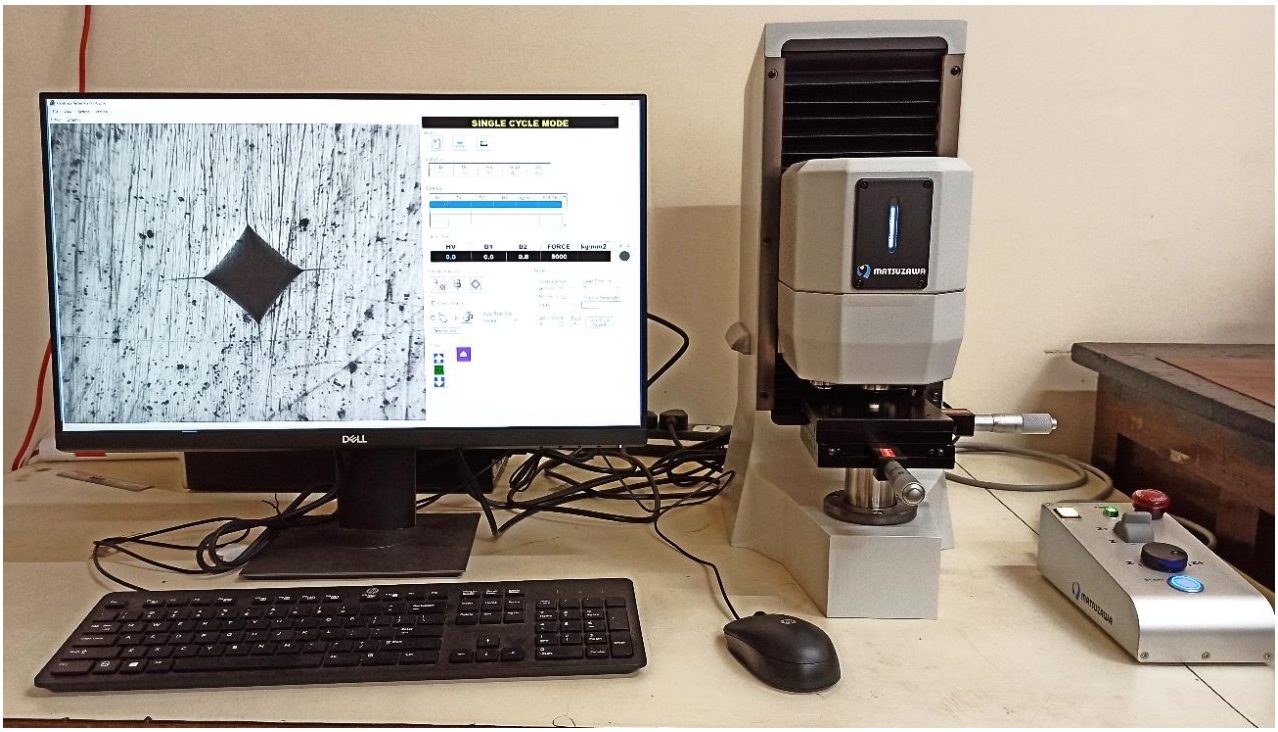

***Fig. 3.10**: Computerized Vickers hardness tester used for measuring hardness and indentation fracture toughness.*

3.6.3.2 Indentation fracture toughness measurement:

Indentation fracture toughness (IFT) of the polished samples was estimated by measuring the crack length of the Vickers indentation (**Fig. 3.11**). The well-known IFT equation given by Anstis et al. was considered to calculate fracture toughness (Anstis et al., 1981).

$$K_{IC} = 0.016.\left(\frac{E}{H}\right)^{1/2}.\left(\frac{P}{C^{3/2}}\right) \qquad \text{(Eq. 3.9)}$$

Where K_{IC} is the fracture toughness, H is the hardness, E is Young's modulus, C is the crack Length, P is applied load, and 0.016 is the "calibration" constant.

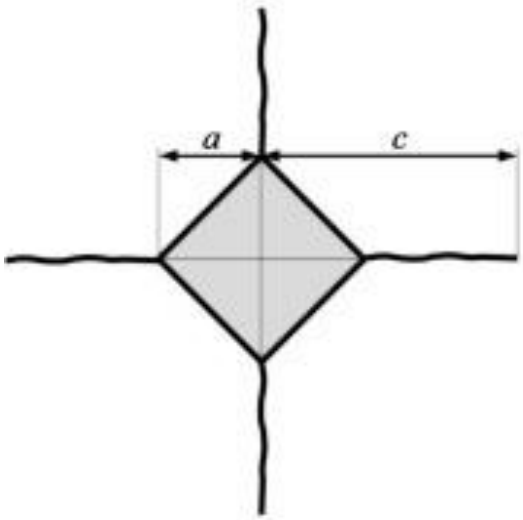

Fig. 3.11*: Schematic image of Vickers' indentation with cracks at the edges*(Anstis et al., 1981).

3.6.3.3 Wear study:

Tribological properties were evaluated (in dry condition) using "pin and ball on disc wear testing machine" (Model: TR-20, Ducom, India) in pin on disc configuration following ASTM G 99 standard (ASTM International, 2017b).

A schematic representation and a photograph indicating different parts of the pin on disc wear machine is presented in **Fig 3.12**. A commercially available alumina disc (99.7 % density) was used as a counter body to the pin type specimen. The test loads were chosen based on the simplification developed by Adelina Borruto for possible loads acting on the femoral head in the hip joint during different human activities like walking, running etc. (Borruto, 2010).

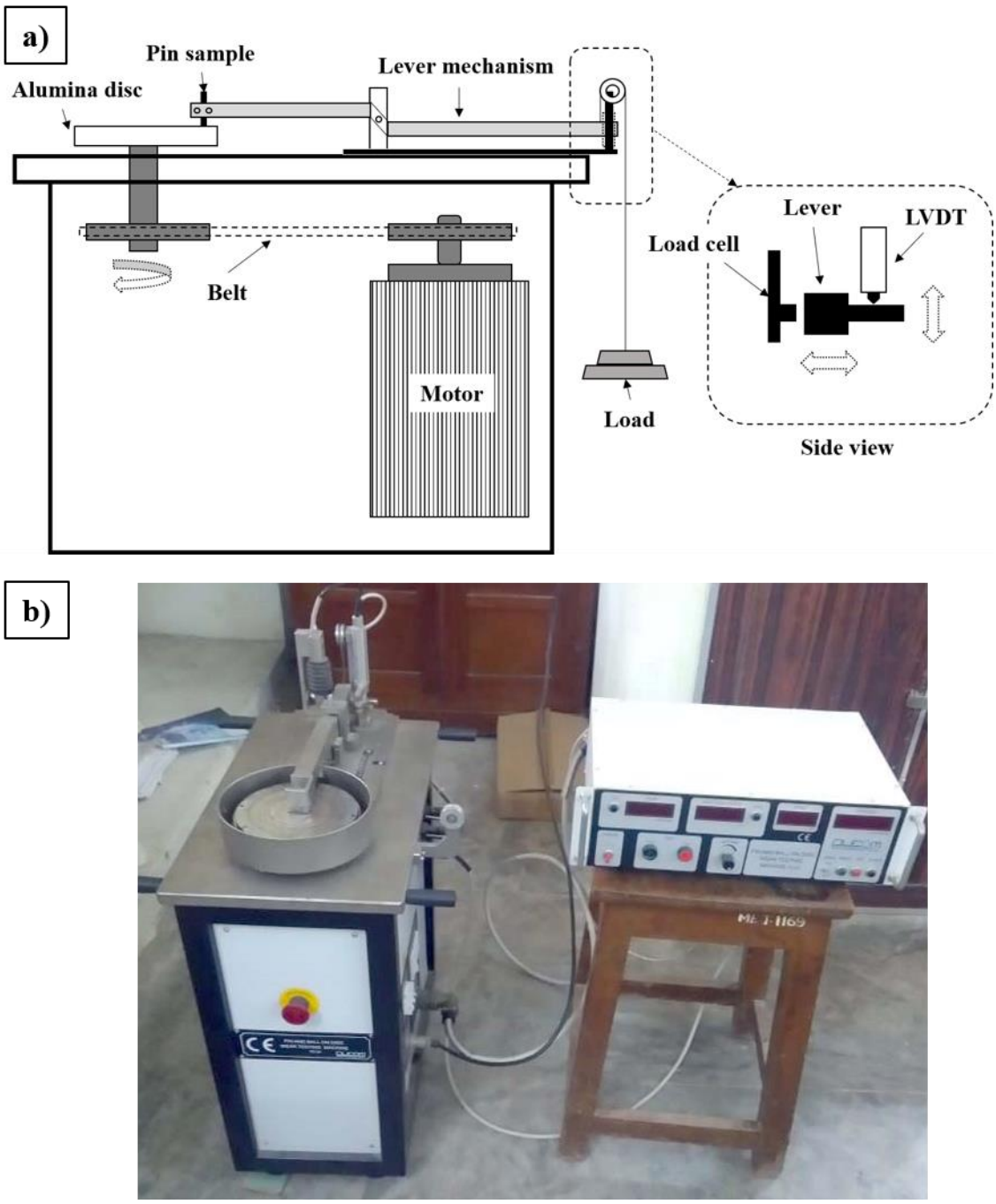

Fig. 3.12:a) *Schematic representation and b) Photograph of pin on disc wear testing machine.*

The tests were carried out for 500 meters sliding distance with different loads (30, 40, 50 N) at a rotational speed of 200 RPM. The generated frictional force and wear depth data were collected using a frictional force sensor (load cell), and Linear Variable Differential Transducer (LVDT) attached to the machine. The weight of the samples was measured before and after testing using a high precision (0.01mg) digital balance (Sartorius, India). The coefficient of friction, volume loss, and specific wear rate of samples was measured using the following equations as per ASTM G 99 standard (ASTM International, 2017b).

- Co-efficient of friction = $\frac{Frictional\ force\ (N)}{Normal\ load\ (N)}$ (Eq. 3.10)
- Volume loss (mm^3) = $\frac{Mass\ loss\ (g)}{Density\ (\frac{g}{cm^3})}$ x 1000 (Eq. 3.11)
- Specific wear rate (mm^3/N-m) = $\frac{Volume\ loss\ (mm^3)}{Applied\ load(N)\ X\ Sliding\ distance(m)}$ (Eq. 3.12)

The wear surfaces of samples were ultrasonically cleaned and observed in Scanning Electron Microscopy (SEM) for surface damage and study of wear mechanism.

3.6.4 Biological characterization:

The samples of optimized compositions were analyzed for *In-vitro* biological characterization such as Hydrothermal aging, Bioactivity, Cytocompatibility.

3.6.4.1 Hydrothermal aging:

For the evaluation of low-temperature degradation properties of developed materials, an accelerated aging study was carried out according to ISO 13356 standard (ISO, 2015) on an optimized sample. Sintered and metallographically polished samples were placed in a low-temperature autoclave chamber containing distilled water (**Fig.3.13**), and the chamber is appropriately sealed. During the test, then the temperature and pressure inside the autoclave chamber were maintained at 134 °C and 0.2 MPa, respectively. The experimental setup used for the hydrothermal aging study is represented in **Fig.3.14**. After every 10 hours of hydrothermal treatment, the samples were taken out and analyzed for phase and microstructural changes.

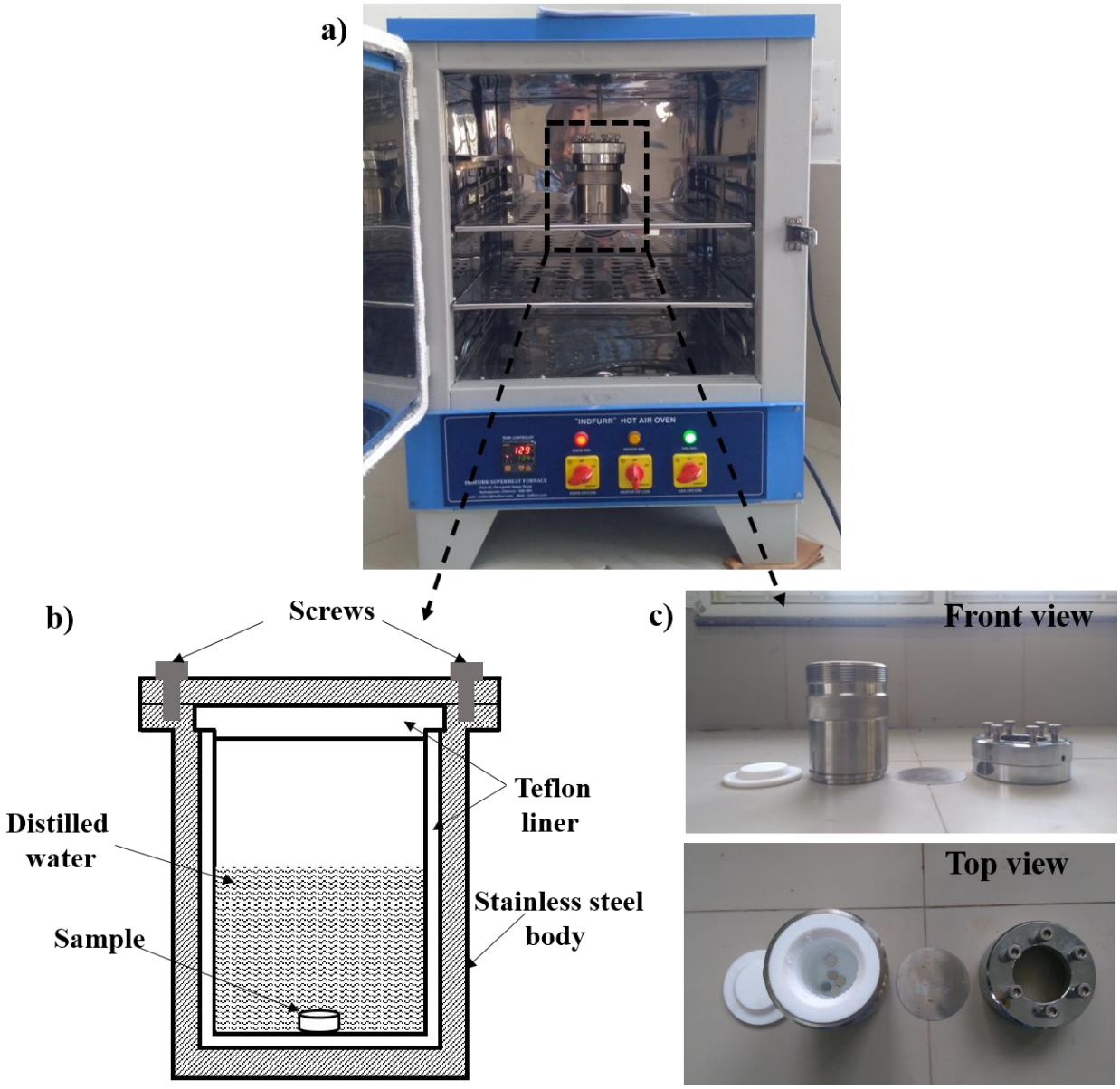

Fig. 3.13.a) Hydrothermal aging setup b) schematic of autoclave c) photograph indicating parts of autoclave used in the study.

3.6.4.2 Bioactivity or Osteo-conduction study:

Osteo-conduction study on sintered samples was carried out to study the bioactivity of samples. The bioactivity of the samples was generally evaluated through the ability of apatite layer formation on the surface of the sample when immersed in a Simulated Body Fluid (SBF).

The SBF solution was prepared by dissolving the reagents mentioned in **Table 3.3** in 1000 ml of distilled water, as described by kokubo et al (Kokubo and Takadama, 2006).

The sintered samples were placed in a polypropylene (plastic) beaker, SBF was added into it and the beakers were kept inside an incubator which maintains a constant temperature of 36.5 °C. After every alternate day, the SBF solution in beakers was replaced with a fresh one.After a period of 7 days, samples were taken out for characterization. After taking out, the samples werecarefully washed with distilled water and dried at room temperature. The dried sample coated with a conductive material and observed under SEM.

Table 3.3.*Reagents required to prepare 1 liter of n-SBF solution* (Kokubo and Takadama, 2006).

Order	**Reagent**	**Amount**
1	NaCl	8.035g
2	$NaHCO_3$	0.355g
3	KCl	0.225g
4	$K_2HPO_4.3H_2O$	0.231g
5	$MgCl_2.6H_2O$	0.311g
6	1M-HCl	39ml
7	$CaCl_2$	0.292g
8	Na_2SO_4	0.072g
9	Tris	6.118g
10	1M-HCl	0-5 ml

3.6.4.3 *In-vitro* bio-compatibility test:

Viability levels or proliferation rates of cells are good indicators of biocompatibility of any material. In this study, the biocompatibility of the developed material is assessed through MTT assay using human osteoblast-like cell (MG63) culture.

3.6.4.3.1 Cell culture study:

The human osteosarcoma cell line (MG-63) obtained from NCCS (Pune, India) was expanded using Dulbecco's Modified Eagles Medium (DMEM, Himedia, India) supplemented with 10% fetal bovine serum and antibiotics. The cells were incubated at standard cell culture conditions (37 °C with 5% CO_2 and 100% relative humidity). The experiments were carried out with the cells when they reached 90% confluence.

3.6.4.3.2 Cellular metabolic activity assay:

The optimized NbCSZ samples were thoroughly cleaned, sterilized and preconditioned with complete medium overnight and placed in a 24 well culture plate for seeding.**Fig. 3.14** represents experimental steps to conduct cellular metabolic activity assay. Initially, cells were counted, and 2 x 10^4 cells were seeded per sample and also into the empty wells as 2D control(**Fig. 3.15 a**). The plates were incubated at standard culture conditions for 2 to 3 h to ensure cell adhesion and incubated for 7 days after adding culture medium and changing the medium every 2 days. At specified intervals, MTT assay was performed by adding 10% MTT solution (Himedia, India) to each plate and incubated for 4 h to allow the formation of purple formazan derivative (**Fig. 3.15 b**). The derivatives were dissolved in dimethyl sulfoxide at room temperature (**Fig. 3.15 c**), and absorbance of the solution was measured using a multi-mode plate reader (Enspire, PerkinElmer, USA).

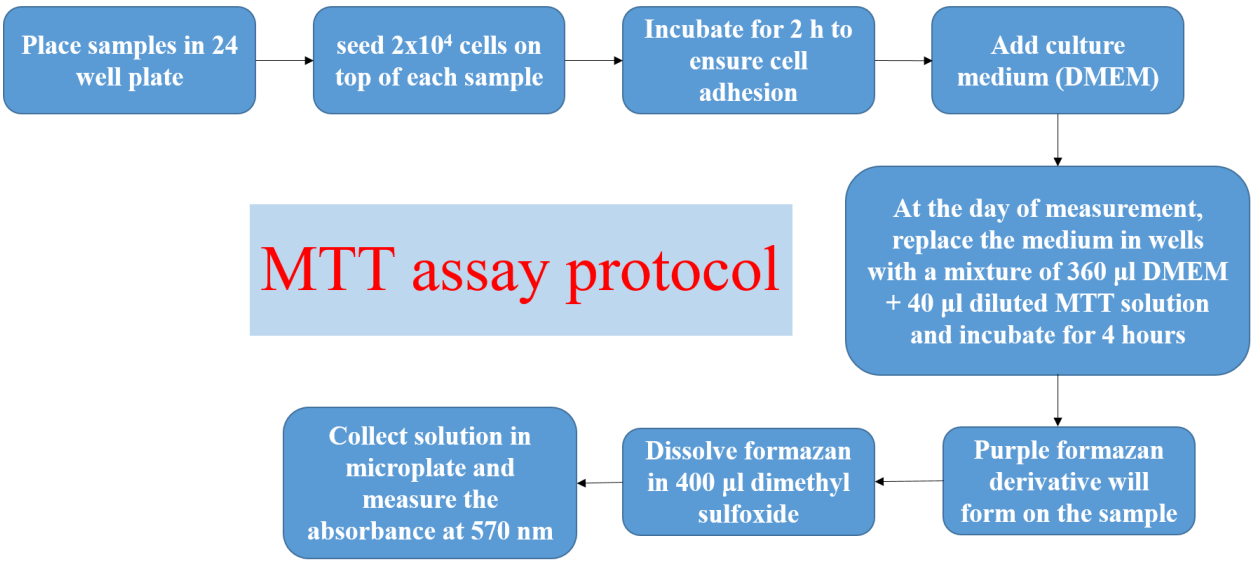

***Fig. 3.14**: Flow chart representing the steps to conduct MTT assay.*

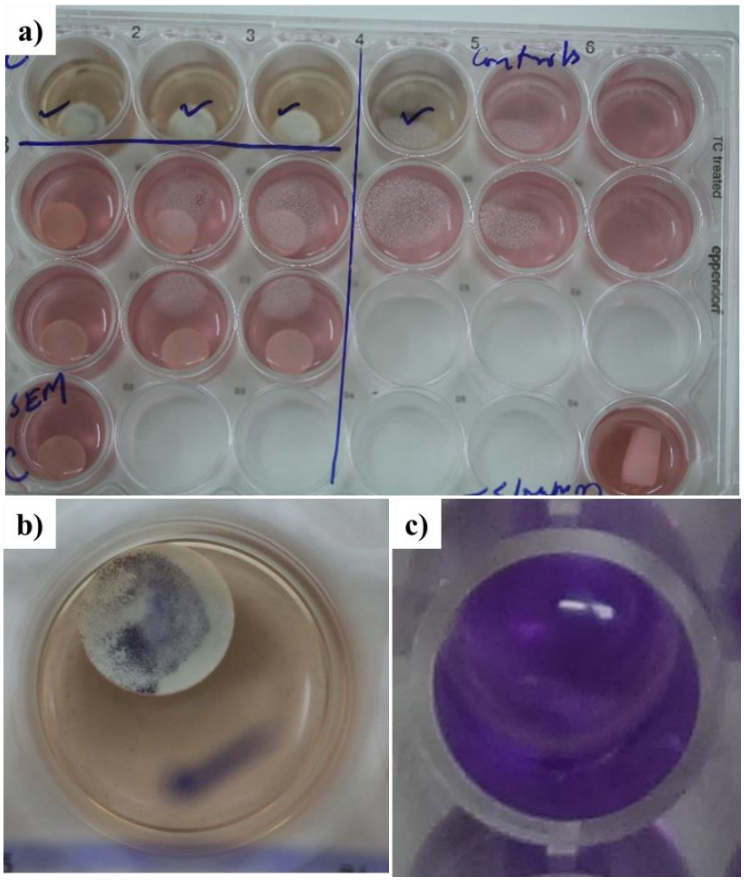

***Fig. 3.15**: Photograph indicating a) 24 well plate with cells attached samples and DMEM medium, b) Sample with purple formazan, c) purple solution obtained after dissolving formazan in dimethyl sulfoxide.*

3.6.4.3.3 Cell morphology study:

The cell morphology on the samples was evaluated by scanning electron microscope imaging. The seeded samples after incubation period were washed with PBS (phosphate buffer saline) and fixed in PBS with 2.5% glutaraldehyde for one hour at room temperature. After fixing, the samples were dehydrated by washing in ascending series of ethyl alcohol solution (50-100%) followed by drying in vacuum. Before observing in SEM, the samples were coated with gold/palladium (80/20) to make the surface conductive.

Chapter-4

Niobium Oxide Doped Ceria Stabilized Zirconia System

This Chapter majorly deals with the synthesis and development of Nb_2O_5 doped ceria stabilized zirconia composite system. Effect of Nb_2O_5 on physical and mechanical properties of ceria stabilized zirconia was also described. The synthesized powders were calcined at different temperatures and then compacted to pellets. The compacted pellets were sintered at different Conventional Single Step (CSS) and Two-Step Sintering (TSS) schedules. Optimization of calcination and sintering schedules were done based on phase, microstructure and mechanical properties of the final product. The details of the characterization techniques used were described in chapter 3.

4.1 Powder characterization:

X-ray diffraction technique was used to analyze the phases present in powders after calcination. XRD patterns of synthesized CSZ powders calcined at different temperatures (600 ℃, 800 ℃, and 1000 ℃) are represented in **Fig. 4.1.**Analysis of the patterns revealed that the peaks in patterns are in match with tetragonal ceria-zirconium oxide (ICSD 98-002-3396) and monoclinic zirconium oxide (ICSD 98-007-1839). As indexed in **Fig. 4.1**the peaks indicating 2θ values of 29.9, 34.2, 34.9, 42.5, 49.7, 50.4, 58.6, 59.6, 62.0, 72.2, 73.9, 80.7, 82.7, 94.2 represents the tetragonal zirconia phase and 24.2, 28.3, 31.4 represents the monoclinic zirconia phase.

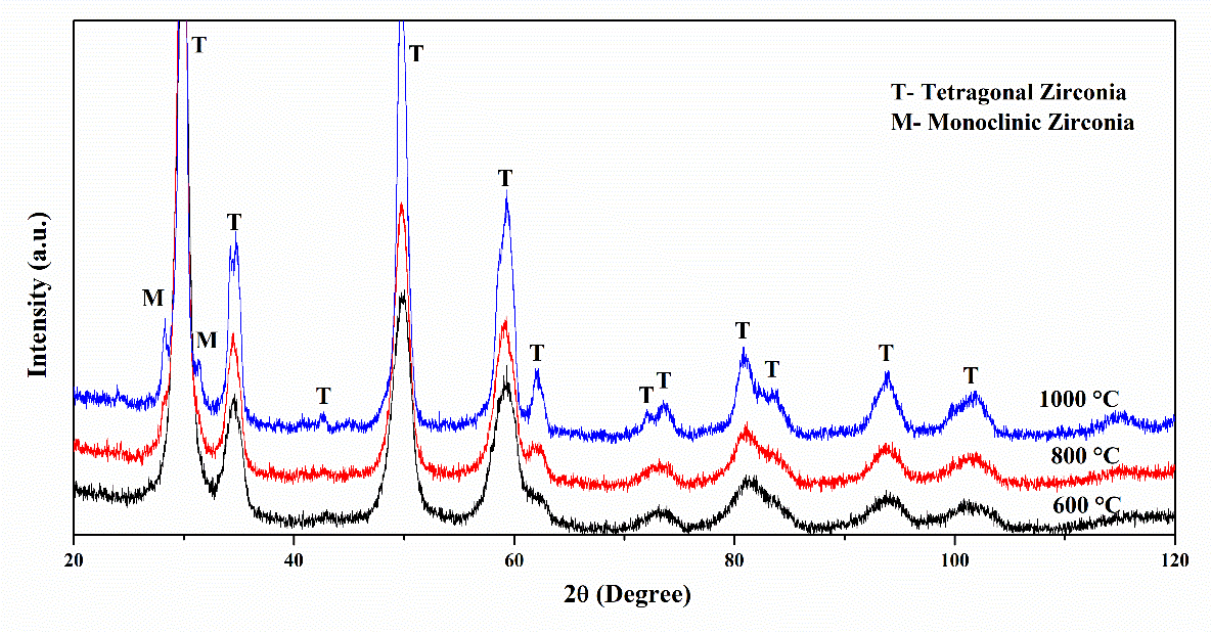

Fig. 4.1: *X-ray diffraction patterns of synthesized CSZ powders calcined at different temperatures.*

To know the phase fractions of Tetragonal and Monoclinic phase, Rietveld analysis for the XRD patterns was performed and found that there are 1%, 4% and 8% monoclinic phase and the remaining amount of tetragonal phase were present in powders calcined at 600 °C, 800 °C and 1000 °C, respectively. The details of Rietveld refinement parameters of the analyzed patterns along with crystallite size are presented in **Table 4.1**. For ideal fit the GOF value should be equal to 1, it can be seen from the table that GOF of all the samples is near to 1, indicating close fit.

Table 4.1: *Crystallite size, relative phase content along with Rietveld refinement parameters of CSZ powders calcined at different temperatures.*

Calcination Temperature (°C)	Crystallite size (nm)	% Phase content		Refinement parameters*			
		Monoclinic	Tetragonal	R_p	R_{exp}	R_{wp}	GOF
600	7	1.2	98.8	6.146	7.6686	7.7713	1.0269
800	13	3.9	96.1	6.3191	7.5268	7.9683	1.1207
1000	26	8.0	92.0	6.2302	7.3993	7.8566	1.1274

* R_p (profile R factor), R_{wp} (weighted profile), R_{exp} (expected profile) and GOF (goodness of fit)

The representative XRD pattern of powder calcined at 1000 °C after Rietveld refinement is shown in **Fig. 4.2**, in which solid line represents the observed profile, dashed line represents calculated profile and plot at the bottom indicates the difference between the observed and calculated profiles. It is known that the lower the difference between observed and calculated profiles (best fit), the higher the accuracy of Rietveld analysis.

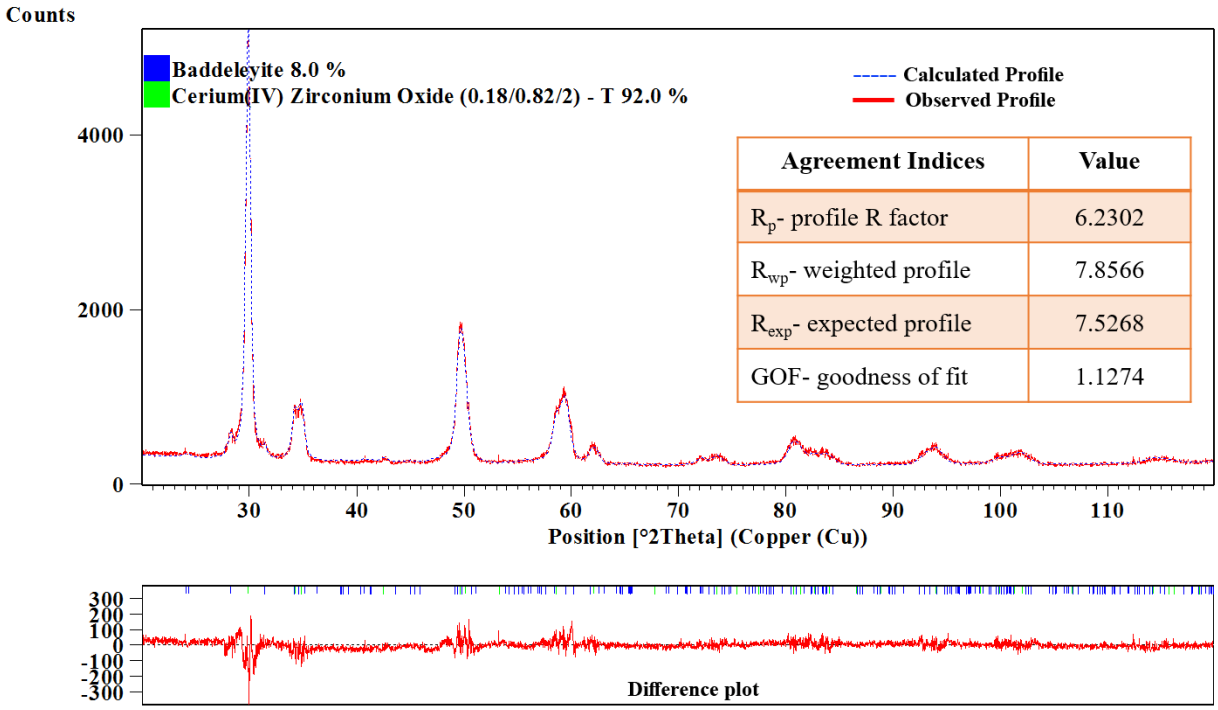

Fig. 4.2: *X-ray diffraction patterns after Rietveld refinement obtained from CSZ calcined at 1000 °C for 2 h.*

It is known that the extent of tetragonal phase stabilization depends on the amount of stabilizer content and size of particles (surface energy). Increase in calcination temperature allows the particles to grow, thereby decreases particle's surface energy which intern reduces the relative amount of tetragonal phase (Bechepeche et al., 1999; Pandey and Biswas, 2011). Average crystallite size at 600 °C, 800 °C, 1000 °C calcination temperature was calculated to be 7, 13 and 26 nm respectively, using Debye-Scherrer equation (Cullity, 1956). Even though some amount of monoclinic phase was present in calcined powder, it got disappeared, and a completely tetragonal phase was observed after sintering at high temperatures (**Fig.4.4**), this is because of the increased solubility of ceria in zirconia at higher temperatures (Ragnhild E . Aune, 1997).

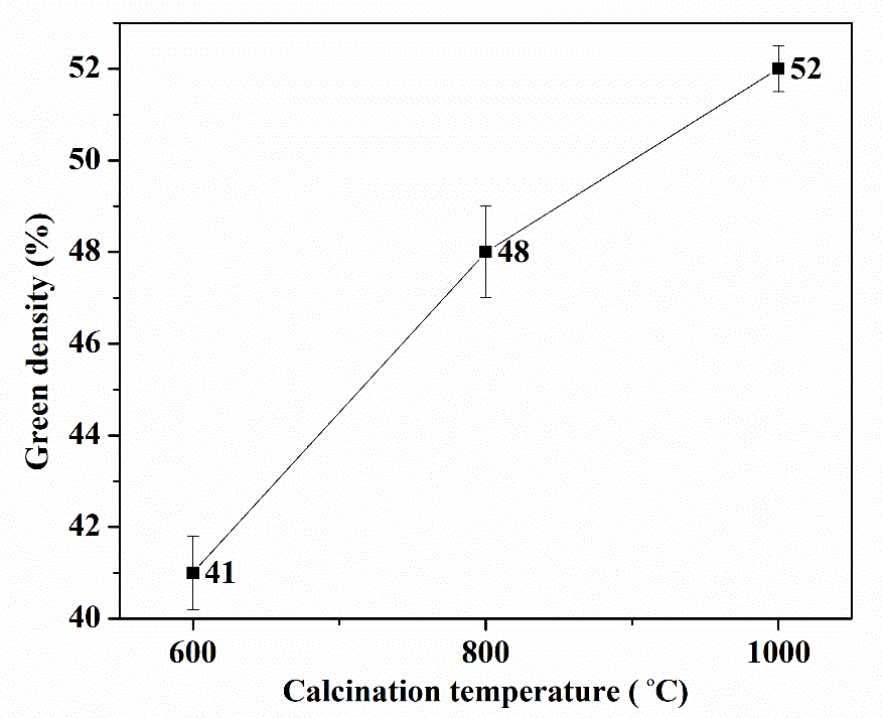

Fig. 4.3: *Green density of pellets made of 600 °C, 800 °C & 1000 °C calcined powders.*

Fig. 4.3shows the green densities of pellets after compaction at 400 MPa. It was observed that green densities of pellets made of 600 °C, 800 °C calcined powders were less compared to 1000 °C. Smaller particles have a higher specific surface area, which experiences more inter-particle friction during compaction and restricts the powder from flowing; resulting in lower green density. Presence of amorphous content in powders calcined below 1000 °C is also a reason for lower green density. So, for a given compaction pressure, smaller the particle size, poorer the green density(Pandey and Biswas, 2014, 2011; Ramabulana et al., 2019). It is known that smaller powder particles exhibit enhanced sintering behaviour, but the extent of sintering or densification also depends on the green density.

4.2 Conventional single step sintering:

Compacted samples of ceria stabilized zirconia powders with varying amounts of niobia (0-2 mol. %) were sintered using various conventional single-step sintering schedules (1300 °C to 1550 °C) represented in **Table. 4.2**. The range of sintering temperatures was chosen based on the literature (Pandey and Biswas, 2011).

Table 4.2: *Different Sintering schedules used in this work.*

Code	Sintering schedule
A	1300 °C for 3 hours
B	1400 °C for 3 hours
C	1450 °C for 3 hours
D	1550 °C for 3 hours

4.2.1 Optimization of Nb_2O_5 content and sintering schedule:

The effect of Nb_2O_5 content on phase formation in the sintered component is represented in **Fig. 4.4**. It is evident that up to 1 mol. % of Nb_2O_5 can be accommodated (solubility limit) by the CSZ matrix at 1450 °C. $CeNbO_4$ phase separates as a new entity as the mol. % of Nb_2O_5 content is increased above 1%, causing depletion of ceria content in zirconia lattice, resulting in destabilization of tetragonal zirconia and allowing monoclinic phase formation. It is observed that the increase in Nb_2O_5 content within the solubility limit results in peak shift (lattice strain) towards the right side, as shown in the inset of **Fig. 4.4**. It can be noted that the ionic radius of Nb^{+5} is smaller than Zr^{+4}, the substitution of Nb^{+5} for Zr^{+4} reduces lattice spacing, as it is known that d spacing is inversely proportional to the diffraction angle, decrease in lattice spacing results in peak shifts towards higher angles.

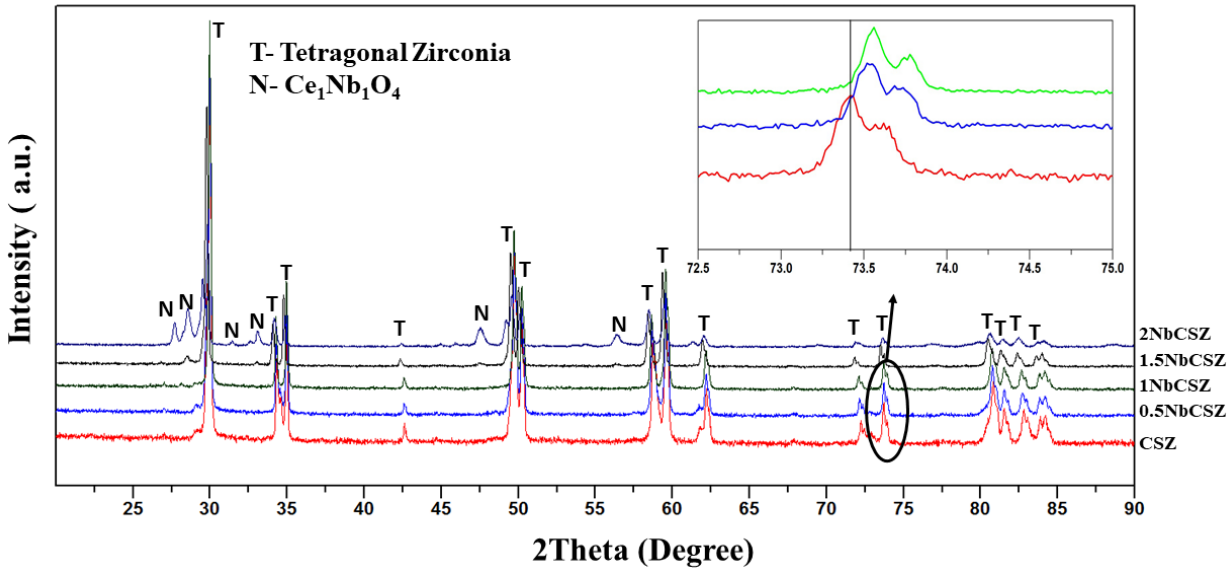

Fig. 4.4: *X-ray diffraction patterns of specimens sintered at 1450 ℃ for 3 h.*

Effect of calcination temperature and sintering schedule on the relative density of the samples are shown in **Fig. 4.5**. Sintered densities of pellets made of 1000 °C calcined powders are higher compared to 600 °C and 800 °C because of optimum particle size and green density combination (**Fig. 4.3**). So, samples made of 600 °C & 800 °C calcined powders were discarded from further analysis. An increasing trend in sintered density was found with the increase in Nb_2O_5 content (0 to 1%) irrespective of the sintering schedule. As discussed earlier ionic radius of Nb^{+5} is smaller than that of Zr^{+4} and O^{-2}, doping of Nb^{+5} ions into CSZ will distort the crystal structure leading to the formation of defects as was observed in case of Fe^{+3} doped YSZ, reported elsewhere (Shon et al., 2009). The defects caused by the Nb^{+5} promote diffusion rate of Zr^{+4} ions (Naga et al., 2015). Nb^{+5}ions might have substituted Zr^{+4}ions which lead to a cation vacancy, as shown in equation 4.1.

$$2Nb_2O_5 \xrightarrow{5ZrO_2} 4Nb'_{Zr} + V''''_{Zr} + 10O_O^X \qquad \text{(Eq. 4.1)}$$

The vacancy diffusion enhances Zr^{+4} ion migration during the sintering process and accelerates diffusion rate, which leads to increased density (Hassan et al., 2015).

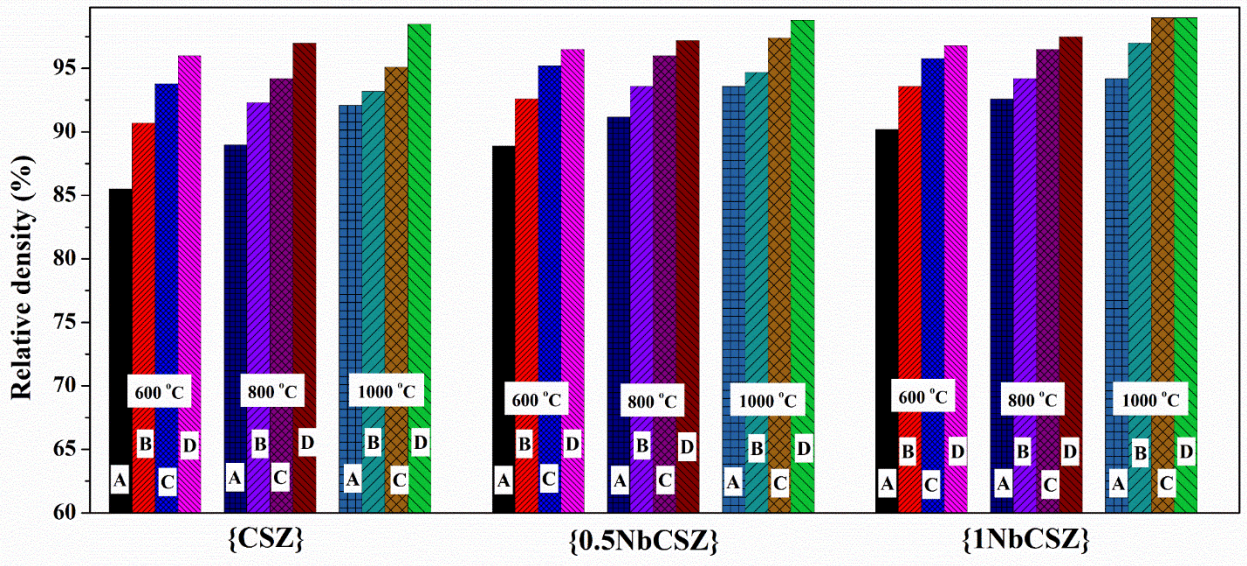

Fig. 4.5:*The relative density of doped and pure CSZ samples at different sintering schedules.*

4.2.2 Microstructural and mechanical characterization:

Vickers hardness of pure CSZ and NbCSZ samples for different sintering schedules are represented in **Fig. 4.6.**An increasing trend of Vickers hardness was found with the increase in Nb_2O_5 content at 1450 °C; it is because of the improved densities of the doped samples, as shown in **Fig. 4.5**. At 1550 °C sintering temperature, an opposite trend was observed, i.e. the hardness values decreased with the doping content, the reason for this might be the effect of grain size, as we know that all the samples were densified to near full density at 1550 °C but the doped samples shown more grain size compared to undoped samples.It is well known that the samples with lower grain size show better hardness. The SEM images shown in **Fig.4.7**represents the microstructure along with their average grain size of full dense samples CSZ (**Fig. 4.7a**) and NbCSZ (**Fig. 4.7b**) sintered at 1550 °C and NbCSZ sintered at 1450 °C (**Fig. 4.7c**). Through the samples shown in **Fig.4.7**are of similar density, the sample NbCSZ sintered at 1450 °C shown a higher hardness of 1047 HV10 which is 17.5 % more compared to the CSZ sintered at 1550 °C. The improvement of hardness value in doped specimens is because of two reasons: firstly; Nb^{5+}ions might have increased the cohesion between the grains (Naga et al., 2015) and secondly; due to improved sinterability (higher densification with finer grain size) of doped CSZ as discussed in the section 4.2.1 (Hassan et al., 2015; Hsu, 2005).

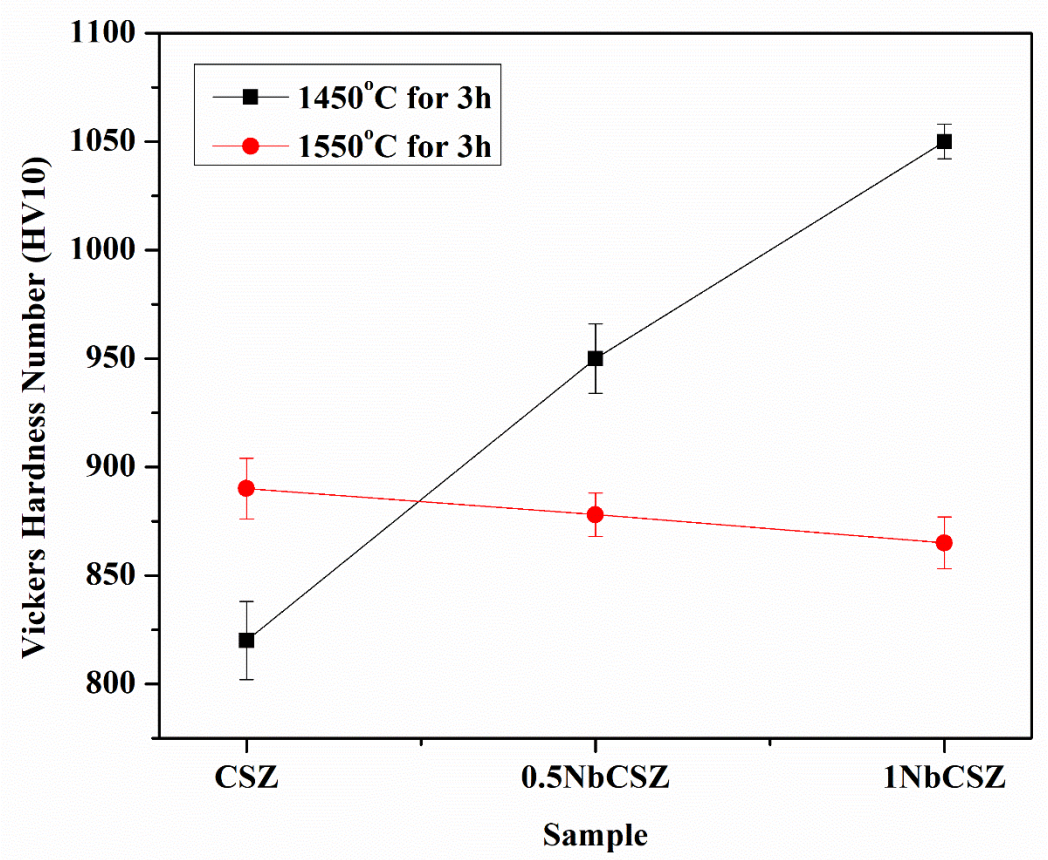

***Fig. 4.6**: Vickers hardness of NbCSZ samples with the variation of Niobium content at different sintering schedules.*

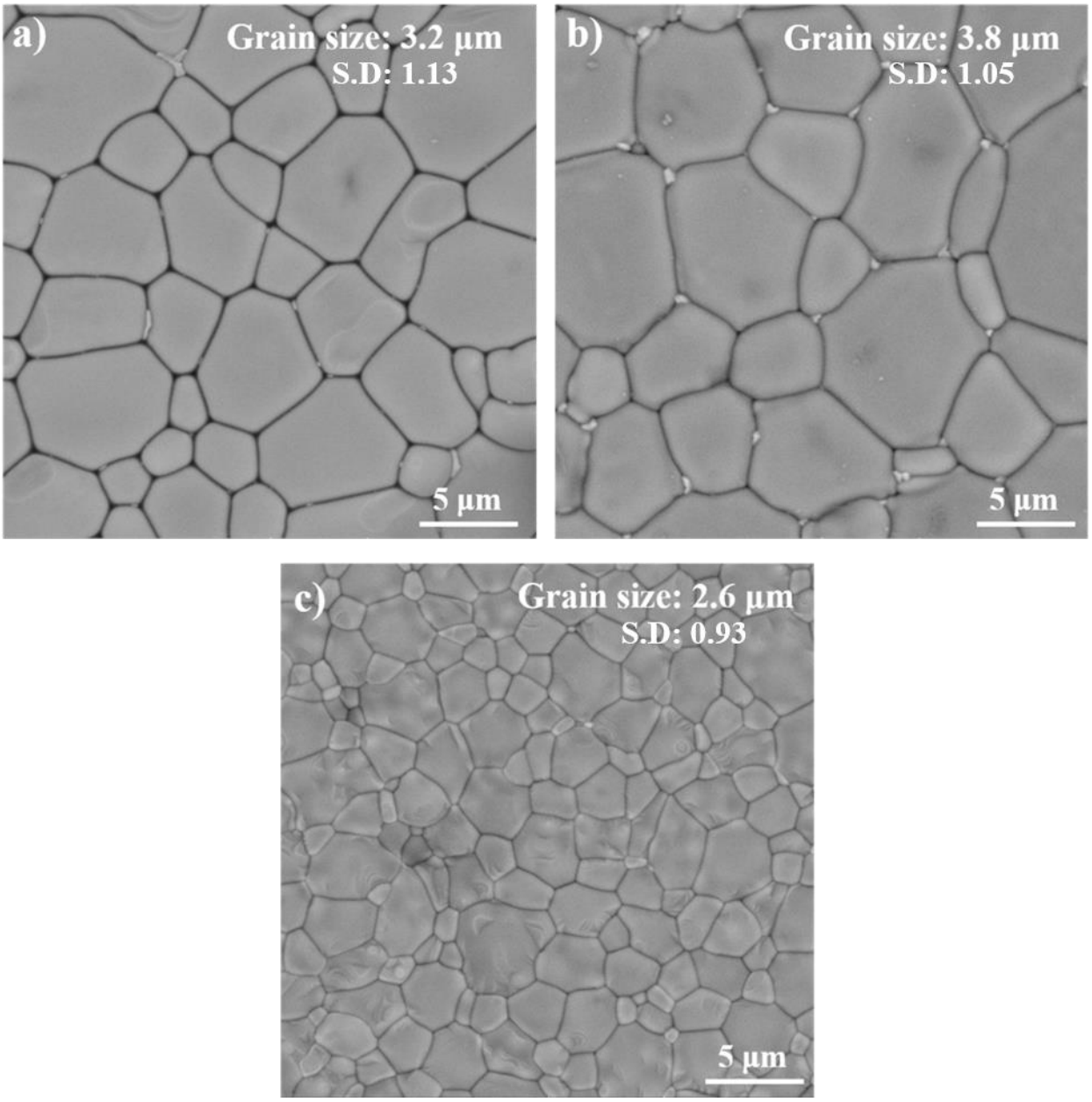

Fig. 4.7: *SEM images of polished and thermally etched specimens a) CSZ b) 1NbCSZ sintered at 1550 °C and c) 1NbCSZ sintered at 1450 °C.*

The effect of Nb_2O_5 addition on indentation fracture toughness is represented in **Fig. 4.8**. It is observed that fracture toughness of doped CSZ samples is higher in comparison to pure CSZ, irrespective of the sintering schedule. A maximum toughness of 6.8 MPa $m^{1/2}$ was observed for the sample NbCSZ sintered at 1550 °C, and it is decreased to 6.2 MPa $m^{1/2}$ for sample sintered at 1450 °C, the decrease in toughness value is attributed to the decrease in grain size. In general, the

improved toughness of zirconia ceramics is majorly due to the mechanism of transformation toughening as discussed in earlier chapters, the transformation toughening depends on the ability of tetragonal phase to transform into the monoclinic phase, and the tetragonal phase stability depends on the grain size. According to the Lange (Lange, 1982), smaller grains shows more tetragonal stability and displays lower propensity to transform to monoclinic under stress, thereby lowers the fracture toughness of the sample.

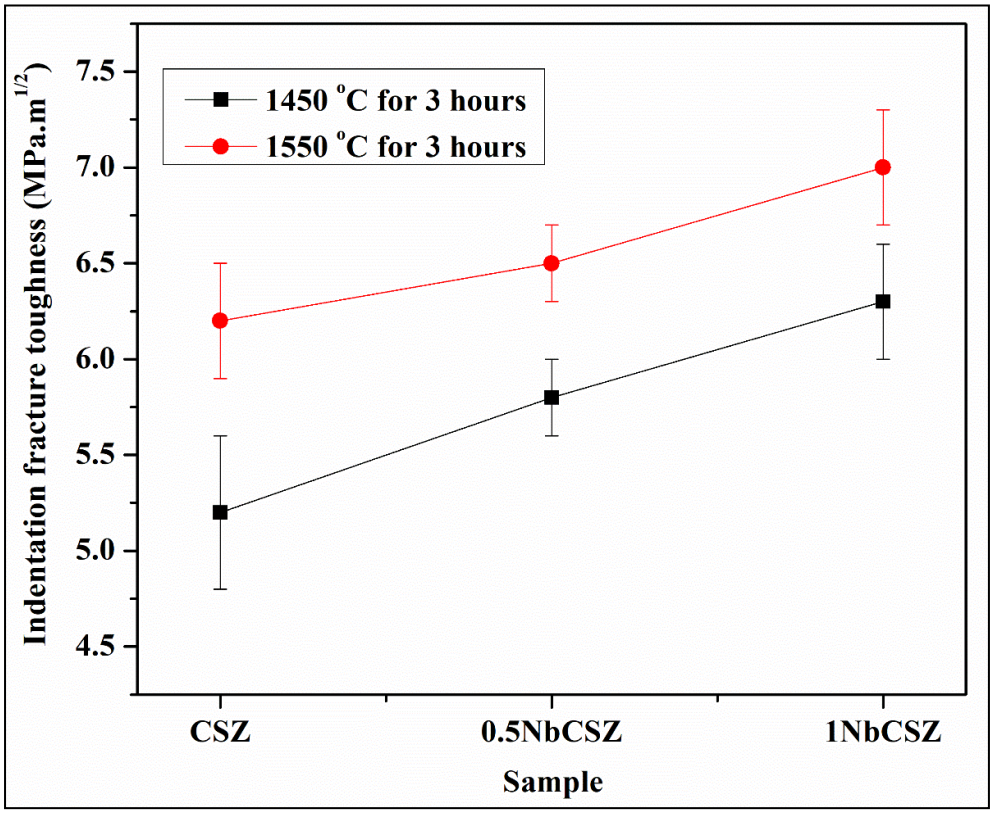

Fig. 4.8: *Indentation fracture toughness of samples sintered at sintering schedule C and D.*

4.3 Effect of two-step sintering on NbCSZ:

It is established that addition of 1 mol. % Nb_2O_5 to CSZ helped in achieving full density with fine grain size compared to pure CSZ by lowering its sintering temperature. It is known that reducing the grain size improves the mechanical properties of ceramics, such as hardness, strength, and wear resistance. Sintering of the ceramics usually carried out through the mechanisms: Grain boundary diffusion and grain boundary migration, former one mainly contributes to the densification of the ceramics and grain boundary migration contribute to the grain growth (Ferreira et al., 2012). Two-step sintering inhibits the grain growth by restricting

grain boundary migration in the final stage of sintering. In this method, samples are first heated to a high-temperature T_1 (first stage temperature) for shorter dwell time, where more than 70% of densification (known as critical density) will be achieved through grain boundary migration and grain boundary diffusion. Then samples cooled to a lower temperature T_2 (second stage temperature) for long dwell time, where Grain boundary migration will be restricted, and rest of the densification will be done through only grain boundary diffusion.

A near full density (>98%) with refined grains can be achieved using two-step sintering process by exploiting proper T_1 and T_2 temperature region, which separates the grain boundary migration and grain boundary diffusion (Ferreira et al., 2012). If sintering condition falls down this region, full density cannot be achieved and above this region grain growth will take place.

4.3.1 Optimization of two-step sintering schedule:

It has been reported in the literature (Chen and Wang, 2000; Lóh et al., 2016; Zhang et al., 2017), that T_1 plays a vital role in achieving critical density, which is required to achieve near full density with finer grains in the two-step sintering process.Initially, to understand the effect of first stage temperature (T_1), different sintering schedules TSS-1 (T_1 = 1600 °C), TSS-2 (T_1 = 1500 °C) and TSS-3 (T_1 = 1450 °C) were chosen by keeping second stage temperature (T_2) fixed at 1300 °C as represented in **Table 4.3.**

Table 4.3: *Different two-step sintering schedules used in this study.*

Schedule ID	Sintering schedule description
TSS-1	1600 °C-1m-1300 °C-15 h
TSS-2	1500 °C-1m-1300 °C-15 h
TSS-3	1450 °C-1m-1300 °C-15 h
TSS-4	1500 °C-1m-1250 °C-15 h
TSS-5	1500 °C-1m-1200 °C-15 h
TSS-6	1500 °C-1m-1100 °C-15 h

Bar charts indicating average grain size and relative density of sintered samples were represented in **Fig.4.9**and **Fig.4.10**, respectively. It can be corroborated from the **Fig.4.9**that, that the

averagegrain size increased with an increase in T_1 temperature as it is already reported non-significant grain growth during single step sintering at 1300 °C (Bejugama and Pandey, 2018).

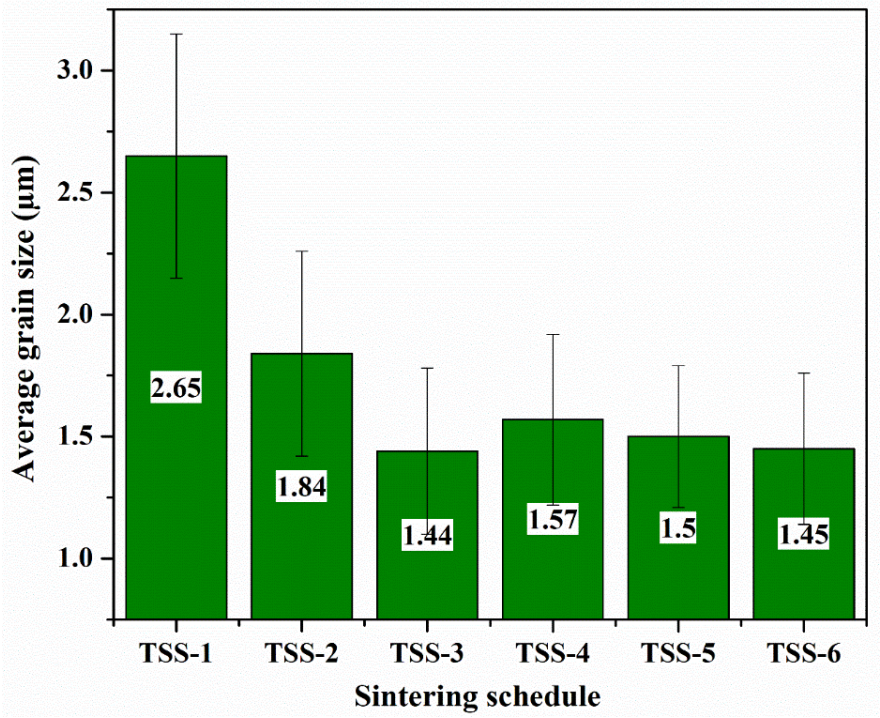

Fig.4.9: *Average grain size of samples sintered at different two-step sintering schedules.*

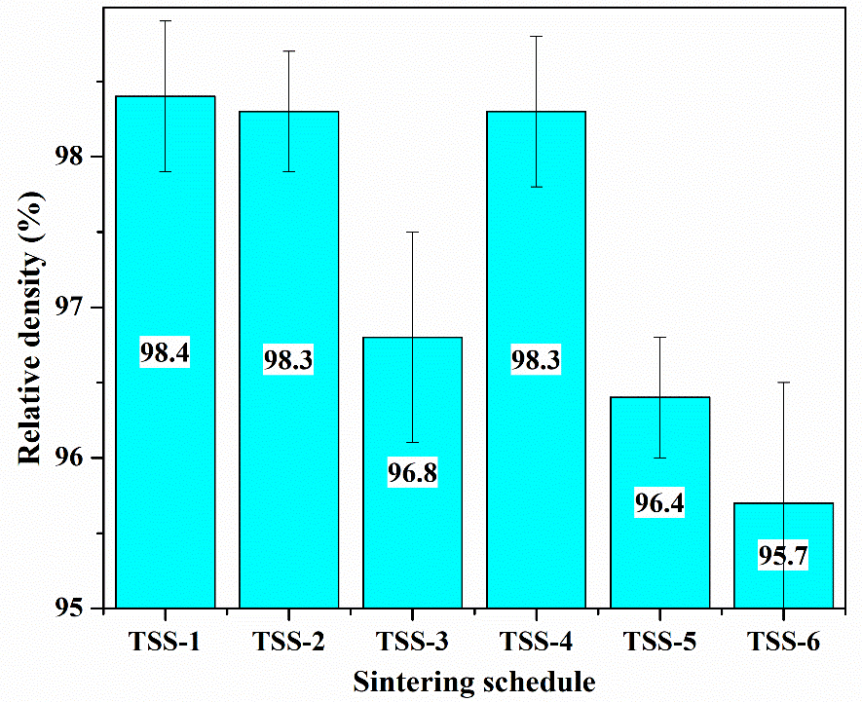

Fig.4.10: *Relative density of samples sintered at different two-step sintering schedules.*

It can be understood that higher temperature provides more activation energy for grain boundary migration, hence increase in temperature always results in grain growth. At schedule TSS-1 (T_1 = 1600 °C), the grain size of the sample observed to be 2.65 µm with a near full density (98.8±0.5), and it is decreased to 1.84 µm at schedule TSS-2 (T_1 = 1500 °C) without affecting its density. Further decrease in T_1 temperature (TSS-3, T_1 = 1450 °C) leads to inadequate density (96.8±0.7).

Now, to understand the effect of T_2 temperature, sintering schedules TSS-4 (T_2 = 1250 °C), TSS-5 (T_2 = 1200 °C), and TSS-6 (T_2 = 1100 °C) were designed by varying T_2 temperature with fixed T_1 temperature at 1500 °C (as near full density with fine grain size was observed at T_1=1500 °C earlier) as represented in **Table 4.3**. It was observed that sample sintered at TSS-4 (T_2 = 1250 °C) shown refined grain size (1.57±0.32) with adequate density (98.3±0.5, similar to TSS-2), however further decrease in T_2 temperature (TSS-5 & TSS-6) resulted in inadequate density.

4.3.2 Phase analysis of sintered samples:

XRD patterns of the sintered samples are represented in **Fig. 4.11**, which shows that all patterns are in complete match with tetragonal zirconia phase (ICSD 98-003-0699) except the pattern of sample sintered at TSS-1, which contains ~ 0.5% of secondary phase $NbCeO_4$ (ICSD 98-008-3094) along with tetragonal zirconia phase.

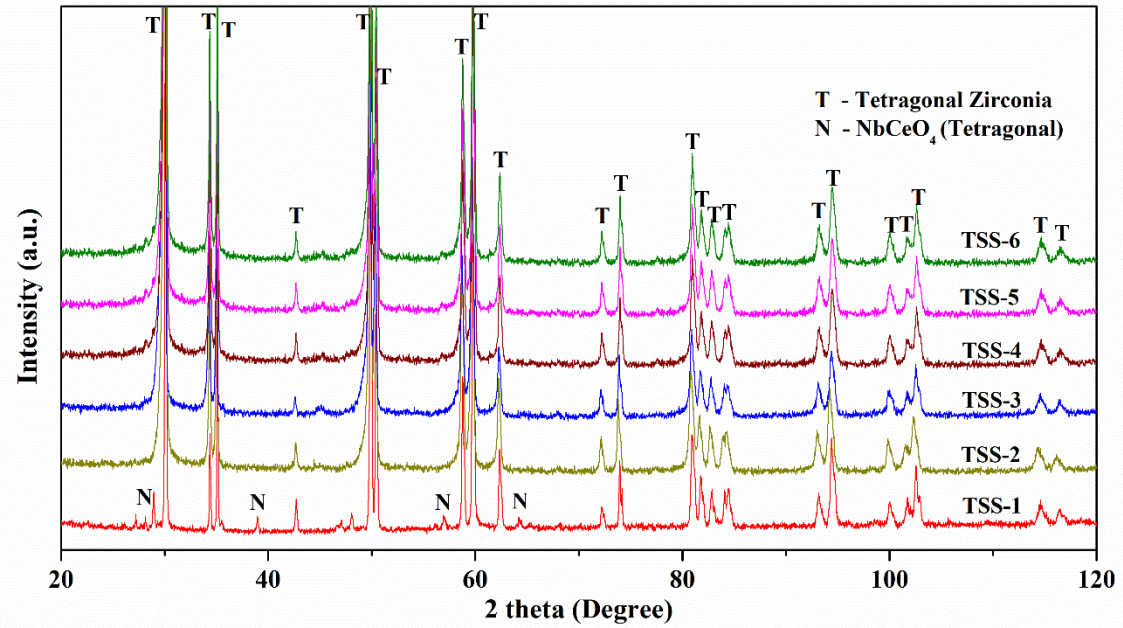

Fig.4.11: *XRD patterns indicating phases present in samples sintered at different two-step sintering schedules.*

4.3.3 Microstructural and mechanical characterization:

Vickers hardness of the sintered samples is shown in **Fig.4.12**, the hardness of 1069 HV10 is observed at TSS-1, which has increased to 1125 HV10 at TSS-2 because of its finer grain size compared to TSS-1 sample. Hardness values have decreased to 935 HV10 at TSS-3 because of its poor density as represented in **Fig. 4.10**. The decrease in T_2 temperature to 1250 °C by maintaining T_1 temperature at 1500 °C in TSS-4 further helped in refining grain size to 1.57 µm resulting in a higher hardness of 1175 HV10. Further decrease in T_2 temperature failed to achieve density leads to lower hardness values. The hardness value obtained in TSS-4 is higher (~ 28-14 %) compared to the previously reported in the literature for similar systems (Bejugama and Pandey, 2018; Pandey and Biswas, 2011).

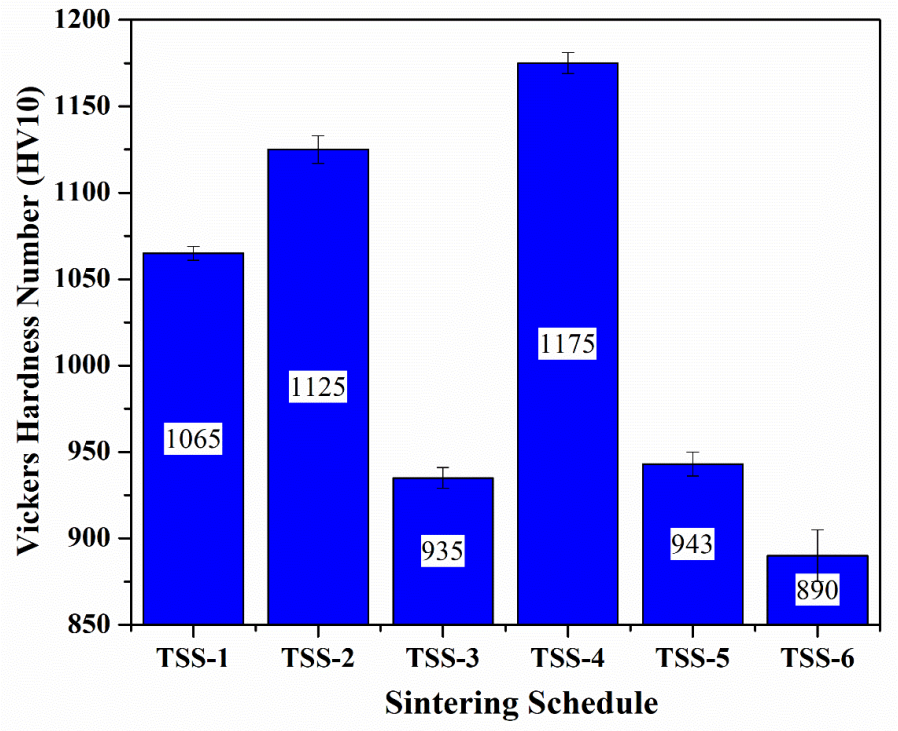

***Fig.4.12**: Effect of different two-step sintering schedules on Vickers hardness of samples.*

Indentation fracture toughness of the near-full density samples was measured and presented in **Fig.4.13**. Fracture toughness of 6.49 MPa√mis observed for sample sintered at TSS-1, and a decreasing trend was found with the increase in hardness values. It is known that fracture toughness of zirconia ceramics depends on the transformability of the tetragonal phase, and

smaller grains have high resistance to transformation, which leads to a decrease in fracture toughness (Bejugama et al., 2019).

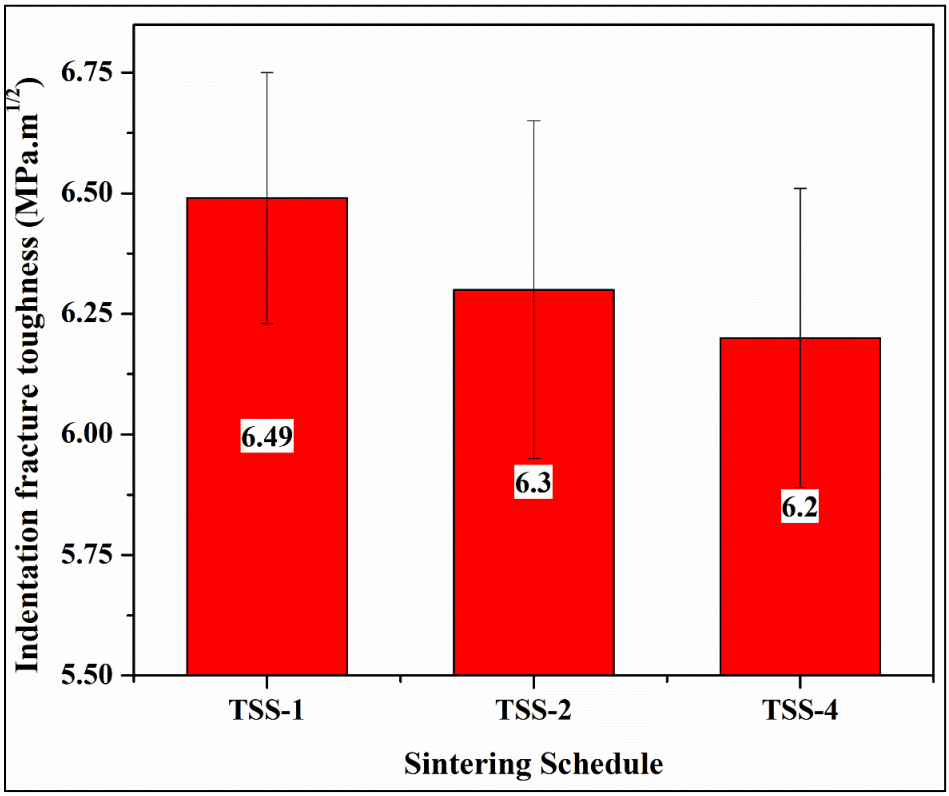

***Fig. 4.13**: Indentation fracture toughness of near full dense samples sintered at different sintering schedule.*

Fig. 4.14shows scanning electron microscope images along with grain distribution of samples sintered at TSS-1 and TSS-4; itis noted that microstructure refinement was prominent in TSS-4 with more homogeneous and smaller grain growth compared with TSS-1. Bright regions in **Fig. 4.14(a)** represents the $NbCeO_4$ phase, which might be formed due to the reaction between Nb_2O_5 and CeO_2 at 1600 °C. The phase formation is also supported by the XRD results, as represented in **Fig. 4.11.**

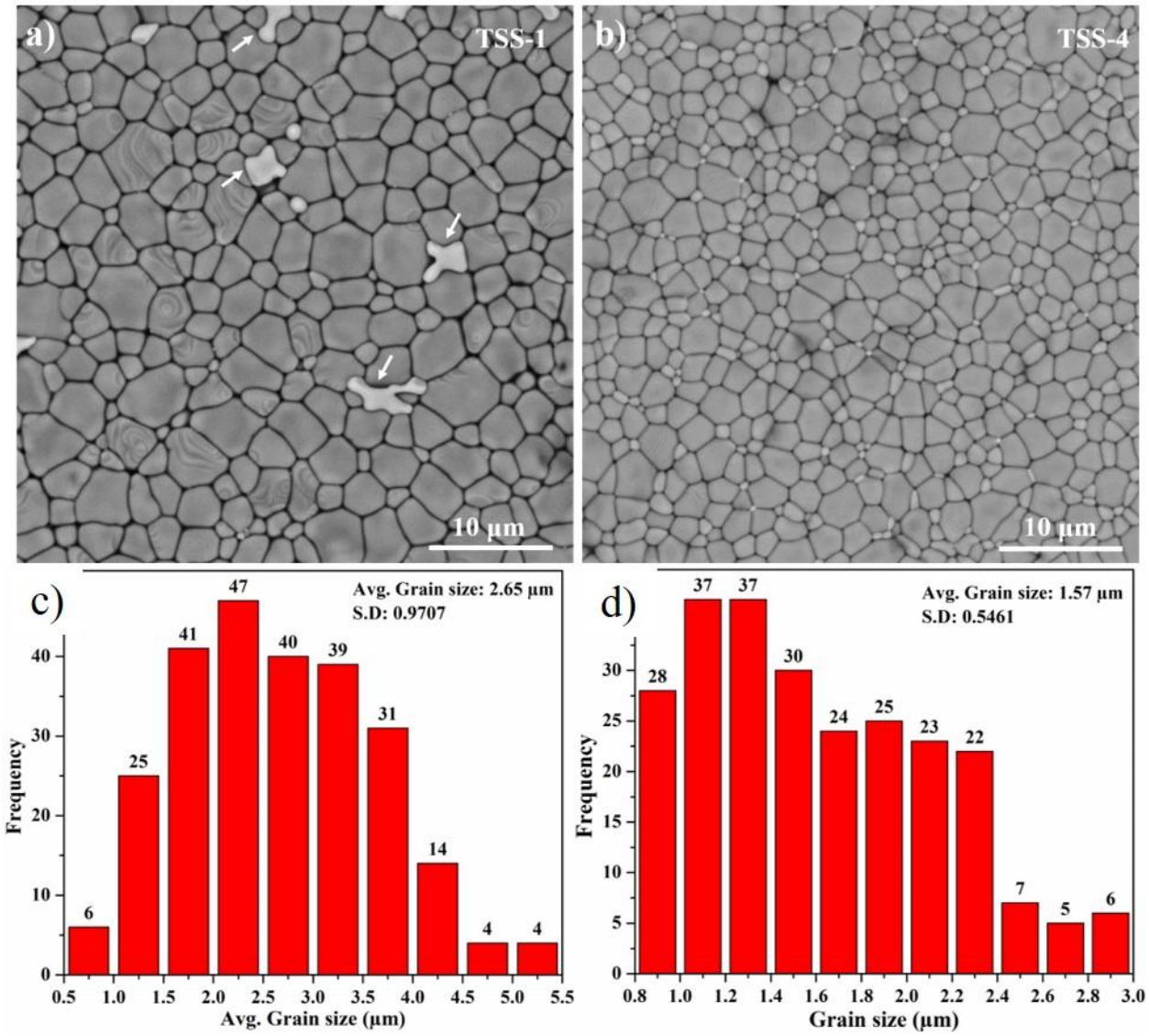

Fig.4.14*: Scanning electron micrographs showing microstructure and grain distribution of samples sintered at (a, c) TSS-1 (b, d) TSS-4 (Arrows indicates $NbCeO_4$ phase).*

4.4 Summary:

- Nb_2O_5 doped ceria stabilized zirconia doped with different amounts of Nb_2O_5 nanopowders were produced successfully using the coprecipitation method.
- Calcination temperature of powders, amount of Nb_2O_5 and sintering schedule of compacts were optimized based on phase, density, microstructure and mechanical properties.
- Addition of Nb_2O_5 improved the sinterability of ceria stabilized zirconia and helped in achieving near full density of samples at temperature 1450 ℃ in single step sintering method.
- Two-step sintering of Nb_2O_5 doped ceria stabilized zirconia effectively reduced the grain size to 1.57 µm from 2.6 µm observed in single step sintering.
- The highest hardness of 1175 HV10 along with an optimum fracture toughness of 6.2 MPa √m was achieved for sample sintered at two-step sintering schedule TSS-4 (1500 °C for 1 minute followed by 1250 ℃ for 15 hours).

Chapter-5

Samarium Oxide Doped Ceria Stabilized Zirconia System

This chapter deals with the synthesis and development of Sm_2O_3 doped ceria stabilized zirconia composite system. Effect of Sm_2O_3 on physical and mechanical properties of ceria stabilized zirconia was described. The synthesized powders were calcined and compacted to pellets. The compacted pellets were sintered at different conventional single step (CSS) and two-step sintering (TSS) schedules. Optimization of composition and sintering schedule was done based on density, microstructure, phases present and mechanical properties of the final product.

5.1 Powder characterization:

As described in the chapter-3, the powders of ceria stabilized zirconia with different amounts of Sm_2O_3 were prepared through coprecipitation method and calcined at 1000 °C for 2h in the air to convert hydroxide powders into crystalline oxide powders. The calcined powders were analyzed for phase using XRD and diffraction patterns were presented in **Fig. 5.1**. It is observed that the patterns are entirely in the match with tetragonal zirconia phase (ICSD 98-002-3396). It indicates that Sm_2O_3 is dissolved in the CSZ and formed a solid solution (ZrO_2-CeO_2-Sm_2O_3).

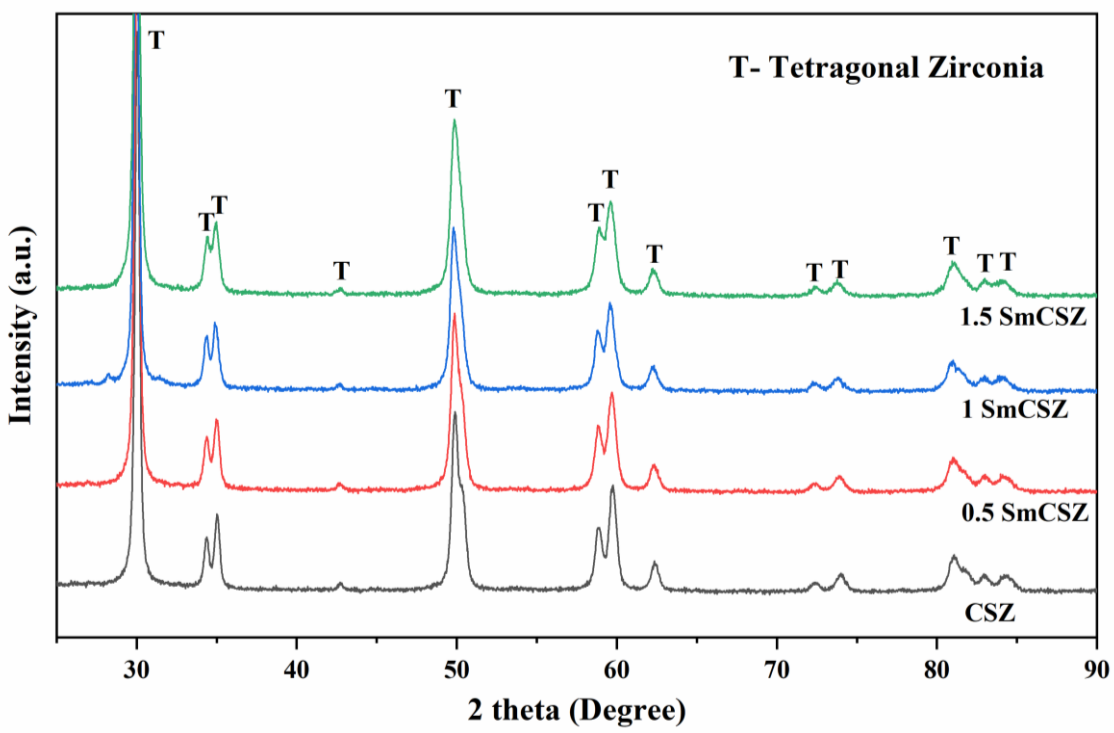

Fig. 5.1*: XRD patterns of calcined powders of samaria doped ceria stabilized zirconia powders.*

5.2 Conventional single step sintering:

Four different sintering schedules (1450 °C to 1600 °C) as represented in**Table 5.1**were chosen to sinter the samples in an air atmosphere. After sintering, samples were characterized for physical, microstructural and mechanical properties.

Table 5.1*: Conventional single step sintering schedules used in this study.*

Schedule ID	Sintering schedule description
CS-1	1450°C for 3 h
CS-2	1500°C for 3 h
CS-3	1550°C for 3 h
CS-4	1600°C for 3 h

5.2.1 Effect of sintering schedule, samaria content on density and grain size:

Relative density and average grain size of the sintered samples were presented in **Fig. 5.2 & Fig. 5.3,**respectively. Increase in sintering temperature has shown enhanced densification and

increased grain size irrespective of sample composition. It is known that high temperature provides more activation energy for both grain boundary diffusion and grain boundary migration, hence increasing the temperature always accompanied by more grain growth. Therefore, the increasing trend of grain size was observed with the increasing temperature irrespective of the dopant concentration. However, it is interesting to note that samaria content helped in improving density. A notable improvement in density for CSZ specimens was observed with the increase in samaria content irrespective of sintering schedules (**Fig. 5.2**). Addition of samaria to the zirconia will distort the crystalline structure of zirconia leading to the formation of defects, as Sm^{+3} ionic radius is greater than Zr^{+4} and Ce^{+4} and also samaria being aliovalent to zirconia has created some oxygen (anion) vacancy (defect), as shown in **equation 5.1**, these defects enhance the solid-state diffusivities during sintering, which might have helped in improving density (Yang et al., 2004).

$$Sm_2O_3 \xrightarrow{ZrO_2} 2Sm'_{Zr} + V_o^{\cdot\cdot} + 3O_o^X \qquad \text{(Eq. 5.1)}$$

It is evident from **Fig. 5.3**that the average grain size of the samples decreases with the increase in samaria content up to 1 mol.% and beyond this grain size increases.

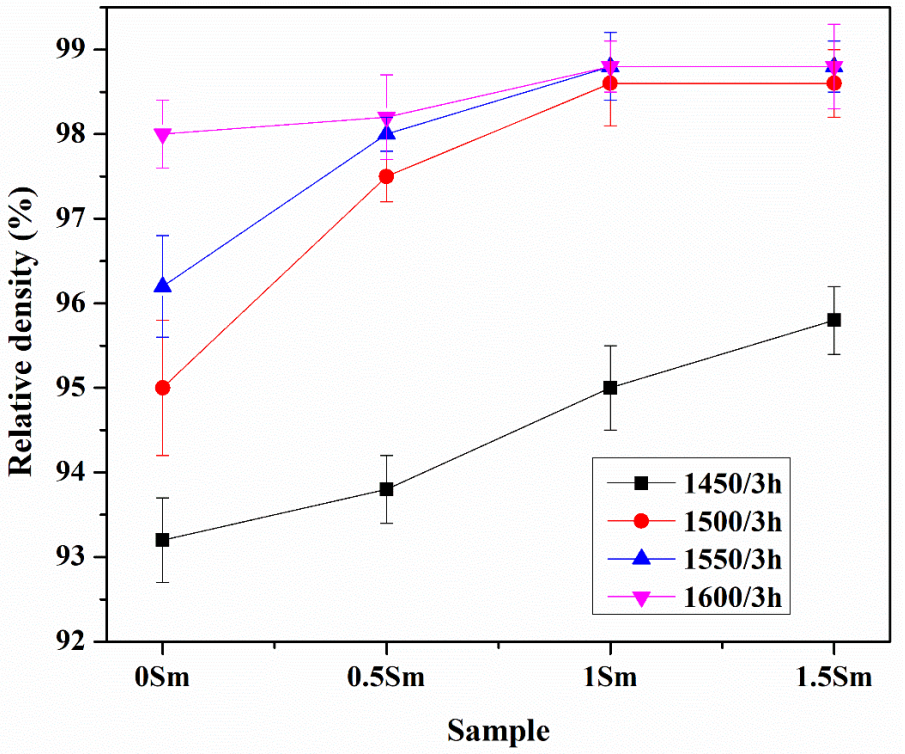

***Fig. 5.2**: The relative density of (0-1.5 mol. %) SmCSZ specimens sintered at different single-step sintering schedules.*

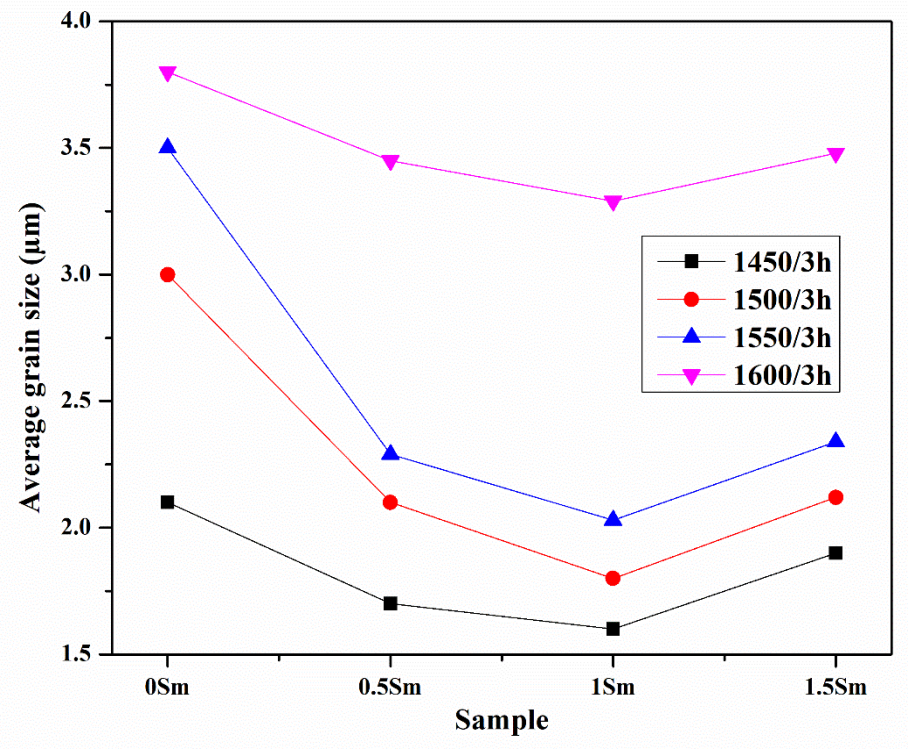

***Fig. 5.3**: Average grain sizes of (0-1.5 mol. %) SmCSZ specimens sintered at different single-step sintering schedules.*

The suppression of grain growth with the addition of samaria is related to the segregation of dopant ions (Sm^{3+}) at the grain boundary during sintering. At high temperature the CSZ-Sm_2O_3 solid solution decomposes, Sm_2O_3 separates from the CSZ. As the grain boundary in tetragonal stabilized zirconia (TZPs) is positively charged, the lower valency cations (i.e. Sm^{3+}) attract towards the grain boundary and forms a negative space charge layer as described in **Fig. 5.4**during sintering (Hwang and Chen, 1990; Lakusta et al., 2018). The drag force caused by these dopant ions present at grain boundaries retards the grain boundary mobility and restricts its growth (Hwang and Chen, 1990).

As the sintering proceeds, a secondary cubic phase was formed at the grain boundaries due to the reaction between zirconia, ceria and samaria (**Fig. 5.5(b,c,d)**), which also helped in restricting the grain growth by pinning the grain boundary (Zhang et al., 2018a). The EDS analysis of bright spots (secondary phase) represented in **Fig. 5.6**revealed the presence of an increased amount of

Sm^{+3} (>6.37 wt. %) and Ce^{+4} (> 20.22 wt.%) compared to tetragonal zirconia grains; it is well known that increase in stabilizer content in zirconia leads to the stabilization of cubic phase.

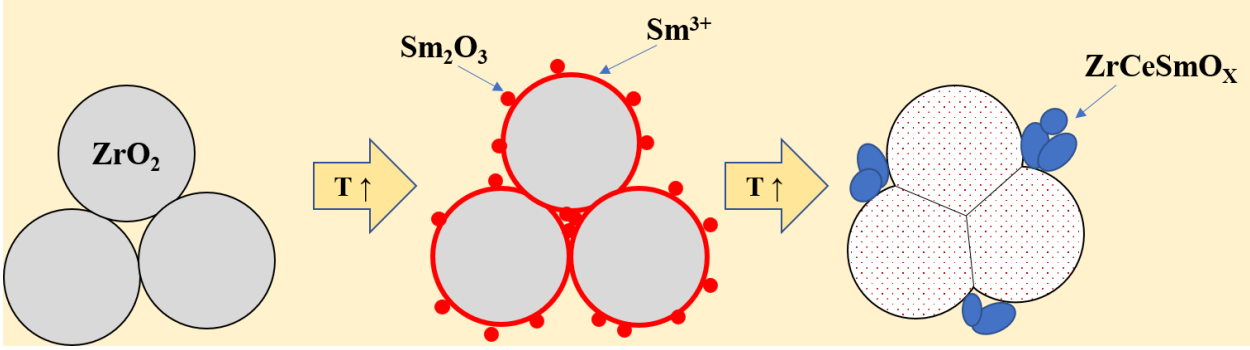

Fig. 5.4:*The scheme of the samarium oxide additive influence on the sintering process of CSZ.*

An increasing amount of samaria beyond 1.5 mol.% lead to the segregation of the secondary phase and get agglomerated to form larger grains. The possibility of grain growth beyond 1.5 mol% samaria addition can further be supported with the fact that grain growth of cubic zirconia is much faster than that of tetragonal zirconia, as reported elsewhere (Allemann et al., 1995).

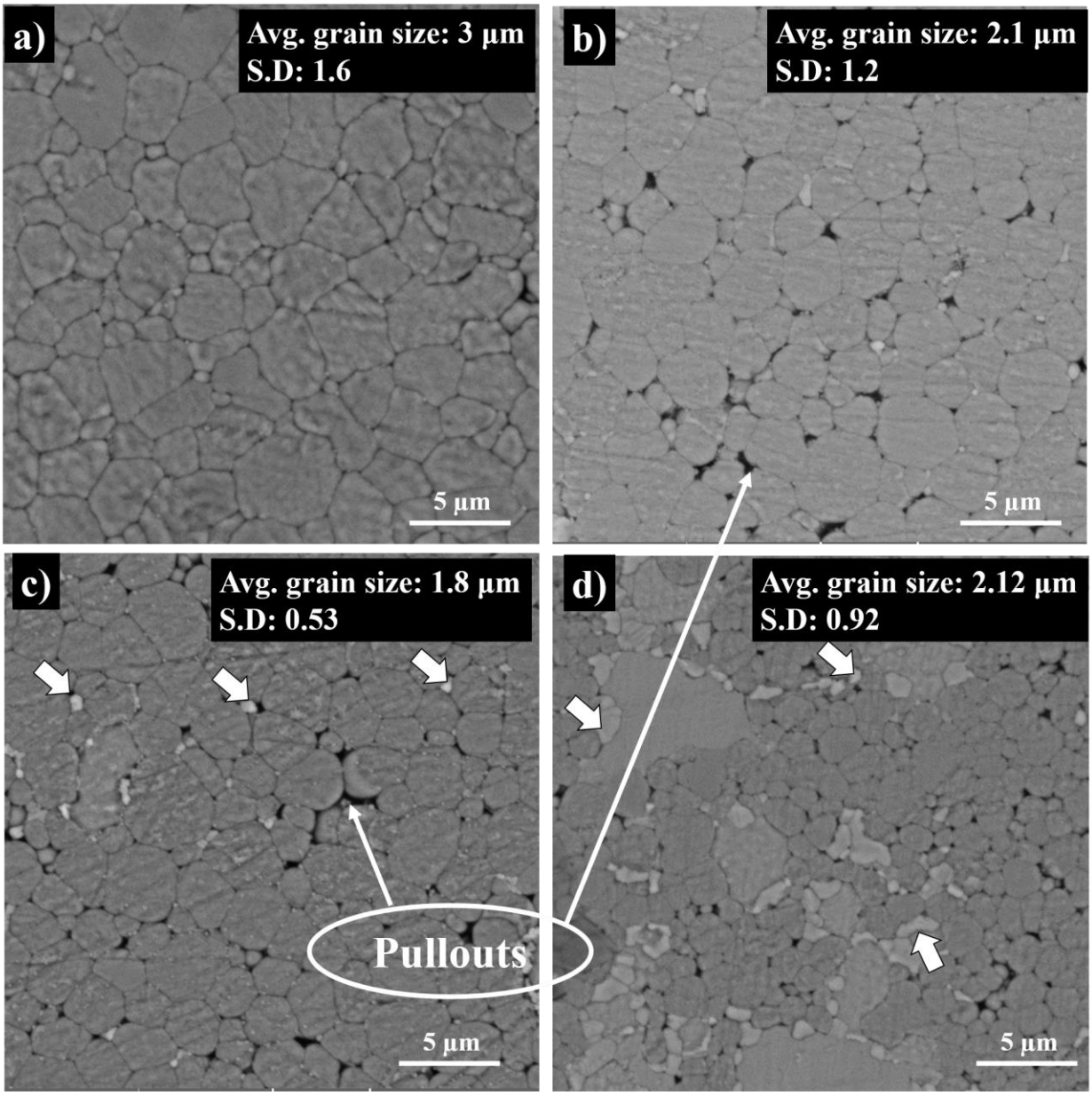

Fig. 5.5*:SEM images of a) CSZ b) 0.5SmCSZ c) 1SmCSZ d) 1.5SmCSZ samples conventionally sintered at 1500 °C for 3 h. Arrowheads are indicating the cubic phase.*

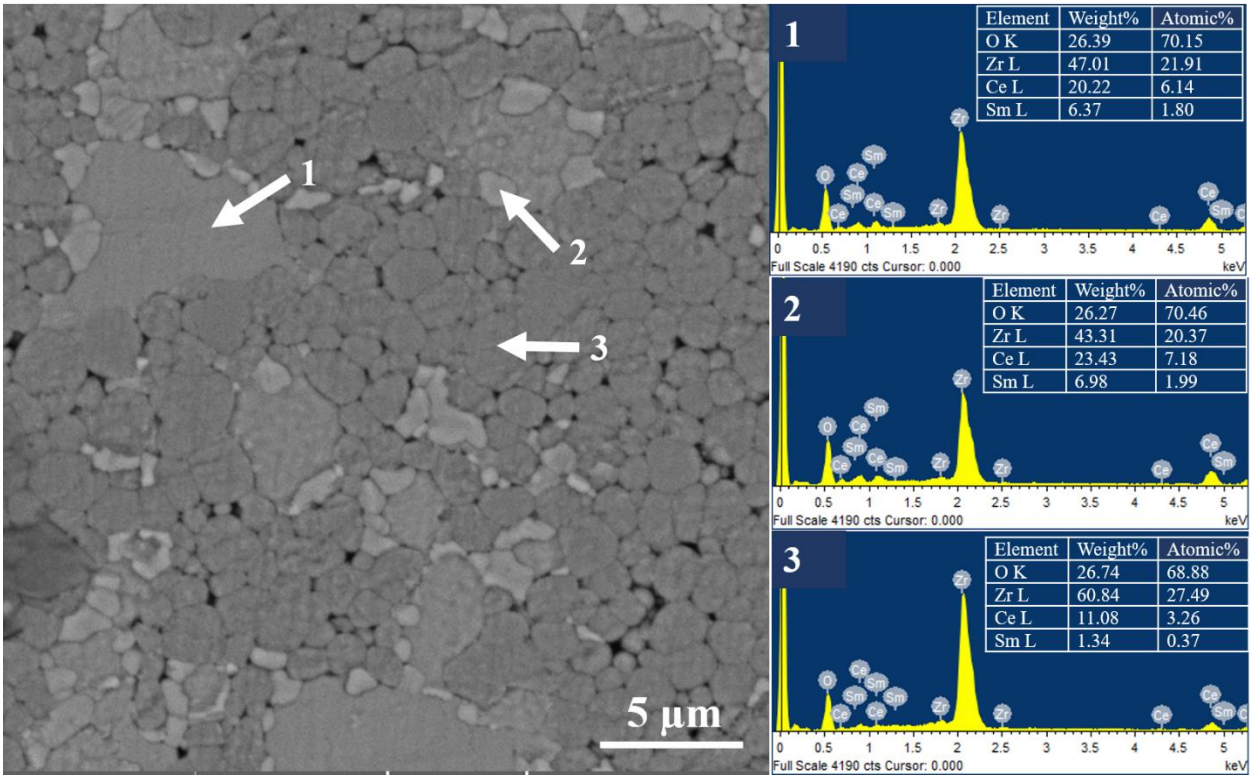

Fig. 5.6*:EDS analysis of different regions of 1.5SmCSZ samples sintered at 1500 °C for 3 h.*

5.2.2 Phase analysis of the sintered sample:

XRD patterns of different specimens sintered at 1500 ℃ for 3 hours are shown in **Fig. 5.7**. The phase analysis revealed that the undoped sample contains only tetragonal zirconia phase and samaria doped samples contain tetragonal zirconia along with cubic zirconia phase. The peaks with 2θ values 30.04, 34.39, 35.01, 42.70, 49.85, 50.31, 58.84, 59.67, 62.31, 72.36, 73.85 were identified as tetragonal zirconia peaks and 29.66, 49.36, 61.82, 80.03 were identified as cubic zirconia peaks.

The phase fractions associated with each pattern were analyzed using the Rietveld method. The details of phases, its quantity, and associated Rietveld refinement parameters were presented in **Table 5.2**for specimen sintered following schedule CSS-2. An increasing trend of cubic phase was observed, from 0% in 0SmCSZ to 27.7% in 1.5SmCSZ. A massive increase in cubic phase content (9.4% to 27.7%) was observed with the increase of samaria from 1 mol% to 1.5 mol%. As samaria is a strong zirconia stabilizer (Gurushantha et al., 2016; Hartmanová et al., 2007; Ouyang et al., 2016) (only 4 mol.% of samaria is sufficient to stabilize tetragonal phase of

zirconia), the addition of samaria to tetragonal CSZ has expectedly stabilized cubic phase of zirconia.

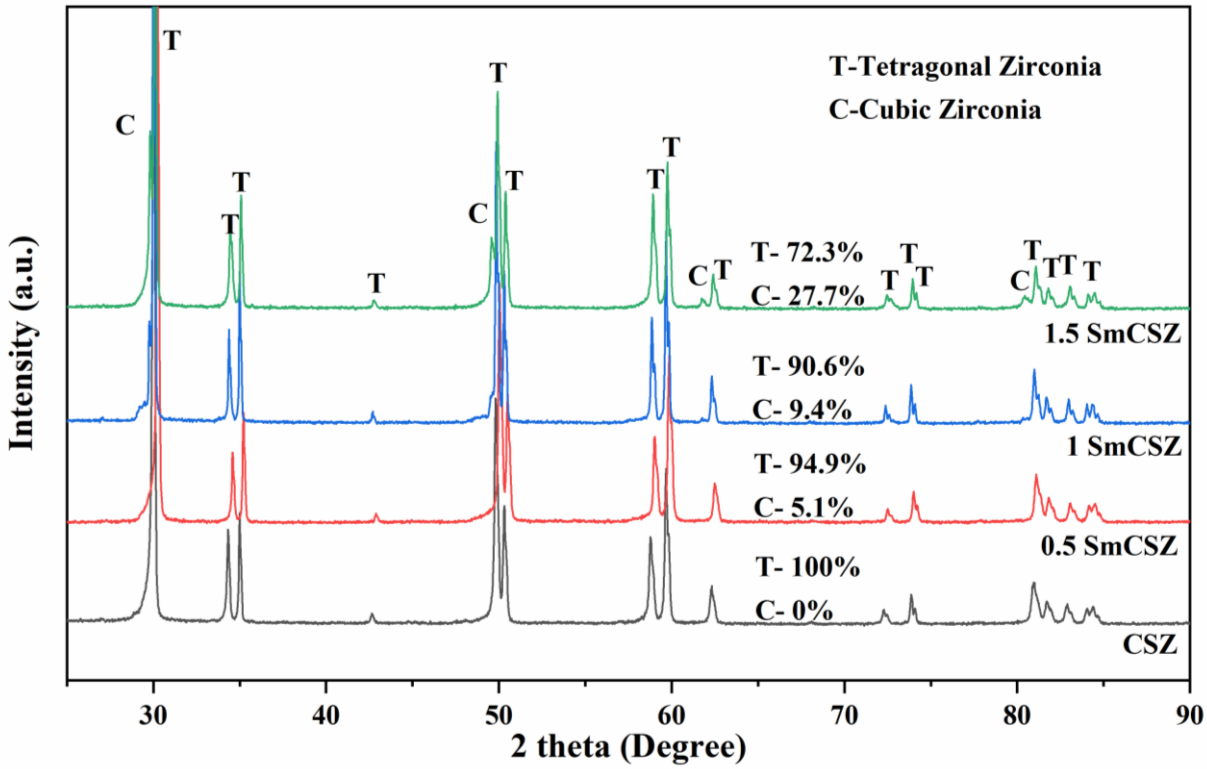

***Fig. 5.7**: XRD patterns representing the phases in samples sintered conventionally at 1500 °C.*

***Table 5.2**. Quantification of phase using Rietveld refinement technique of (0-1.5 mol. %) SmCSZ specimens sintered using CSS-2.*

Sintering Schedule	Sample	Monoclinic	Tetragonal	Cubic	Refinement Parameters			
					R expected	R profile	Wt. R Profile	GOF
CS-2	0SmCSZ	0	100	0				
	0.5SmCSZ	0	94.9	5.1	7.805	7.551	9.510	1.484
	1SmCSZ	0	90.6	9.4	7.813	7.398	9.770	1.563
	1.5SmCSZ	0	72.3	27.7	7.876	8.495	10.632	1.821

5.2.3 Vickers hardness measurement:

Fig. 5.8shows Vickers hardness of the sintered specimens with various composition sintered at different schedules. It is evident that the hardness values increase with the amount of samariaup to 1 mol.% irrespective of the sintering schedule used for near full dense specimens. Maximum hardness up to 1050 HV10 was achieved for sample doped with 1 mol.% samaria sintered using CSS-2 schedule. The schedule offered near full density (98.4±0.5%) with finer grain size (1.8 μm). On the other hand, the highest hardness of 915 HV10 was observed for the undoped sample (0SmCSZ) using a different schedule, i.e., CSS-4.

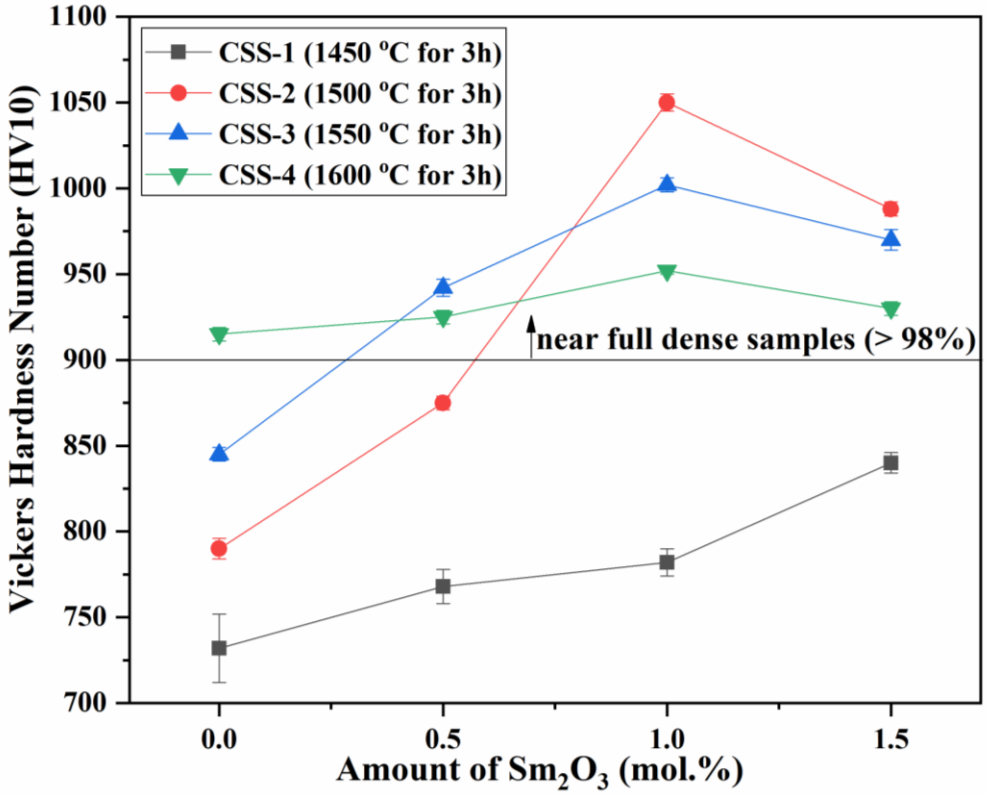

***Fig. 5.8**: Vickers hardness of samples sintered at different conventional single-step sintering schedules.*

5.2.4 Indentation fracture toughness measurement:

Indentation fracture toughness of the sintered samples is represented in **Fig. 5.9**. As expected, toughness decreases with the increase in hardness, irrespective of sintering schedule and composition. Numerous studies have shown that reducing grain size will increase the stability of tetragonal zirconia (Turon-Vinas et al., 2018; Zhang et al., 2018a). As fracture toughness is

associated with the transformability of tetragonal zirconia, it will decline with the decrease in grain size. Lange (Lange, 1982) have given a thermodynamic equation to observe the grain size effect on transformability of tetragonal zirconia. According to Lange as described in the chapter 2, section 2.4 the total free energy per unit volume required for tetragonal to monoclinic phase transformation primarily depends on surface energy, chemical free energy, and strain energy. The surface energy (ΔU_s) can be increased with decreasing grain size and increased surface energy reduces the t-m transformability.

As it is observed, increasing samaria content, decreasing the grain size, which increases ΔU_s thereby decreasing t-m transformation and accordingly resulted in reduced fracture toughness.

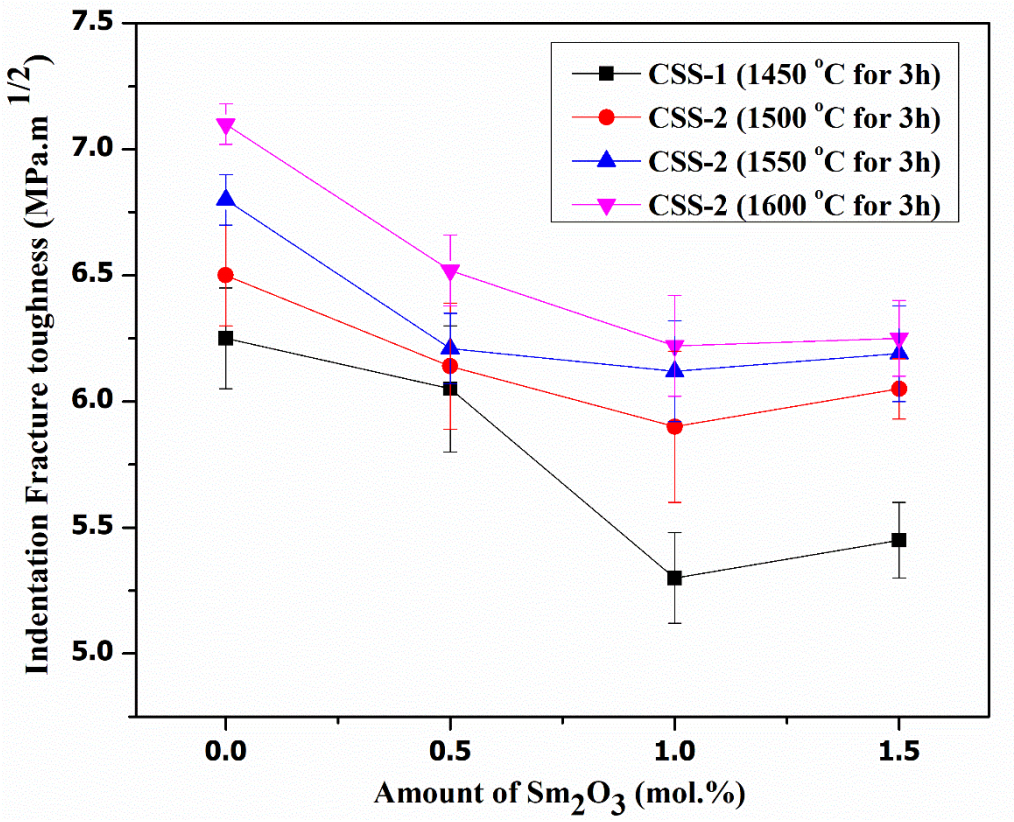

***Fig. 5.9**: Indentation fracture toughness of samples sintered at different conventional single-step sintering schedules.*

5.3 Effect of two-step sintering on SmCSZ:

In order to control the grain size of sintered samples further, two-step sintering method was adopted, and different sintering schedules were designed by varying T_1 and T_2 temperatures. The sintering schedule was optimized based on density, microstructure and mechanical properties of the sintered sample.

5.3.1 Optimization of two-step sintering schedule:

As represented in **Table 5.3**, three different two-step sintering schedules were used to sinter samples. In these sintering schedules, T_1 temperate was fixed at 1500 ℃, as densification of the samples is prominent without much grain growth at this temperature in conventional single-step sintering, and it is expected that grain migration will be active at this temperature. T_2 was varied from 1400 ℃ to 1300 ℃ to know where the grain diffusion is more active to get the samples to densify by restricting grain migration. Initially, samples were sintered at 1500 ℃ for 1 h and 1400 ℃ for 2 h (TSS-1), but at this schedule, neither effective grain size reduction nor densification of the samples was observed. It is because of allowing more dwell time at T_1 and short dwell time at T_2. Then T_1 dwell time was reduced to 1 minute and T_2 temperature to 1300 ℃ for 12 h (TSS-2), at this schedule grain size reduction is more prominent (i.e., T_1 is sufficient). However, samples were not fully densified (T_2 is insufficient). Again, T_2 temperature increased to 1350 ℃ without changing other parameters (TSS-3) to improve the densification. At this schedule, samples 1SmCSZ and 1.5SmCSZ achieved near full density with finer grain size.

Table 5.3*. Relative densities and grain sizes of (0-1.5 mol. %) SmCSZ sintered following different two-step sintering schedules.*

Schedule ID	Sintering Schedule	Relative Density (%)				Average Grain size (μm)			
		0 Sm	0.5 Sm	1 Sm	1.5 Sm	0 Sm	0.5 Sm	1 Sm	1.5 Sm
TSS-1	1500℃-1 h-1400 ℃ -2 h	94.4±0.8	95.3±0.6	97.2±0.5	97.8±0.2	2.25	1.33	1.07	1.12
TSS-2	1500℃ -1 min-1300℃ -12 h	94.1±0.4	94.8±0.6	96.8±0.5	97.6±0.4	1.2	0.82	0.61	0.72
TSS-3	1500℃ -1min-1350℃ -12 h	94.8±0.5	96.9±0.3	98.2±0.6	98.9±0.4	1.23	0.84	0.64	0.76

Relative density, along with the average grain size of the samples sintered using two-step sintering schedules was also represented in **Table 5.3**. A similartrend, as observed in conventional single-step sintering, was observed in densification and grain size reduction of the samples with an increase in samaria content. The finer grain size of 0.65 µm with a near full density (98.2±0.6 %) was achieved for 1SmCSZ at schedule TSS-3, which is the smallest grain size ever reported in the literature for CSZ system (Vleugels et al., 2004; Zhang et al., 2018b, 2017).

5.3.2 Phase analysis of the sintered samples:

Fig. 5.10showsthe XRD patterns of the samples sintered using TSS-3, phases were indexed and quantified using Rietveld refinement method and presented in **Table 5.4**along with refinement parameters. The amount of cubic phase is decreased to 1, 6.2, and 13 % compared with 5.1, 9.4, and 27.7 % observed in a conventional single step for the samples 0.5SmCSZ, 1SmCSZ, and 1.5SmCSZ respectively. This decrease in cubic phase content helped in restricting the agglomeration of secondary phase precipitates to form larger grains, thereby allowing more homogeneous distribution of precipitates along the grain boundaries.

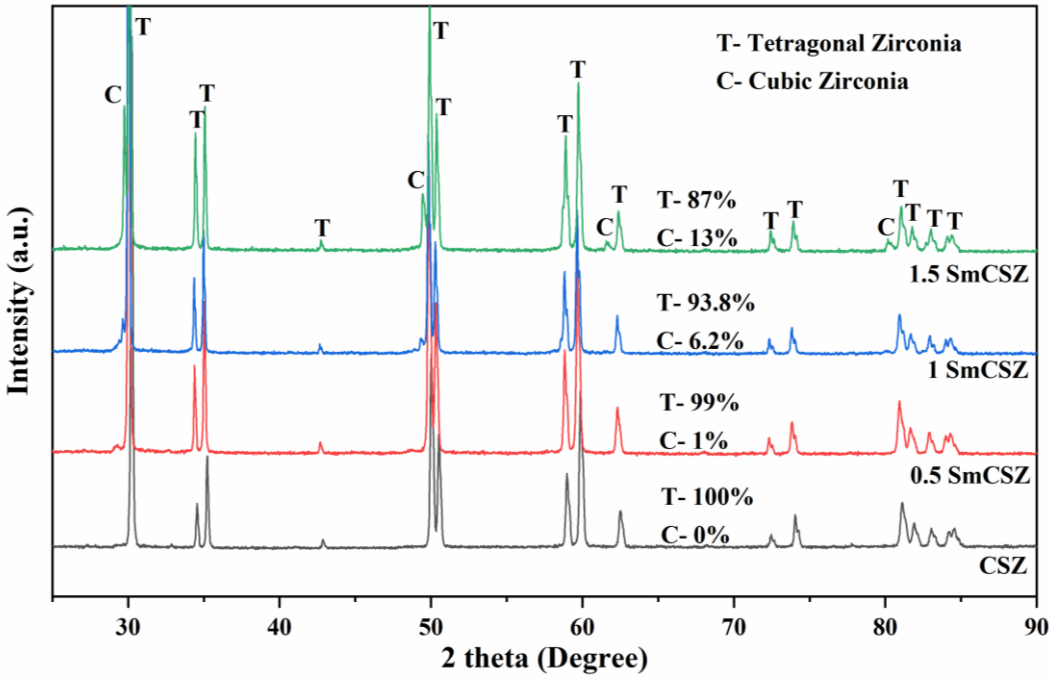

***Fig. 5.10**: XRD patterns representing the phases in samples sintered at TSS-3.*

***Table 5.4**. Quantification of phase using Rietveld refinement technique of (0-1.5 mol. %) SmCSZ specimens sintered using TSS-3.*

Sintering Schedule	Sample	Monoclinic	Tetragonal	Cubic	Refinement parameters			
					R expected	R profile	Wt. R Profile	GOF
TSS-3	0sm	0	100	0				
	0.5sm	0	99	1	8.5451	7.3269	9.1671	1.1508
	1sm	0	93.8	6.2	9.5060	7.6868	9.5925	1.0182
	1.5sm	0	87	13	8.2601	7.2970	9.1028	1.2144

5.3.3 Microstructural analysis:

The scanning electron micrographs of the polished samples sintered using TSS-3 schedule were represented in **Fig.5.11**. As expected, a significant microstructural refinement was observed in the samples sintered using two-step sintering. The microstructure of samples shows the finer grains with more homogeneous distribution as compared to conventional sintering schedules. The average grain size of 1.23 µm, 0.84 µm, 0.64 µm and 0.76 µm observed for the samples 0SmCSZ, 0.5SmCSZ, 1SmCSZ, and 1.5SmCSZ respectively, which is approximately 50 % less than the average grain size found at CSS-2.

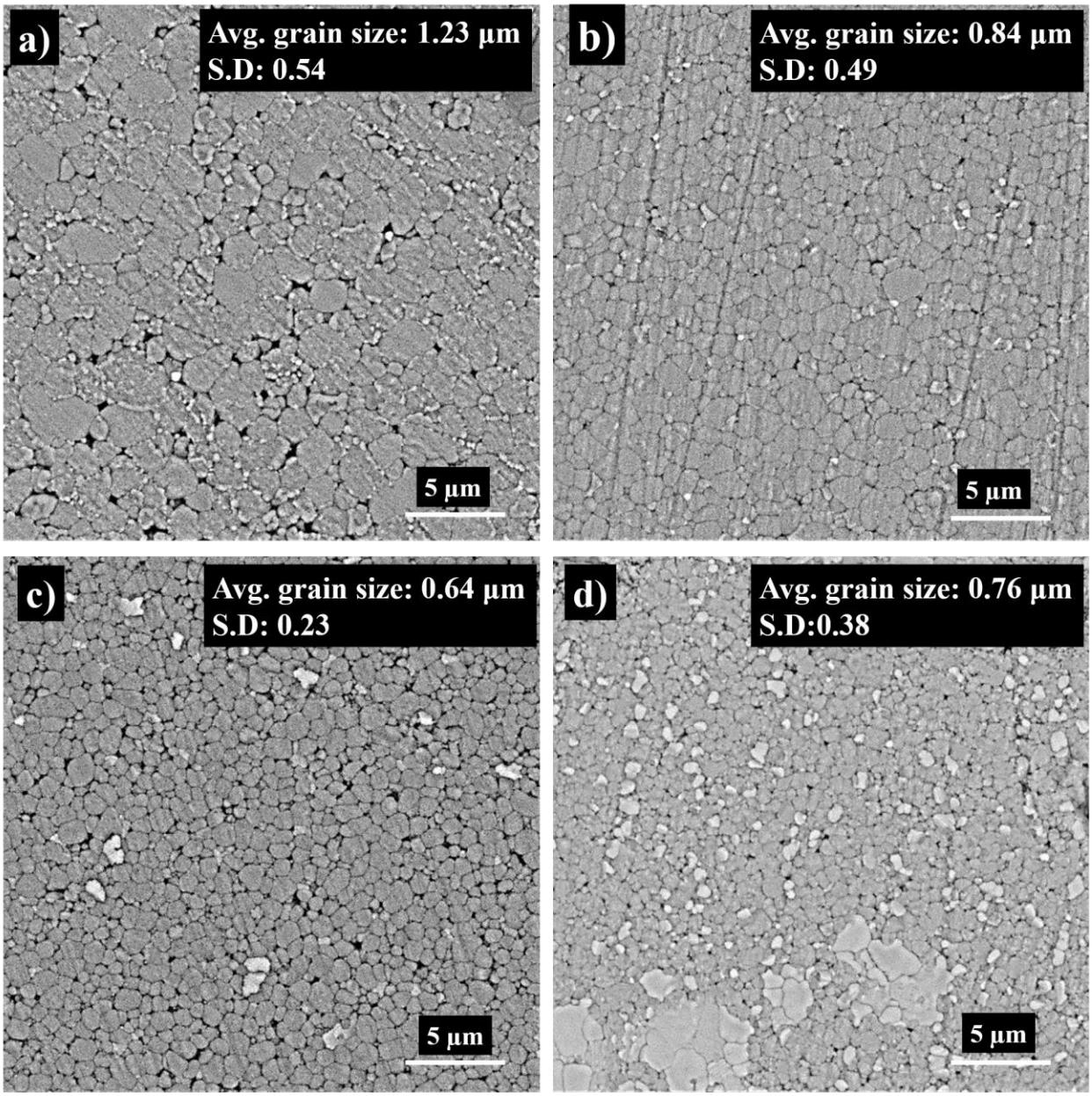

Fig. 5.11*: SEM images of a) CSZ b) 0.5SmCSZ c) 1SmCSZ d) 1.5SmCSZ samples sintered using TSS-3.*

5.3.4 Vickers hardness and indentation fracture toughness measurement:

Fig. 5.12shows Vickers hardness of the two-step sintered samples. A remarkable improvement of hardness value to 1288 HV10 was achieved for 1SmCSZ using TSS-3. The obtained hardness value is 22.6 % higher than the sample sintered using a conventional sintering process and also higher than reported values the on CSZ elsewhere (Bejugama and Pandey, 2018; Pandey and Biswas, 2011; Zhang et al., 2018a). The improvement can mainly be attributed to the effective

reduction in average grain size in two-step sintering schedule along with the solute drag mechanism by offered by Sm_2O_3 addition [21,25].

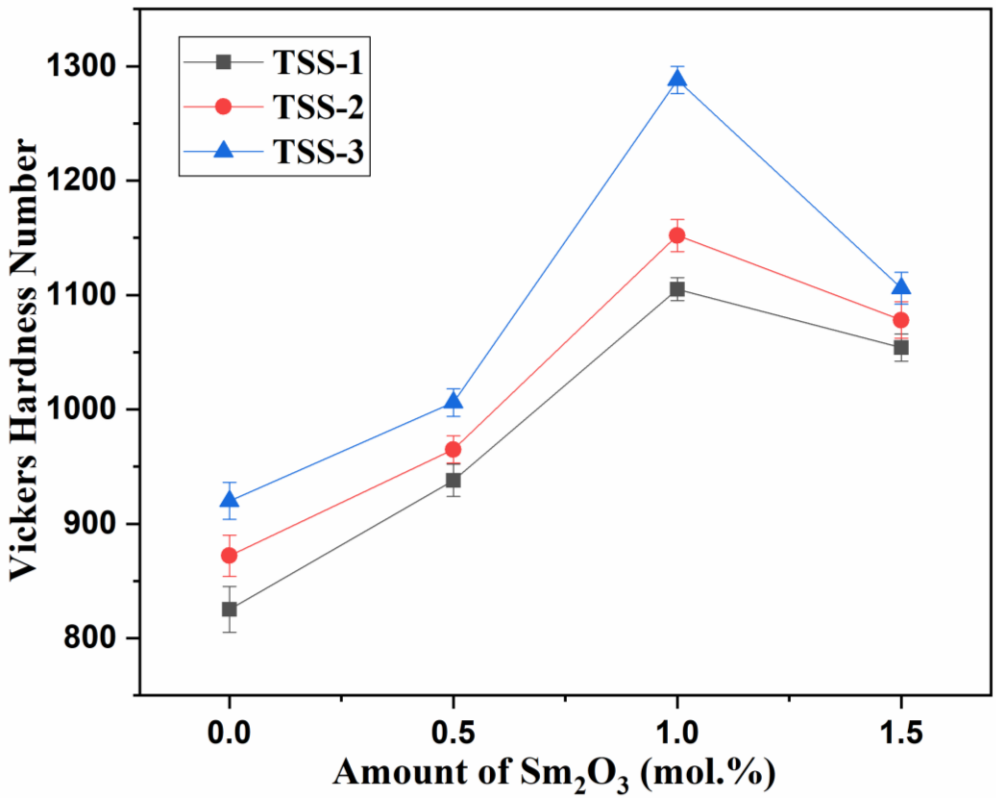

***Fig. 5.12**: Vickers hardness of samples sintered at different two-step sintering schedules.*

As discussed in the conventional singles step sintering, the fracture toughness of the samples shows anopposite trend from the hardness values as represented in **Fig. 5.13**. A toughness of 5.37 MPa.$m^{1/2}$is observed for the sample 1SmCSZ at TSS-3.

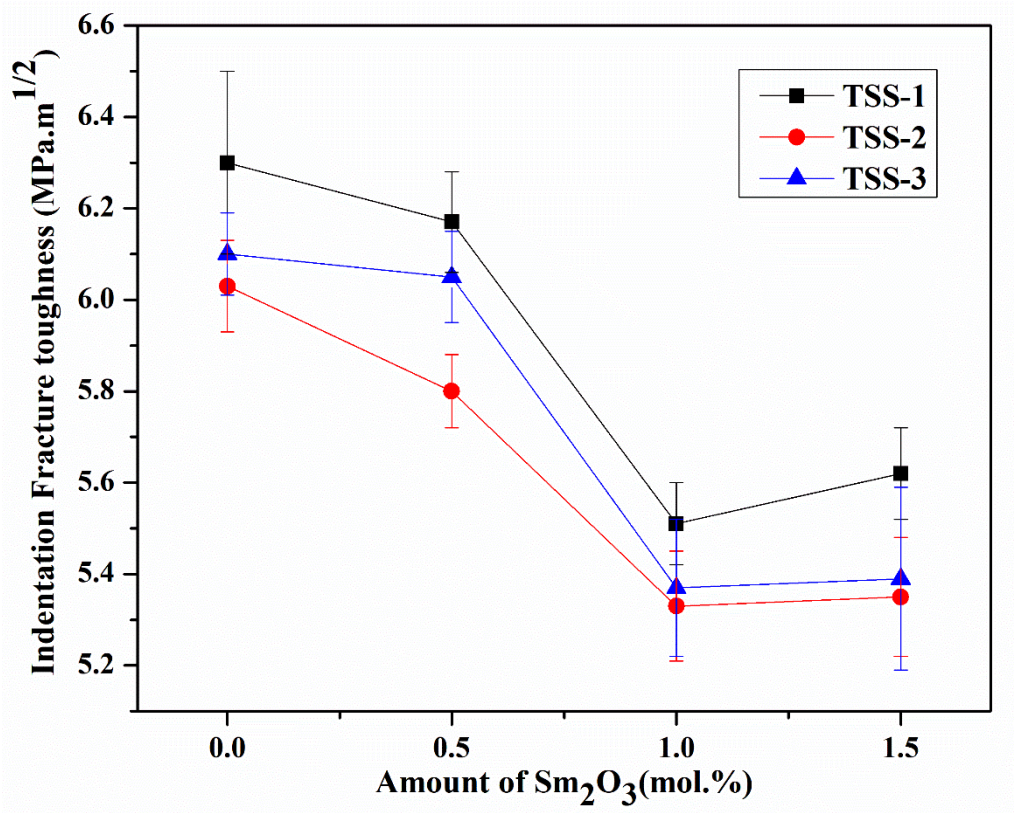

***Fig. 5.13**: Indentation fracture toughness of samples sintered at different two-step sintering schedules.*

5.4 Summary:

- Sm_2O_3 doped ceria stabilized zirconia doped with different amounts of Sm_2O_3 nanopowders were produced successfully using the coprecipitation method.
- Amount of Sm_2O_3 and sintering schedule of compacts were optimized based on density, microstructure, phases present, and mechanical properties.
- Addition of Sm_2O_3 to CSZ improved the densification and helped in restricting the grain growth of CSZ by solute drag mechanism.
- Two-step sintering of the compacts further inhibited the grain growth and assistedin the useful microstructure refinement of Sm_2O_3 doped CSZ.
- An optimum combination of 1288 HV10 Vickers hardness with 5.37 MPa.m$^{1/2}$ fracture toughness is achieved for sample doped with 1 mol.% Sm_2O_3 sintered at 1500 °C for 1 minute followed by 1350 °C for 12 h.

Chapter-6

Tribology and *In-vitro* biological characterization

This chapter devoted to the evaluation of tribological properties such as specific wear rate, coefficient of friction and wear mechanism of niobia doped ceria stabilized zirconia (NbCSZ), and samaria doped ceria stabilized zirconia (SmCSZ). The biological characterization such as low-temperature degradation behaviour, bioactivity and cytocompatibility of the niobia doped ceria stabilized zirconia, and samaria doped ceria stabilized zirconia were also studied.

6.1 Pin on disc wear test:

As described in chapter 3, the pin on disc wear setup was used to determine the tribological properties of NbCSZ and SmCSZ. The wear depth and coefficient of friction plots were drawn, the specific wear rate and average co-efficient of friction (μ) were calculated for the samples at each test load. The results are compared with the conventionally sintered undoped ceria stabilized zirconia.

6.1.1 Ceria stabilized zirconia system:

The change in wear depth and co-efficient of friction with time during the pin on disc wear test of CSZ sample were plotted and presented in **Fig. 6.1**. It can be seen that the wear depth is significantly increasing and the coefficient of friction is decreasing with the increase in load. A wear depth of 96 μm was observed for the sample tested at 30 N load and which is increased to 198 μm at 50 N load. The specific wear rate (SWR) and average co-efficient of friction (μ) were calculated and summarized in **Table 6.1**.

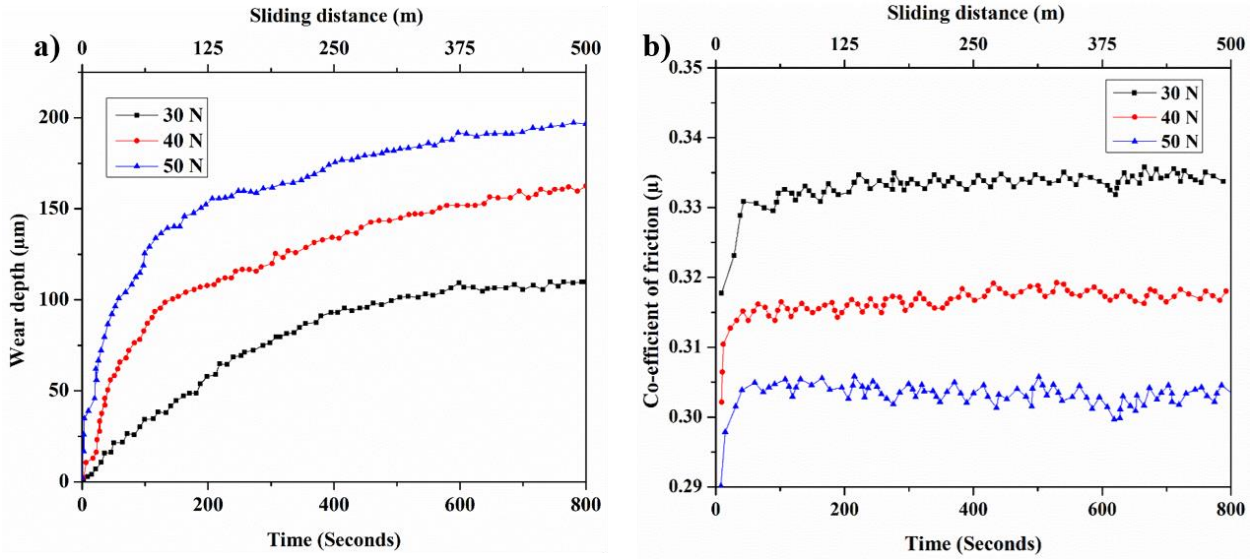

***Fig.6.1**: Comparative plots of a) Wear depth b) Co-efficient of friction of CSZ specimen at different loads.*

The worn surfaces of samples were observed under a scanning electron microscope to understand the severity of damage and wear mechanisms. The micrographs were presented in **Fig. 6.2**.The presence of deeper grooves, grain pullouts and fractured grains can be observed from the micrographs (**Fig. 6.2**). The frequency of grain pullouts and fractured grains were more at 50 N load compared to 30 N as evident from **Fig. 6.2**. The possible reason for grain pullouts probably because of the increase in surface roughness due to volume change accompanied by the stress-induced transformation of tetragonal to monoclinic phase (Basu et al., 2002).

***Table 6.1**: Average coefficient of friction and the specific wear rate of CSZ specimens at different test loads.*

Sample	Test Load	Average µ	Specific wear rate (mm^3/N-m)
CSZ	30 N	0.33	$1.1x10^{-4}$
	40 N	0.31	$1.3x10^{-4}$
	50 N	0.30	$1.5x10^{-4}$

The debris generated due to grain pullouts acts as a third body between the sample and counter body resulting in increased abrasive wear (deeper grooves observed in **Fig. 6.2** are evident for abrasive wear) (Jansen et al., 1998). The grain pullouts, along with increased abrasive wear, caused the severe wear damage in CSZ samples.

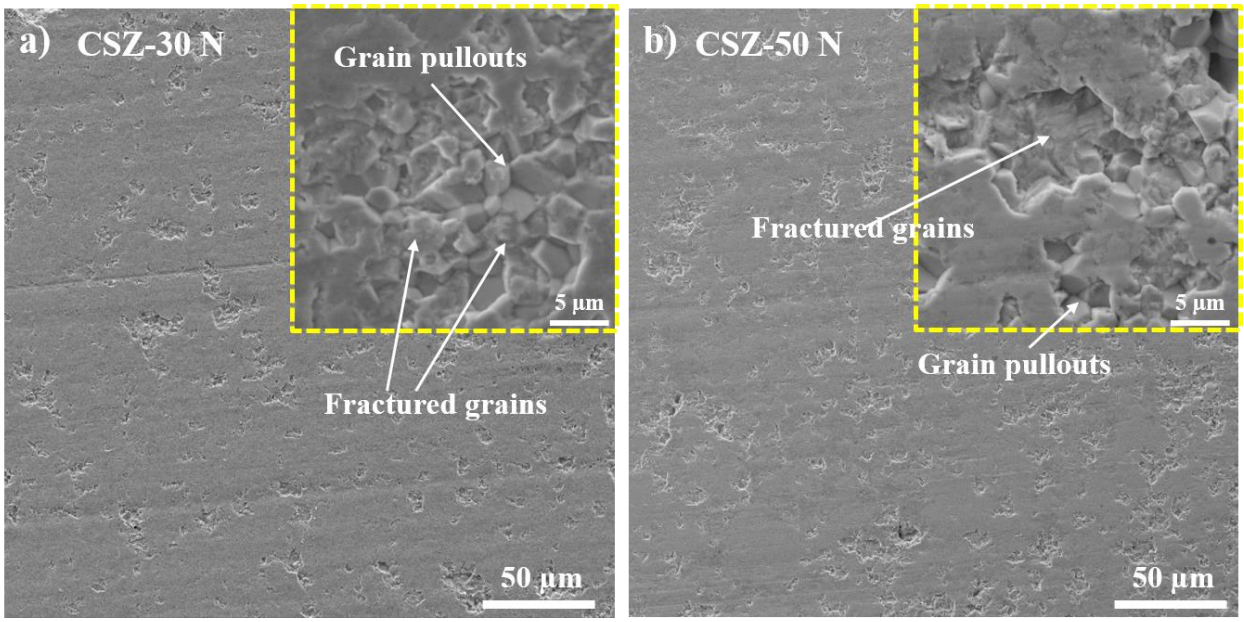

Fig.6.2: *Scanning electron micrographs of worn surfaces of CSZ at a) 30 N, b) 50 N test loads (Inset images indicates enlarged micrographs).*

6.1.2 Niobia doped ceria stabilized zirconia system:

The plots showing wear depth and co-efficient friction of NbCSZ are presented in **Fig. 6.3**. A maximum wear depth of 65 µm was observed for the sample tested at 30 N load and which is increased to 142 µm at 50 N load. The specific wear rate (SWR) and average co-efficient of friction (µ) were calculated and summarized in **Table 6.2**. The specific wear rate is decreased by a percentage of 33%, 36%, 40% for a test load of 30 N, 40 N and 50 N respectively in comparison with CSZ samples.

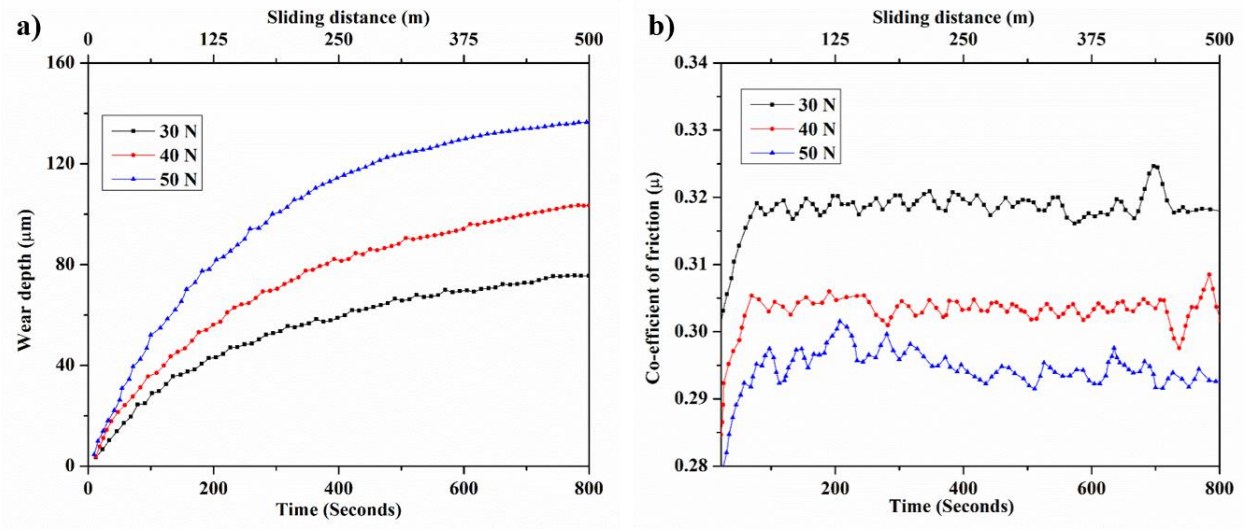

***Fig.6.3**: Comparative plots of a) Wear depth b) Co-efficient of friction of NbCSZ specimen at different loads.*

***Table 6.2**: Average coefficient of friction and the specific wear rate of NbCSZ specimens at different test loads.*

Sample	Test Load	Average μ	Specific wear rate (mm^3/N-m)
NbCSZ	30 N	0.318	$7.3x10^{-5}$
	40 N	0.302	$8.2x10^{-5}$
	50 N	0.294	$8.9x10^{-5}$

SEM images of NbCSZ samples tested at 30 N load represented in **Fig. 6.4** shows only a few grain pullouts and no evidence of fractured grains, whereas at 50 N load more grain pullouts were observed along with some fractured grains.

The results indicate that for a particular experimental condition, the extent of wear damage is less for NbCSZ compared to CSZ. The wear resistance is significantly increased in the case of NbCSZ irrespective of test loads. The increase in wear resistance of NbCSZ might be attributed to its improved hardness and decreased grain size (Bejugama and Pandey, 2018).

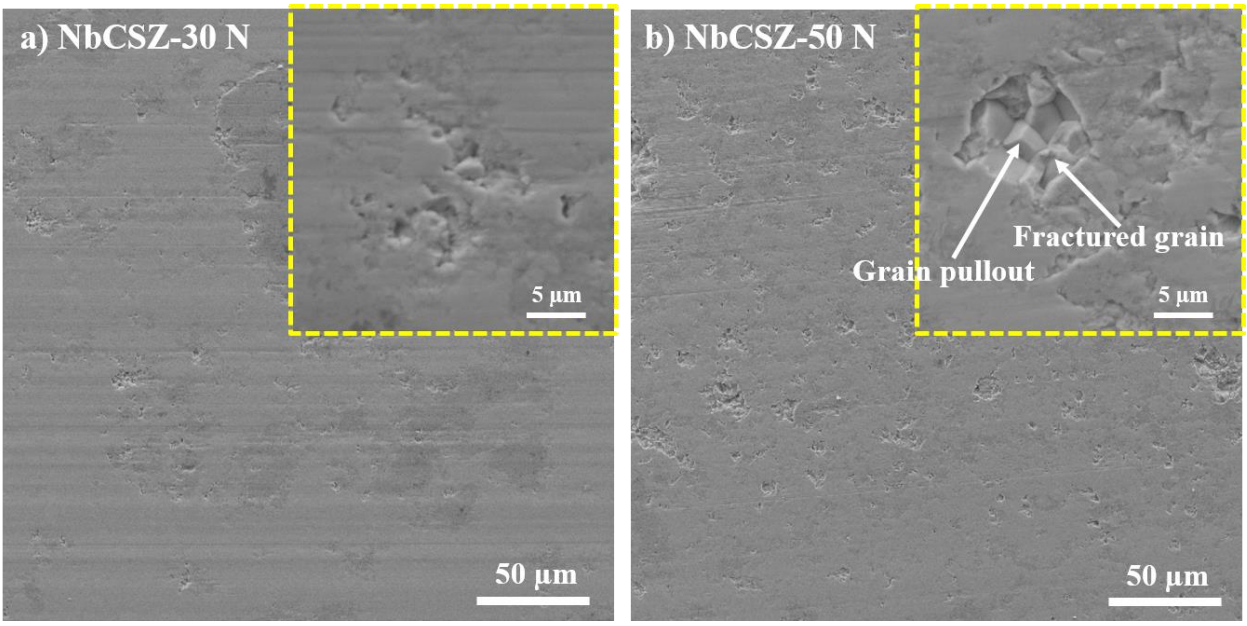

***Fig.6.4**: Scanning electron micrographs of worn surfaces of NbCSZ at a) 30 N, b) 50 N test loads (Inset images indicates enlarged micrographs).*

6.1.3 Samaria doped ceria stabilized zirconia system:

Wear depth and co-efficient of friction plots of SmCSZ samples represented in **Fig. 6.5** clearly shows the improved tribological properties compared to both CSZ and NbCSZ specimens. A maximum wear depth of only 35 µm was observed for the sample tested at 30 N load and which is increased to 72 µm at 50 N load. The specific wear rate (SWR) and average co-efficient of friction (µ) were calculated and summarized in **Table 6.3**. It can be seen that lower co-efficient of friction values were observed for SmCSZ samples compared to CSZ & NbCSZ samples at a particular load. The specific wear rate is decreased by a percentage of 59 %, 63 %, 61 % for a test load of 30 N, 40 N and 50 N respectively in comparison with CSZ samples, which indicates the better wear resistance of SmCSZ samples. The increase in wear resistance of the SmCSZ sample is attributed to its fine grain size and high hardness (Bejugama et al., 2019).

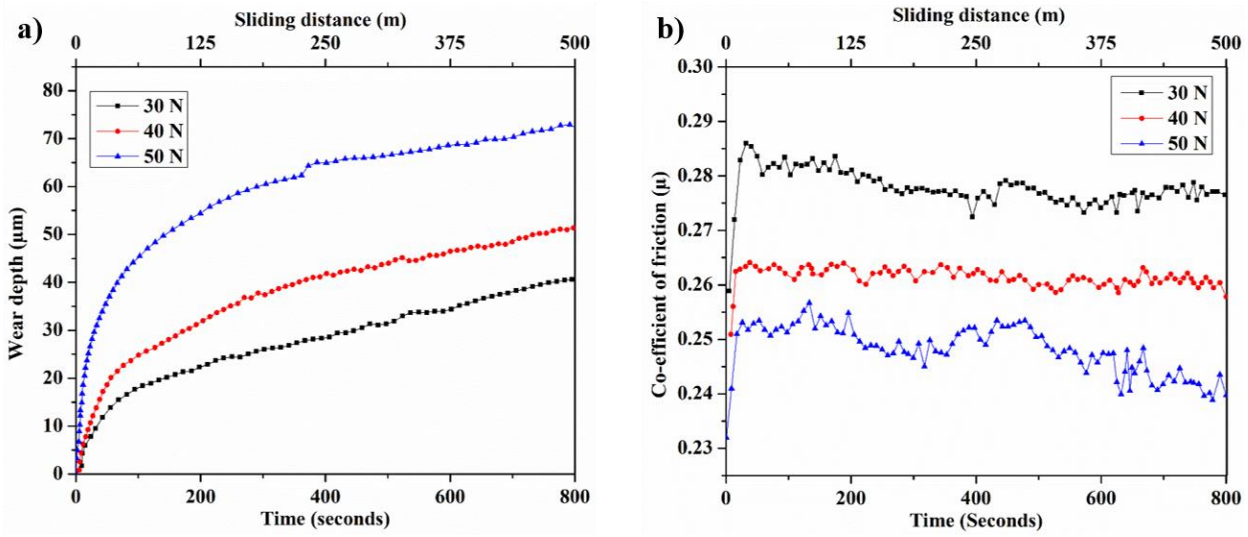

***Fig.6.5**: Comparative plots of a) Wear depth b) Co-efficient of friction of SmCSZ specimen at different loads.*

***Table 6.3**: Average coefficient of friction and the specific wear rate of SmCSZ specimens at different test loads.*

Sample	Test Load	Average µ	Specific wear rate (mm^3/N-m)
SmCSZ	30 N	0.27	$4.5x10^{-5}$
	40 N	0.26	$4.7x10^{-5}$
	50 N	0.24	$5.8x10^{-5}$

The SEM images of the worn surface of the SmCSZ sample shown negligible damage at 30 N **(Fig. 6.6(a))** and there were only a few grain pullouts observed at 50 N **(Fig. 6.6(b))** load and no fractured grains were seen, which confirms that only mild wear occurred in the sample and it can be noted that SmCSZ can work in even more severe conditions. The absence of grain fracture in SmCSZ may be attributed to the improved tetragonal phase stability due to its finer microstructure.

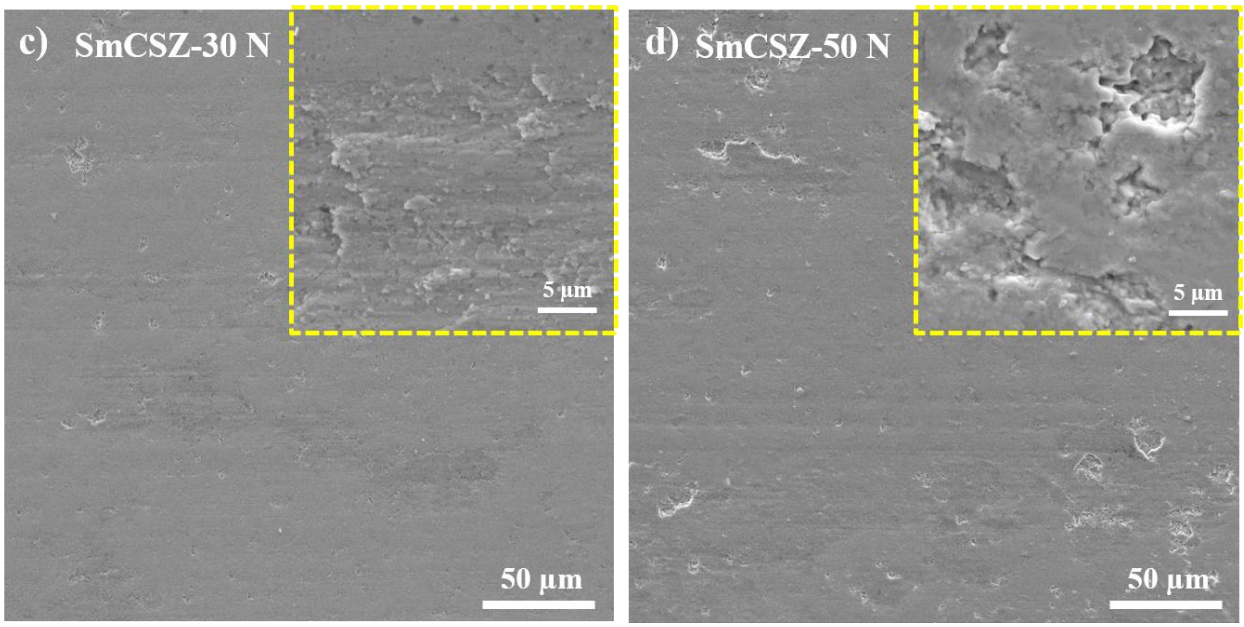

Fig.6.6: *Scanning electron micrographs of worn surfaces of SmCSZ at a) 30 N b) 50 N test loads (Inset images indicates enlarged micrographs).*

6.2 Accelerated Hydrothermal aging:

As described in chapter 3, accelerated hydrothermal aging study was conducted on the optimized samples to understand the low-temperature degradation behaviour of ceria stabilized zirconia, Niobia doped ceria stabilized zirconia, and samaria doped ceria stabilized zirconia. The samples undoped CSZ sintered at 1600 °C for 3 hours, NbCSZ sintered at 1500 °C for 1 minute followed by 1250 °C for 15 hours and SmCSZ sintered at 1500 °C for 1 minute followed by 1350 °C for 12 h were chosen for the accelerated aging study. A commercially available yttria-stabilized zirconia ceramic sintered at 1450 °C for 3 hours was also tested along with the samples for comparison purposes.

6.2.1 Effect of hydrothermal aging on yttria-stabilized zirconia ceramics:

X-ray diffraction patterns of hydrothermal tested yttria-stabilized zirconia samples for a specified hour of treatment were presented in **Fig. 6.7**. It is observed that a significant amount of increase in the monoclinic phase (from 47.7 % from the initial 6 %) was observed in the YSZ sample only after 10 hours of hydrothermal treatment. The monoclinic phase increased further with the duration of the hydrothermal study, as represented in **Fig. 6.7**. As discussed in the literature (Section 2.6), the volume expansion involved in tetragonal to monoclinic phase transformation (~ 4%) caused the formation of microcracks, surface upliftment, and in turn grain pullouts as

evident from the SEM image shown in **Fig. 6.8 (b & c)** (Sato et al., 1986; Tsukuma et al., 1983; Watanabe et al., 1983). The reason for low-temperature degradation in YSZ is due to the presence of yttria as a stabilizer or the annihilation of oxygen vacancies (responsible for tetragonal stabilization in YSZ) as discussed in chapter 2. The oxygen vacancy in YSZ lattice can be seen from the following Kröger–Vink equation.

$$Y_2O_3 \xrightarrow{ZrO2} 2Y'_{Zr} + 3O_o^x + V_o^{\cdot\cdot} \qquad (6.1)$$

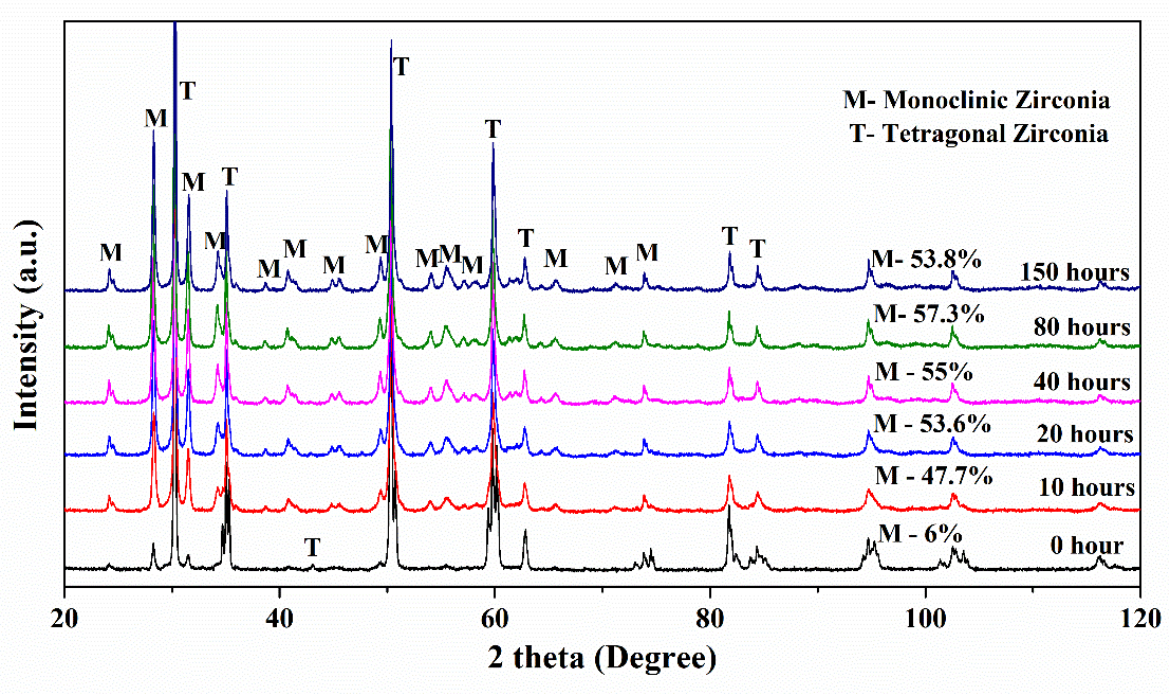

***Fig. 6.7**: XRD patterns of YSZ sample along with monoclinic fraction after different durations of hydrothermal treatment.*

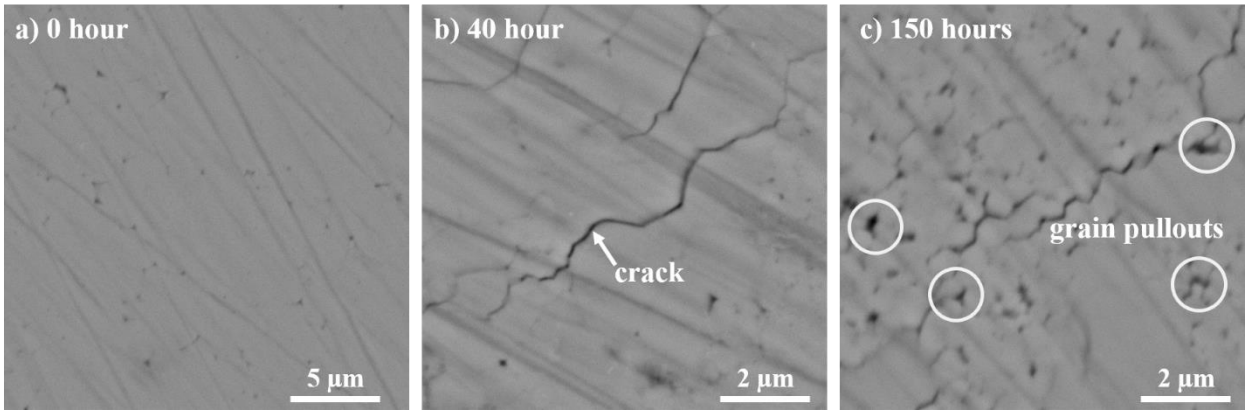

***Fig. 6.8**: SEM images of hydrothermally treated 3YSZ samples indicating the extent of surface damage after a) 0-hour b) 40 hours c) 150 hours of treatment.*

6.2.2 Effect of hydrothermal treatment on ceria stabilized zirconia:

The XRD patterns of the CSZ sample at specified intervals of hydrothermal aging were presented in **Fig. 6.9**. Expectedly, CSZ did not show any phase change and retained its tetragonal phase even after 200 hours of accelerated aging. It is the absence of oxygen vacancies, which made CSZ more resistant to LTD (Pandey and Biswas, 2014). It is known that the stabilization of high-temperature phases in ceria stabilized zirconia is different from YSZ and oxygen vacancies has no role in the stabilization of CSZ (Li et al., 1994b). SEM images of hydrothermal treated CSZ samples are presented in **Fig. 6.10**, there is no surface damage observed even after 200 hours of treatment, and these results are also in agreement with XRD analysis.

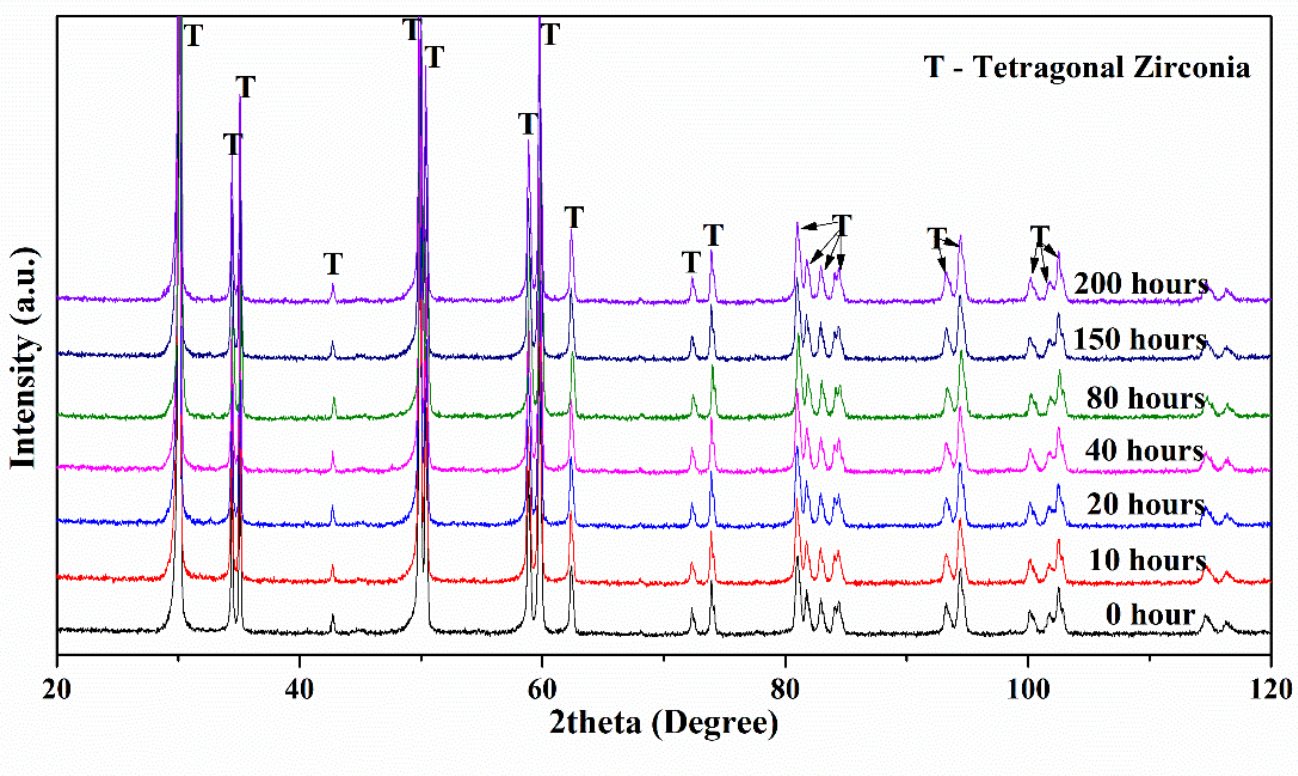

***Fig. 6.9**: XRD patterns of CSZ samples indicating phases present after different durations of hydrothermal treatment.*

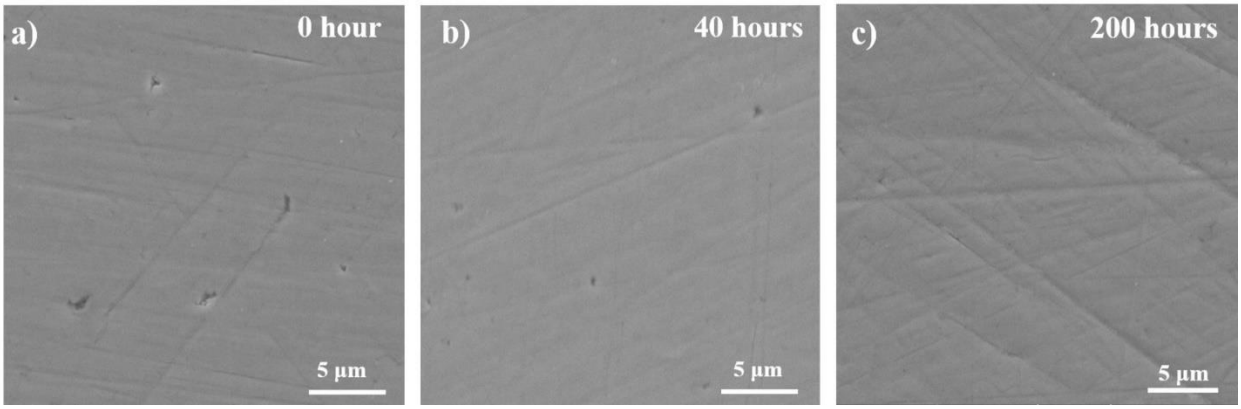

***Fig. 6.10**: SEM images of hydrothermally treated CSZ samples indicating the extent of surface damage after a) 0-hour b) 40 hours c) 200 hours of treatment.*

6.2.3 Effect of hydrothermal treatment on Niobia doped ceria stabilized zirconia:

Similar results, as observed in CSZ samples after hydrothermal treatment, were also found in NbCSZ samples. XRD patterns of NbCSZ samples after different hours (up to 200 hours) of hydrothermal treatment as represented in **Fig.6.11** did not show any traces of monoclinic phase, which confirms the high resistance of NbCSZ to low-temperature degradation.

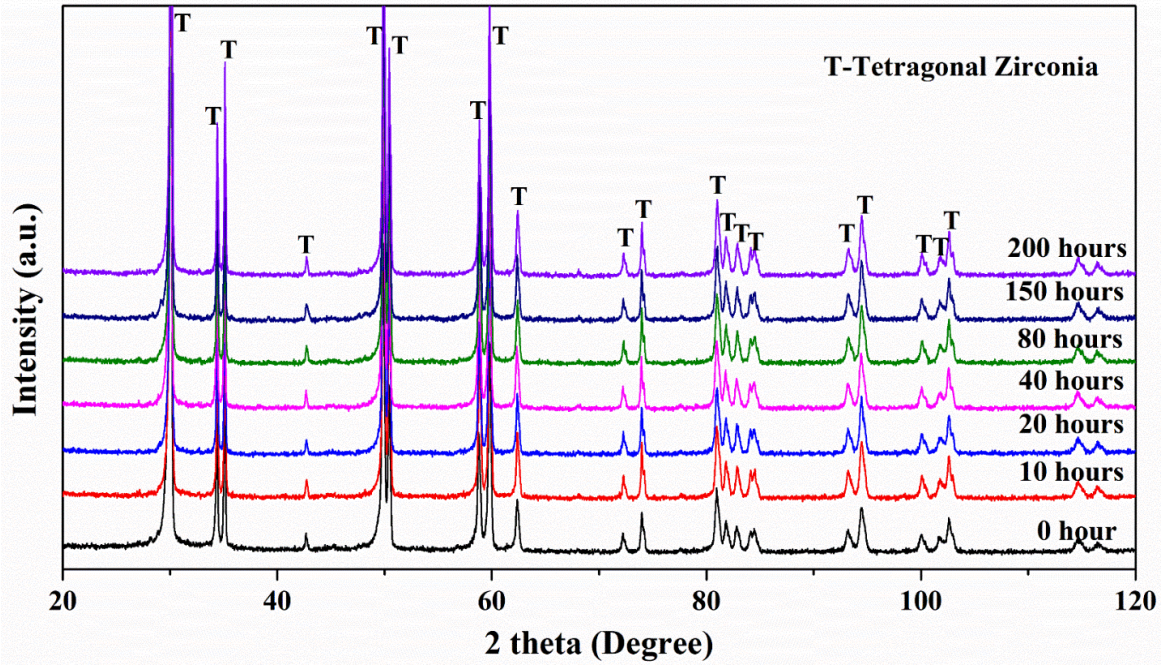

***Fig. 6.11**: XRD patterns of NbCSZ samples indicating phases present after different durations of hydrothermal treatment.*

As discussed in the earlier section, the reason for the resistance to LTD is the absence of oxygen vacancies in the NbCSZ lattice. The SEM images of hydrothermal tested sample surfaces were also taken to support the XRD results and presented in **Fig. 6.12**; SEM images did not show any surface damage like surface uplifts or grain pullouts.

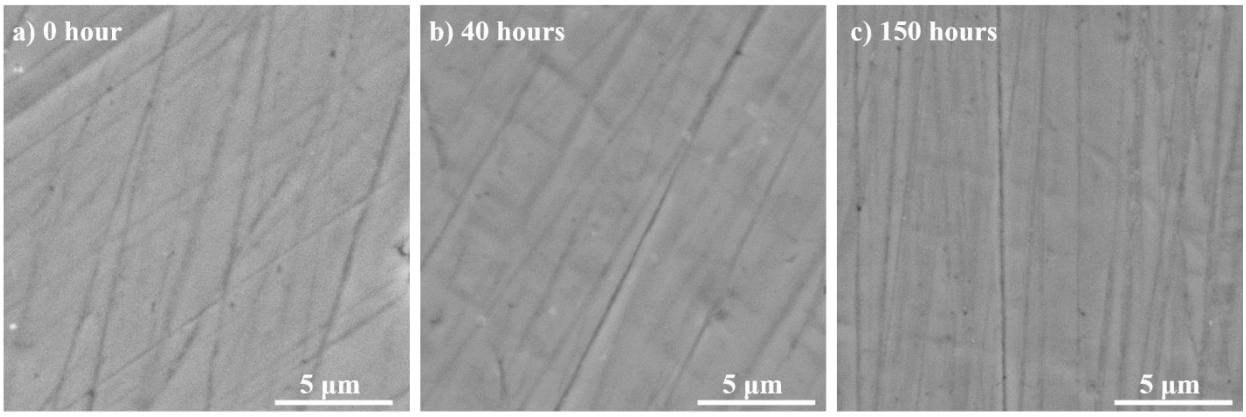

Fig. 6.12: *SEM images of hydrothermally treated NbCSZ samples indicating the extent of surface damage after a) 0-hour b) 40 hours c) 200 hours of treatment.*

6.2.4 Effect of hydrothermal treatment on Samaria doped ceria stabilized zirconia:

The XRD patterns of the SmCSZ sample at specified intervals of hydrothermal aging were presented in **Fig. 6.13**. Interestingly, SmCSZ also did not show any phase changes even after 200 hours of accelerated aging. It can be noted that the SmCSZ contains cubic and tetragonal zirconia phases as indexed in **Fig. 6.13** before hydrothermal treatment. However, the cubic and tetragonal phases retained, and no monoclinic phase transformation was observed in the SmCSZ sample after aging**(Fig. 6.14)**. Even though, SmCSZ contains oxygen vacancies (equation 6.2), which are introduced by doping Sm_2O_3 into CSZ, the quantity of oxygen vacancies are very low, and they are not entirely responsible for stabilization (Turon-Vinas et al., 2018). The scanning electron micrographs (**Fig. 6.15**) are also in support with the XRD results and did not show any surface damage even after 200 hours of hydrothermal treatment. Hence, the accelerated hydrothermal aging study of SmCSZ concludes that the material is highly resistant to low-temperature degradation.

$$Sm_2O_3 \xrightarrow{ZrO_2} 2Sm'_{Zr} + V_o^{\cdot\cdot} + 3O_o^X \qquad (6.2)$$

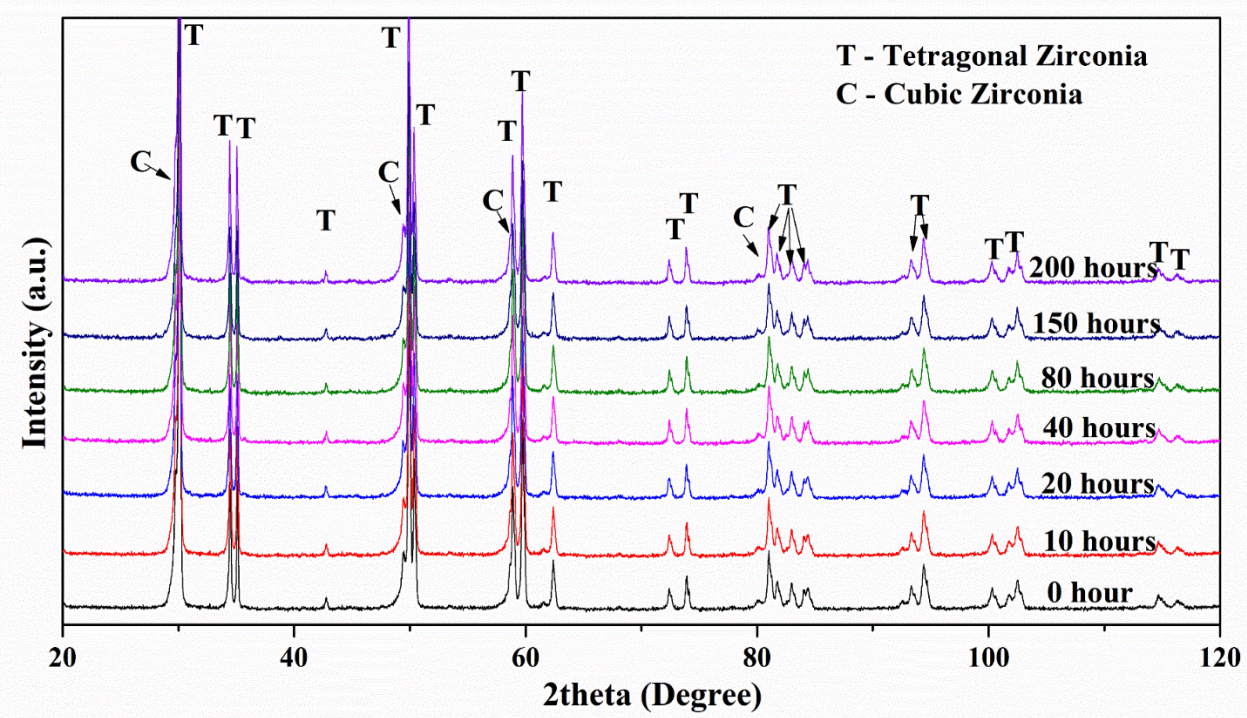

Fig. 6.13: *XRD patterns of SmCSZ samples indicating phases present after different durations of hydrothermal treatment.*

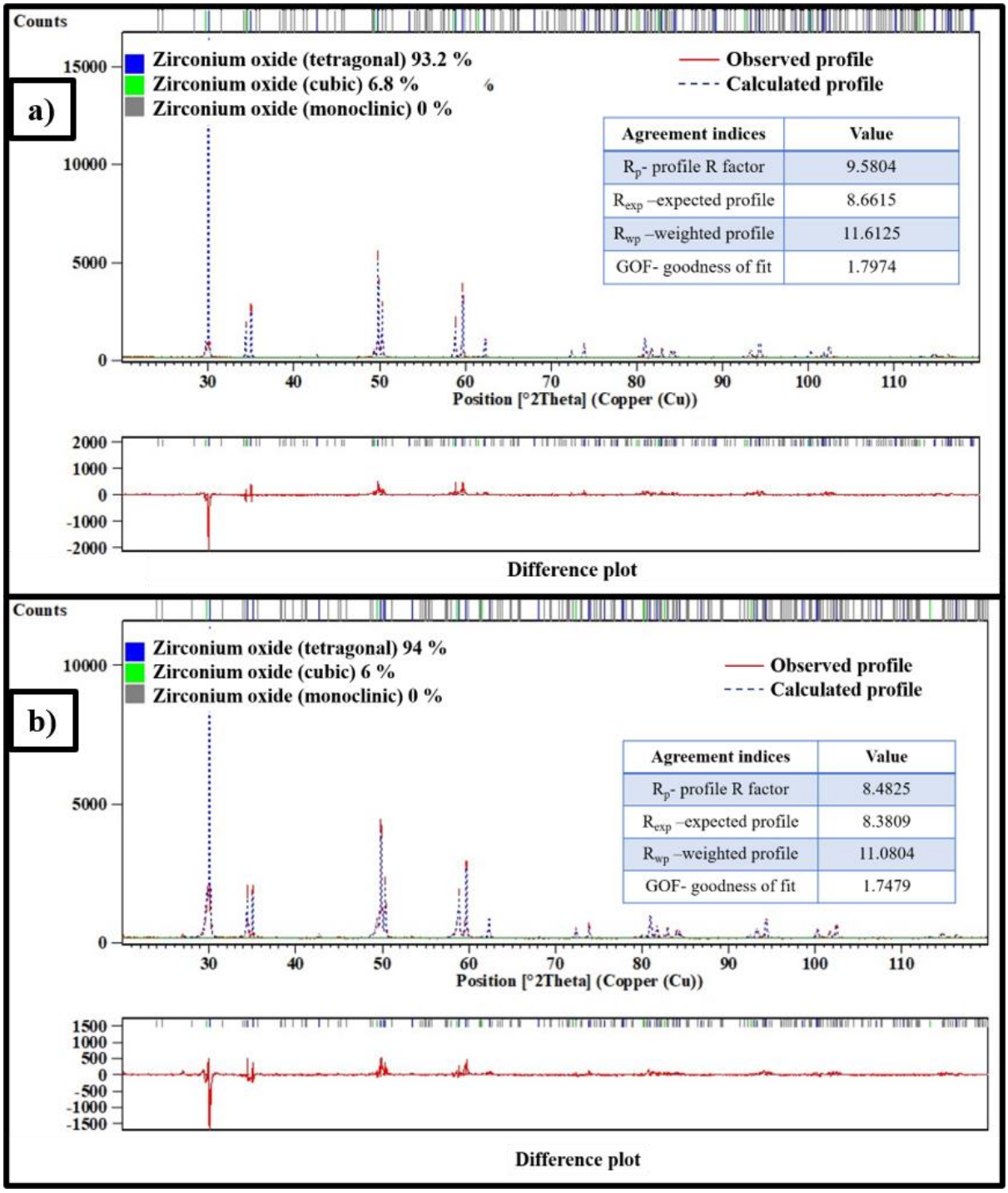

Fig. 6.14: *XRD patterns of SmCSZ samples after Rietveld refinement a) before and b) after 200 hours of hydrothermal treatment.*

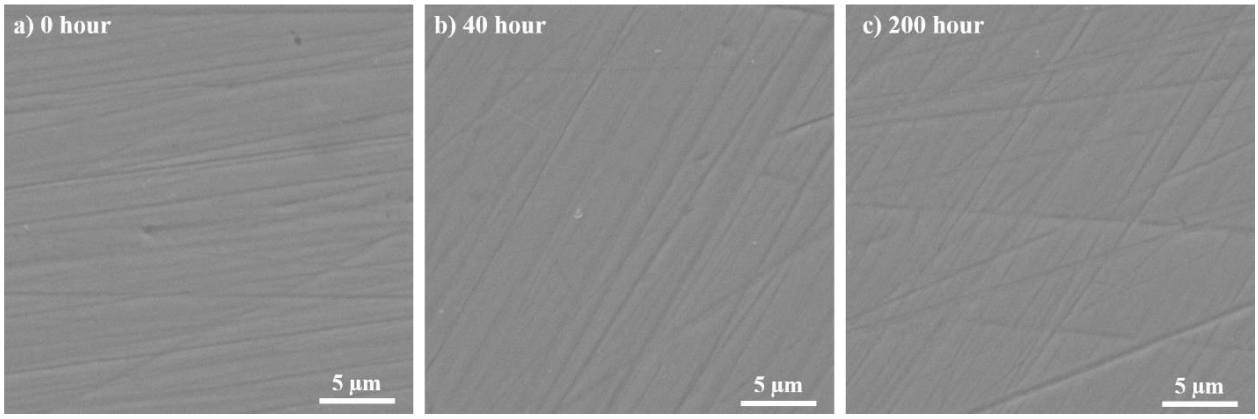

***Fig. 6.15**: SEM images of hydrothermally treated SmCSZ samples indicating the extent of surface damage after a) 0-hour b) 40 hours c) 200 hours of treatment.*

6.3 Osteo-conductivity or bioactivity study:

The samples' bioactivity was generally evaluated through the ability of apatite layer formation on the surface when immersed in a Simulated Body Fluid (SBF). The SBF solution was prepared by dissolving the reagents mentioned in chapter 3, section 3.6.4.2 in 1000 ml of distilled water, as described by kokubo et al. (Kokubo and Takadama, 2006). Before immersing the samples in SBF, one set of samples were kept in 5M H_3PO_4 solution at 90 °C for 4 days; after that, samples were taken out of the solution, cleaned with distilled water, dried at room temperature. Then the untreated and chemical treated samples were placed in polypropylene beakers, SBF solution was added into them and placed inside an incubator, which maintains a constant temperature of 36.5 °C. After every alternate day, the SBF was replaced with a fresh one, and the samples were taken out after 7 days for characterization. After taking out, the samples were gently washed with distilled water and dried in a desiccator. The dried samples were characterized for phase and also observed under SEM.

SEM micrographs of SBF immersed samples were shown in **Fig. 6.16**. It is observed that there is no layer formation on untreated CSZ, NbCSZ and SmCSZ samples (**Fig. 6.16 (a, b, c)**), whereas cauliflower-like mineral layer deposition of considerable thickness was observed in 5M H_3PO_4 treated samples (**Fig. 6.16 (d, e, f)**). The formed layer's chemical analysis was carried through EDS and presented in **Fig. 6.16 (g, h, i)**. The Ca/P (wt.%) ratio of the layer was calculated and found to be 1.61±0.04 for the treated CSZ sample, 1.71±0.06 for treated NbCSZ samples and 1.67±0.04 for the treated SmCSZ sample, which confirms that the formed layer is hydroxyapatite (Ca/P ratio of hydroxyapatite is ~1.67). The XRD analysis of chemical treated and SBF

immersed samples represented in the **Fig. 6.17** also confirms the presence of hydroxyapatite phase (HAP). The functional groups like Si-OH, Ti-OH, Zr-OH, or Ta-OH are expected to acts as nucleating sites for apatite formation in bioactive ceramics (Nakamura and Inuzuka, 2011; Uchida et al., 2002b, 2001). As untreated zirconia doesn't have any -OH groups on its surface, it will not induce an apatite layer when immersed in SBF solution. However, chemical treatment with 5M H_3PO_4 at 90 °C induces Zr-OH bonds on the surface, later when immersed in SBF these Zr-OH functional sites acted as nucleating sites for apatite formation as described in the chapter 2, section 2.14(Aguiar et al., 2008; Uchida et al., 2002a).

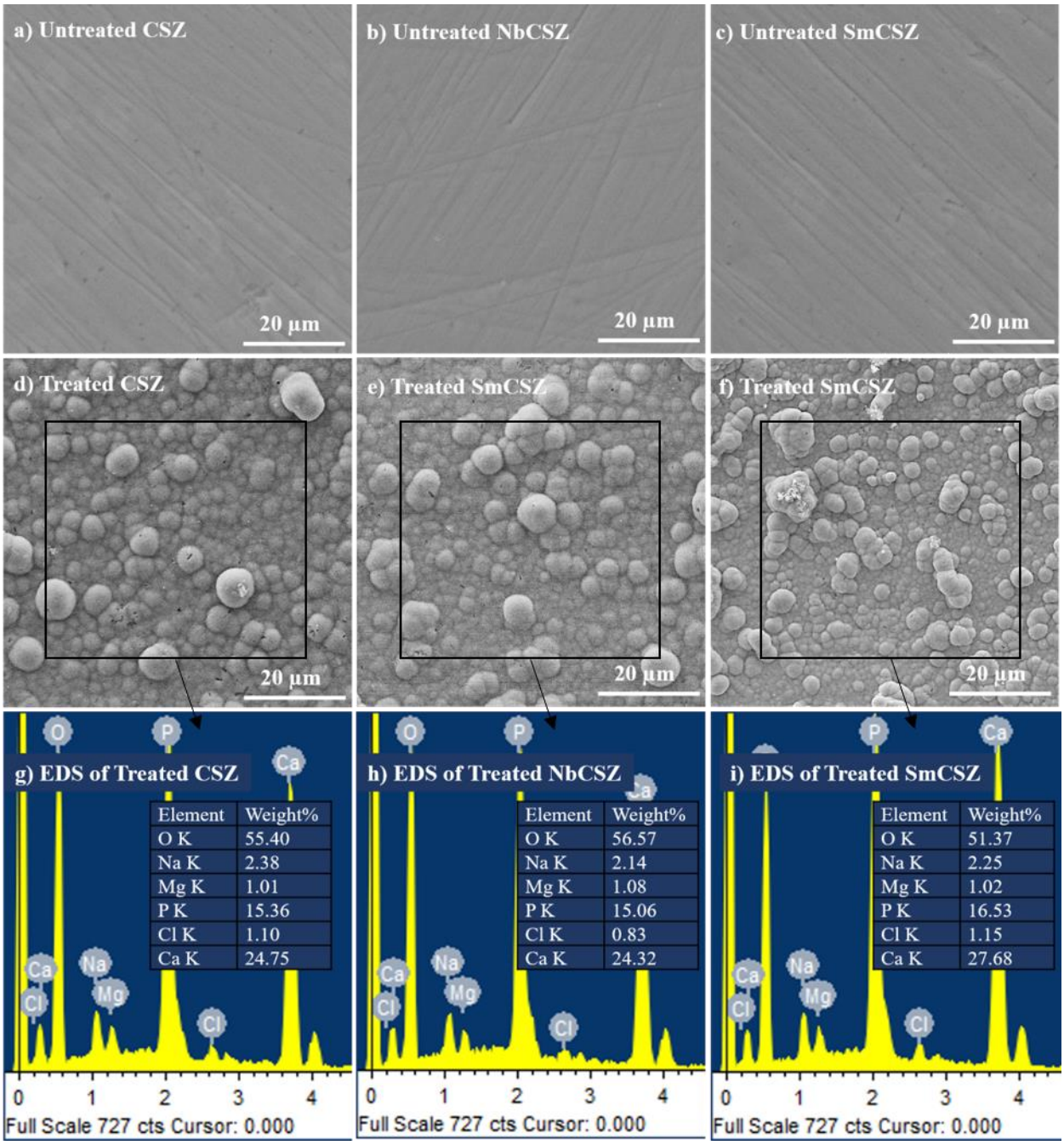

***Fig. 6.16**: The SEM images of SBF immersed (a, b, c) Untreated samples, (d, e, f) 5M H_3PO_4 treated samples, (g, h, i) EDS analysis of treated samples.*

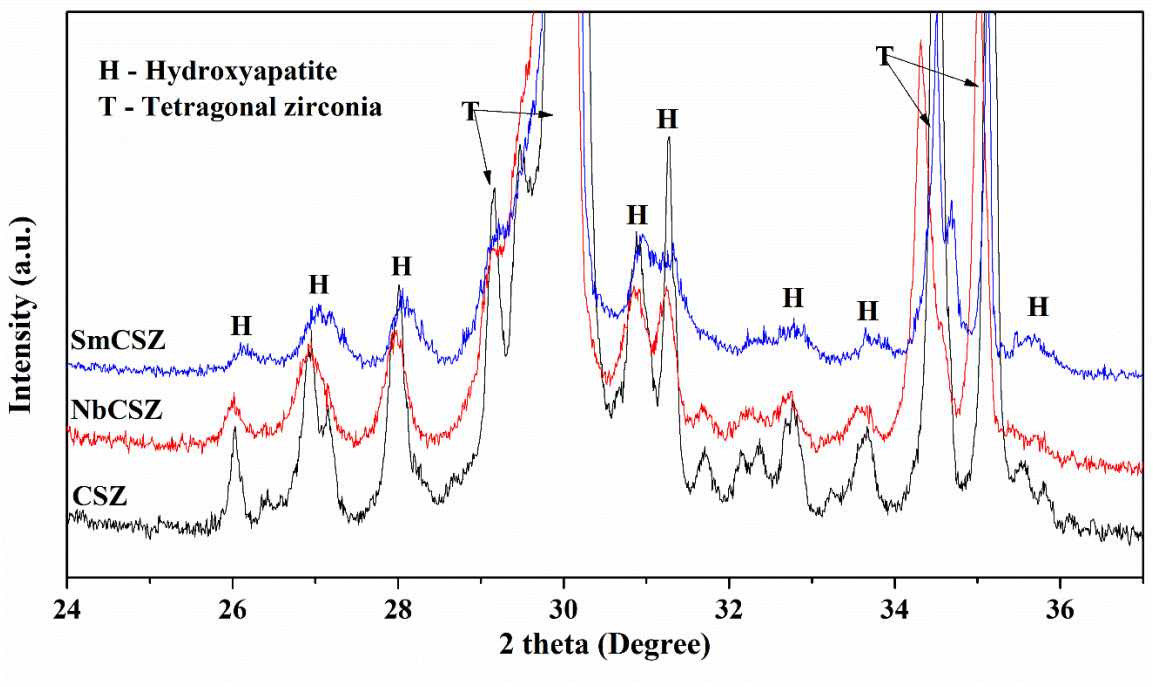

***Fig. 6.17**: XRD patterns of SBF immersed 5M H_3PO_4 treated samples indicating hydroxyapatite phase.*

6.4 *Invitro* cellular response of developed materials:

Invitro cell culture study was conducted to understand the toxic behaviour of material on the human osteoblast-like cells. The Scanning electron microscope was used to analyze the cell attachment and its morphology on the surface of the samples. Cellular metabolic activity assay (MTT assay) was conducted to understand the proliferation and viability of cells on the samples.

6.4.1 Cell attachment and morphology:

The surface of the samples seeded with MG 63 cells (human osteoblast-like cells) was observed under a scanning electron microscope for cell morphology and attachment. The micrographs representing typical morphology of attached human osteoblast-like cells after 1 and 7 days of culture are shown in **Fig. 6.18**, **Fig. 6.19** and **Fig 6.20**for CSZ, NbCSZ and SmCSZ samples, respectively. All the three substrates support intimate cellular attachment to the substrate by cellular extension and continuous growth of cells. It is observed that the cells retained their typical polygonal morphology with some variations due to the underlying surface topography as described by Herath et al. (Herath et al., 2015). The cells on the surface were connected to each other and spread most of the sample surface after seven days of incubation and also colonized multilayered cells with numerous cell-cell contacts were observed. Similar morphological

features for osteoblast cells were seen on all samples (CSZ, NbCSZ and SmCSZ ceramics). A significant increase in cell density can be seen in day 7 sample compared to day 1 sample, which confirms the active proliferation of cells.

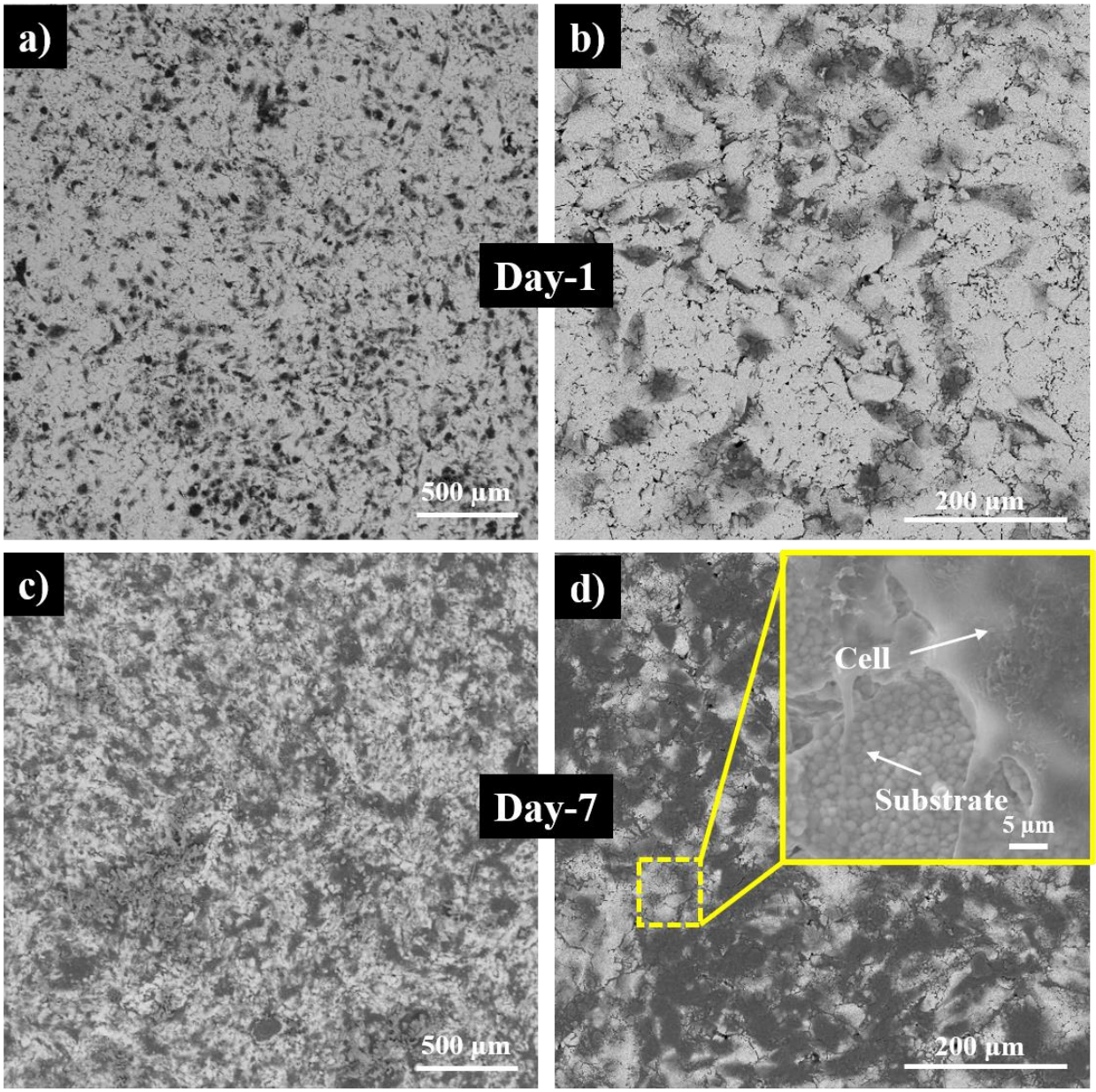

***Fig. 6.18**: SEM images indicating cell morphology and proliferation on CSZ sample, (a & b) SEM image of sample surface after 1 day of culture. (c & d) SEM image of sample surface after 7 days of culture (inset image indicates a magnified view of sample).*

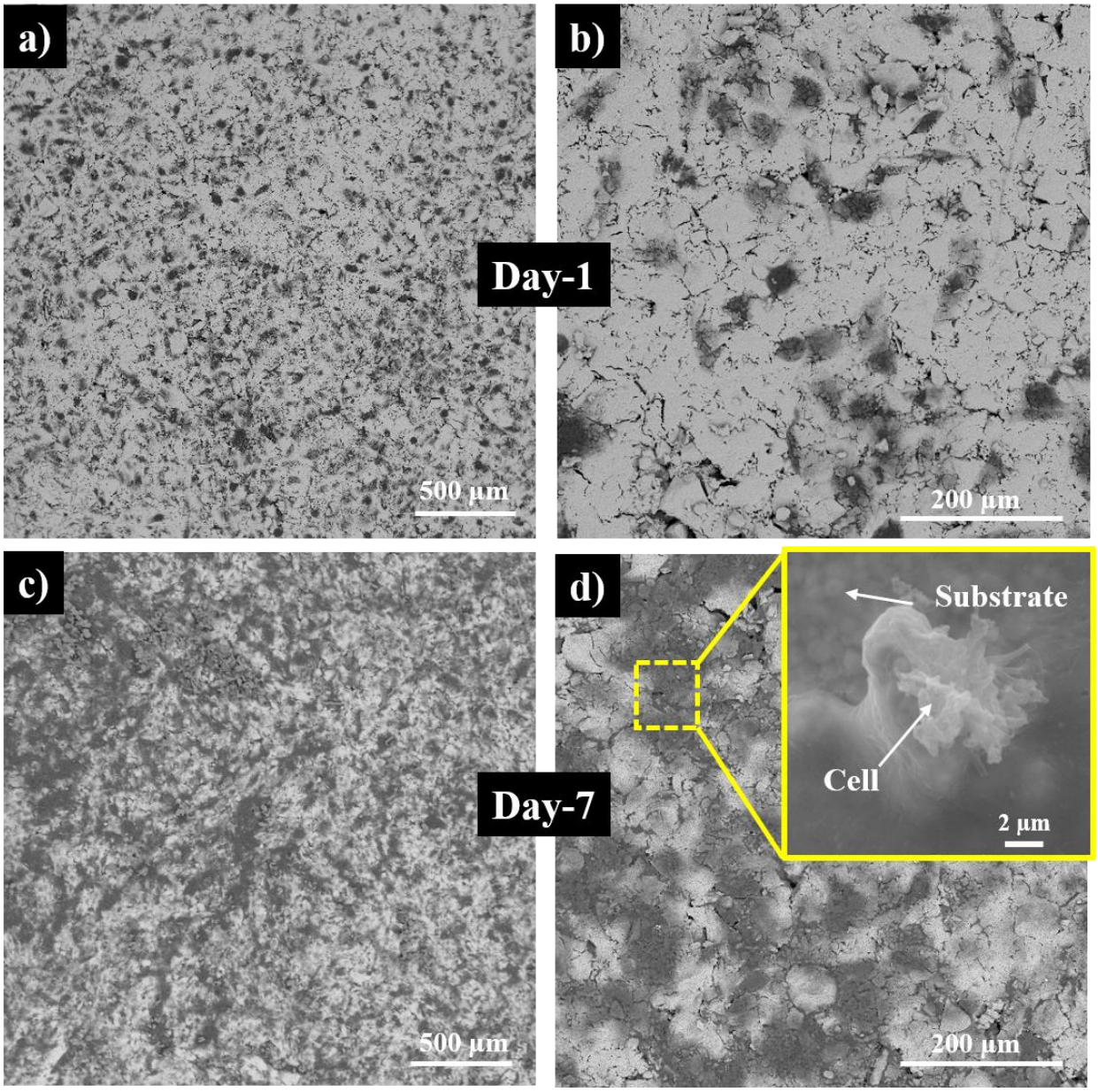

***Fig. 6.19**: SEM images indicating cell morphology and proliferation on NbCSZ sample, (a & b) SEM image of sample surface after 1 day of culture. (c & d) SEM image of sample surface after 7 days of culture (inset image indicates a magnified view of sample).*

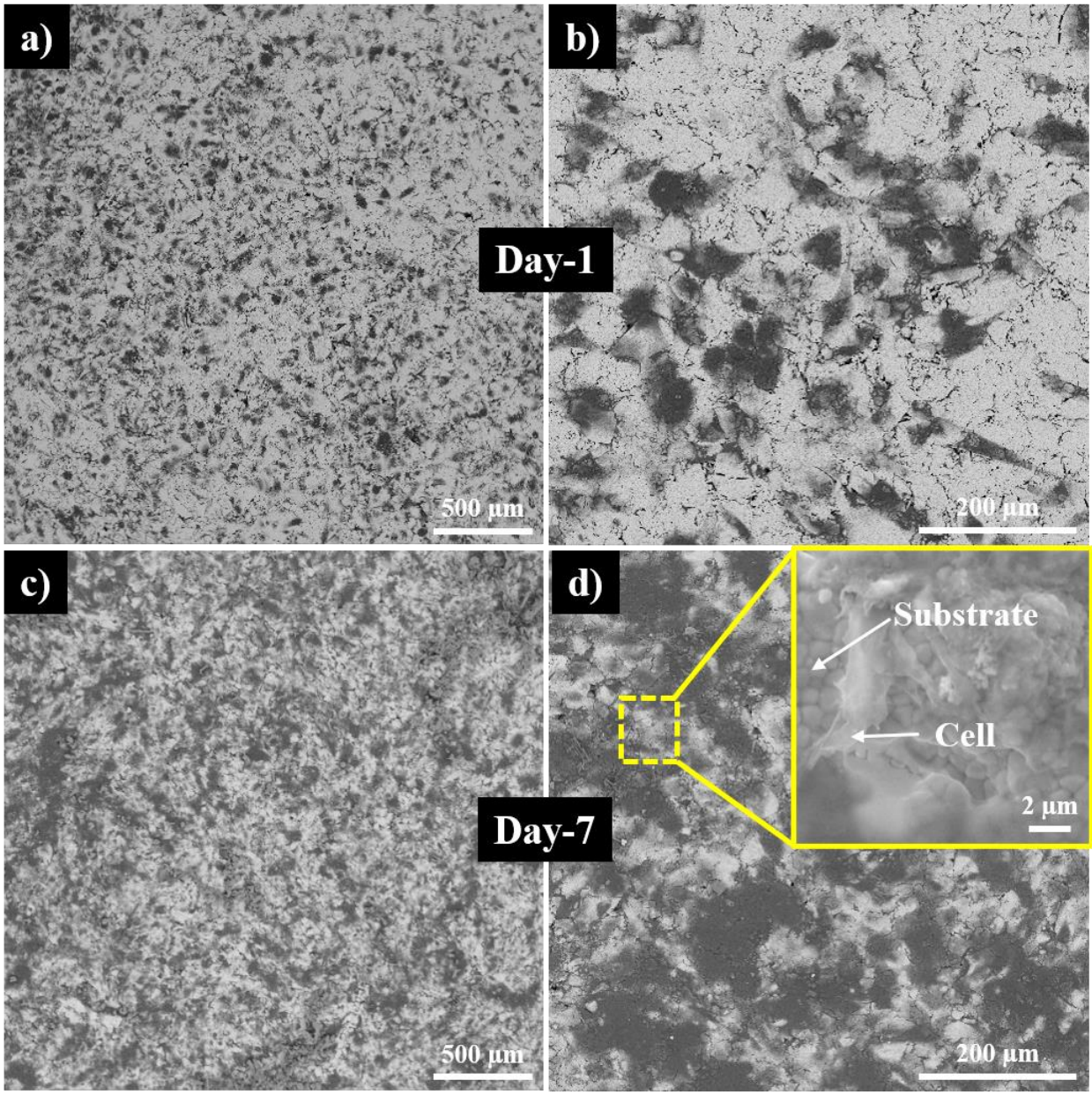

***Fig. 6.20**: SEM images indicating cell morphology and proliferation on SmCSZ sample, (a & b) SEM image of sample surface after 1 day of culture. (c & d) SEM image of sample surface after 7 days of culture (inset image indicates a magnified view of the sample).*

6.4.2 Cellular metabolic activity assay:

Cell metabolic activity and viability of MG63 cells on samples (CSZ, NbCSZ & SmCSZ) were measured by performing MTT assay on samples and control (empty well) incubated for 1, 4, and 7 days.

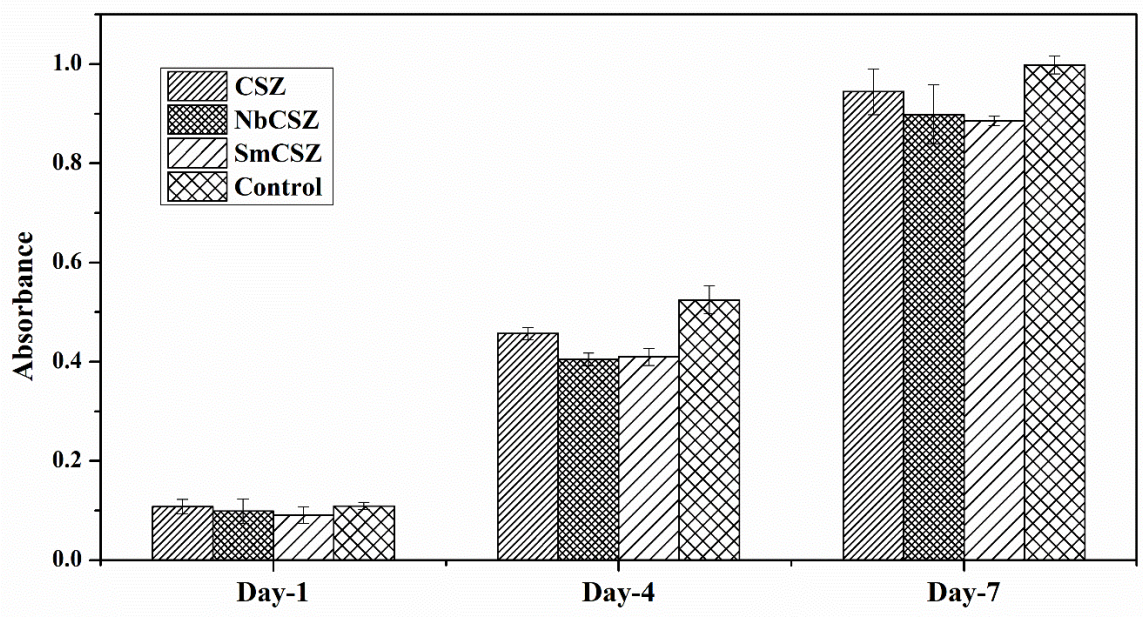

Fig.6.21: *MTT assay plot representing the absorbance values of CSZ, NbCSZ, SmCSZ sample and control.*

Fig. 6.21 represents the absorbance values of NbCSZ sample and control; there was no significant difference observed between samples and control, and more than 95% cell viability (absorbance of sample to the absorbance of control) was observed when compared with control. Also, an increasing trend was seen in absorbance values with the increase in the number of days. A similar trend was also observed in case of yttria-stabilized zirconia (Lee et al., 2016; Pandey et al., 2013) and ceria stabilized zirconia (Pandey and Biswas, 2014) in literature, which confirms that the cells are metabolically active and proliferating on the material. Therefore, it can be assumed that the addition of Nb_2O_5 or Sm_2O_3 to CSZ did not induce any undesirable effects on cell proliferation. As per the ISO 10993-5:2009 standard "biological evaluation of medical devices: tests for in vitro cytocompatibility", if the cell viability of the material is more than 70%, then the material can be considered as cytocompatible. Overall, the results confirm that the NbCSZ material is biocompatible and also, not leaching any cytotoxic material, indicating its potential for usage as implants. Overall, the results indicate that the NbCSZ and SmCSZ

ceramics are cytocompatible and also, not leaching any toxic material, indicates its potential for usage as implant materials.

6.5 Summary:

- The pin on disc wear test successfully conducted on the CSZ, SmCSZ and NbCSZ samples and tribological properties were compared.
- NbCSZ and SmCSZ samples were shown better wear resistance compared to CSZ.
- The Accelerated hydrothermal aging is conducted to understand the low-temperature degradation behaviour of NbCSZ, SmCSZ samples and results were compared with the YSZ samples.
- The Accelerated aging studies have shown high resistance to low-temperature degradation for NbCSZ and SmCSZ samples.
- 5M H3PO4 treated CSZ, NbCSZ, SmCSZ samples shown enhanced bioactivity compared with the untreated samples.
- *Invitro* cell-culture studies were conducted on samples by culturing MG 63 cells on the surfaces of NbCSZ and SmCSZ.
- Cellular metabolic activity assay (MTT assay) and Scanning electron micrographs of samples with cells did not show any toxic effects and revealed active proliferation of cells.

Chapter-7

Summary, conclusions and scope for future work

This chapter summarizes the significant findings and concludes the outcomes of the research work carried out and also presents the scope for future work.

7.1 Powder synthesis:

Nanopowders of Ceria stabilized zirconia (CSZ), Niobia doped ceria stabilized zirconia (NbCSZ), and Samaria doped ceria stabilized zirconia (SmCSZ) are synthesized through co-precipitation synthesis. The co-precipitated powders (hydroxides) are amorphous in nature, contains bonded water molecules and volatile impurities. Calcination is required to convert these powders into crystalline oxide powder. The calcination removes water and volatile matters, and breaks the hydroxide bonds, converts them into oxide powders. The crystallite size of the powders depends on the calcination temperature. The calcination temperature of powders is optimized based on the relative density, grain size and mechanical properties of sintered product.

7.2 Compaction and sintering:

The powders are mixed with a binder and compacted to different sizes of circular pellets using a uniaxial hydraulic press. The compacted pellets are sintered using conventional single step and two-step sintering schedules. The composition of powders and sintering schedule of the samples are optimized based on the phases present, relative density, microstructure and mechanical properties.

7.3 Effect of Niobia doping on ceria stabilized zirconia:

The addition of Niobia to ceria stabilized zirconia improved the sinterability by creating defects in the lattice and decreased the sintering temperature of ceria stabilized zirconia to 1450 ℃, which refined the microstructure and improved the mechanical properties. The average grain size of 2.6±0.93 μm along with a hardness of 1047±20 HV10 and fracture toughness of 6.2±0.5 $Mpa.m^{1/2}$ is achieved for 1 mol.% Niobia doped ceria stabilized zirconia sintered at 1450 ℃ for 3 hours.

7.4 Effect of two-step sintering on Niobia doped ceria stabilized zirconia:

Different sintering schedules are used to sinter NbCSZ samples, and sintering schedule is optimized based on relative density, microstructure and mechanical properties of the sintered sample. The two-step sintering of Nb_2O_5 doped ceria stabilized zirconia effectively reduced the grain size to 1.57 ± 0.54 µm from 2.6± 0.93 µm observed in single step sintering.The highest hardness of 1175 ± 18 HV10 along with an optimum fracture toughness of 6.2 ± 0.5 MPa $m^{1/2}$ was achieved for sample sintered at 1500 ℃ for 1 minute, followed by 1250 ℃ for 15 hours.

7.5 Effect of Samaria doping on ceria stabilized zirconia:

Addition of Sm_2O_3 to CSZ improved the densification by inducing defects in the lattice and helped in restricting the grain growth through solute drag mechanism. The average grain size of 1.8± 0.53 µm along with a hardness of 1050± 10 HV10 and fracture toughness of 6.0± 0.4MPa √m is obtained for sample 1 mol.% samaria doped ceria stabilized zirconia (SmCSZ) sintered at 1500 ℃ for 3 hours.

7.6 Effect of two-step sintering on Samaria doped ceria stabilized zirconia:

The two-step sintering of Samaria doped ceria stabilized zirconia effectively suppressed the grain growth (0.64 ± 0.23 µm) and also decreased the cubic zirconia content in the sample. Which helped in achieving a higher hardness of 1288± 12HV10 Vickers along with an optimum fracture toughness of 5.37± 0.45 MPa $m^{1/2}$ sample sintered at 1500 °C for 1 minute followed by 1350 °C for 12 h sintering schedule.

7.7 Tribological properties of NbCSZ and SmCSZ materials:

The pin on disc wear test is conducted for NbCSZ and SmCSZ samples to evaluate the tribological properties, and the results are compared with the undoped ceria stabilized zirconia (CSZ).It is observed that NbCSZ and SmCSZ samples are shown better wear resistance compared to CSZ. The SEM images revealed that the grain pull-outs and grain fractures are major wear mechanisms in CSZ and NbCSZ, whereas only grain pull-outs are observed in SmCSZ, indicating its improved resistance to wear.

7.8 Low-temperature degradation of NbCSZ and SmCSZ materials:

The low-temperature degradation behaviour of NbCSZ andSmCSZ samples are analyzed through accelerated aging study, and results are compared with 3YSZ and CSZ samples. It is observed that the NbCSZ and SmCSZ samples did not show any monoclinic transformation even after 200 hours of treatment similar to CSZ samples, whereas 3YSZ samples shown significant monoclinic transformation with severe surface damage only after 10 hours of treatment. It is concluded that

the absence of oxygen-vacancies is a major reason for the resistance to LTD of CSZ, NbCSZ and SmCSZ samples.

7.9 Bioactivity of NbCSZ and SmCSZ materials:

SBF immersion tests were carried out to study the bioactivity of samples. After SBF immersion for 7days, the samples were characterized for phase and microstructure. As the untreated samples are bioinert in nature they did not induced any apatite layer formation on surface indicating poor bioactivity. However, samples after chemical treatment with 5M H_3PO_4 solution were able to form apatite layer on surface of samples, indicating their enhanced bioactivity.

7.10 Biocompatibility of NbCSZ and SmCSZ materials:

In vitro cell culture studies with human osteoblast-like cells (MG-63) on samples are conducted to evaluate the biocompatibility. The cellular metabolic activity assay (MTT assay) and scanning electron microscope analysis are used to understand the proliferation, viability, morphology and attachment of cells on samples. All the samples showed similar results, and cells are actively proliferated, and more than 85 % of cell viability is observed in comparison with the control sample. Hence, it can be concluded that the NbCSZ and SmCSZ did not show any toxic effects on cells, and samples are biocompatible.

7.11 Scope for future work:

As discussed in the previous chapters, NbCSZ and SmCSZ ceramics are developed and tested for physical, mechanical and biological behaviour. However, to use these materials for commercial biomedical applications further analysis/development is required as discussed below.

1) The time for sintering SmCSZ and NbCSZ can be reduced by using rapid/pressure-assisted sintering methods (Vleugels et al., 2004).
2) In the present study wear behavior is studied in dry condition, however, considering the application area the wear behavior in simulated body fluid condition using different counter bodies need to be evaluated(Baykal et al., 2014).
3) *In vivo* studies of developed materials to understand the biocompatibility more precisely(Kurtz et al., 2014).
4) Development of porous structures with the developed composition can enable them to use as scaffolds for tissue engineering(Fadli and Alfarisi, 2015).

References:

Abd El-Ghany, O.S., Sherief, A.H., 2016. Zirconia based ceramics, some clinical and biological aspects: Review. Futur. Dent. J. 2, 55–64. https://doi.org/10.1016/j.fdj.2016.10.002

Aguiar, A.A., Ussui, V., Ribeiro, C., Scapin, M.A., Ricci, D.R., De Lima, N.B., 2008. Characterization of the apatite formation on the surfaces of zirconia and alumina ceramics in body environments. Mater. Sci. Forum 591–593, 697–702.

Allemann, J.A., Michel, B., Märki, H.B., Gauckler, L.J., Moser, E.M., 1995. Grain growth of differently doped zirconia. J. Eur. Ceram. Soc. 15, 951–958. https://doi.org/10.1016/0955-2219(95)00073-4

Anselme, K., 2000. Osteoblast adhesion on biomaterials. Biomaterials 21, 667–681. https://doi.org/10.1016/S0142-9612(99)00242-2

Anstis, G.R., Chantikul, P., Lawn, B.R., Marshall, D.B., 1981. A Critical Evaluation of Indentation Techniques for Measuring Fracture Toughness: I, Direct Crack Measurements. J. Am. Ceram. Soc. 64, 533–538. https://doi.org/10.1111/j.1151-2916.1981.tb10320.x

ASTM International, 2019. C1327-15 Standard Test Method for Vickers Indentation Hardness of Advanced Ceramics. ASTM Int. 15, 1–10. https://doi.org/10.1520/C1327-15R19.2.

ASTM International, 2017a. B962-17 Standard Test Methods for Density of Compacted or Sintered Powder Metallurgy (PM) Products Using Archimedes' Principle. i, 1–7. https://doi.org/10.1520/B0962-13.2

ASTM International, 2017b. G99-17 Standard Test Method for Wear Testing with a Pin-on-Disk Apparatus. ASTM Int. https://doi.org/10.1520/G0099-05R10.2

Basu, B., Vitchev, R.G., Vleugels, J., Celis, J.P., Van Der Biest, O., 2002. Fretting wear of self-mated tetragonal zirconia ceramics in different humidity. Key Eng. Mater. 206, 783–786.

Baykal, D., Siskey, R.S., Haider, H., Saikko, V., Ahlroos, T., Kurtz, S.M., 2014. Advances in tribological testing of artificial joint biomaterials using multidirectional pin-on-disk testers. J. Mech. Behav. Biomed. Mater. 31, 117–134.https://doi.org/10.1016/j.jmbbm.2013.05.020

Bechepeche, A.P., Treu, O., Longo, E., Paiva-Santos, C.O., Varela, J.A., 1999. Experimental and theoretical aspects of the stabilization of zirconia. J. Mater. Sci. 34, 2751–2756. https://doi.org/10.1023/A:1004698026465

Bejugama, S., Gadwal, N.K., Pandey, A.K., 2019. Two-step sintering of Sm_2O_3 doped ceria stabilized zirconia. Ceram. Int. 45, 10348–10355. https://doi.org/10.1016/j.ceramint.2019.02.091

Bejugama, S., Pandey, A.K., 2018. Effect of Nb_2O_5 on sintering and mechanical properties of ceria stabilized zirconia. J. Alloys Compd. 765, 1049–1054. https://doi.org/10.1016/j.jallcom.2018.06.280

Borruto, A., 2010. A new material for hip prosthesis without considerable debris release. Med. Eng. Phys. 32, 908–913. https://doi.org/10.1016/j.medengphy.2010.06.007

Boutz, M.M.R., Winnubst, A.J.A., Burggraaf, A.J., 1994. Yttria-ceria stabilized tetragonal zirconia polycrystals: Sintering, grain growth and grain boundary segregation. J. Eur. Ceram. Soc. 13, 89–102. https://doi.org/10.1016/0955-2219(94)90106-6

Boutz, M.M.R., Winnubst, A.J.A., Van Langerak, B., Olde Scholtenhuis, R.J.M., Kreuwel, K., Burggraaf, A.J., 1995. The effect of ceria co-doping on chemical stability and fracture toughness of Y-TZP. J. Mater. Sci. 30, 1854–1862. https://doi.org/10.1007/BF00351622

Chen, I.W., Wang, X.H., 2000. Sintering dense nanocrystalline ceramics without final-stage grain growth. Nature 404, 168–171. https://doi.org/10.1038/35004548

Chen, P.C., Cheng, C.W., Kao, I.C., Tuan, W.H., Lian, T.W., Naito, M., 2016. Effect of co-doping NiO and Nb_2O_5on phase stability and mechanical properties of Y_2O_3stabilized ZrO_2/Al_2O_3composites. Adv. Powder Technol. 27, 877–881. https://doi.org/10.1016/j.apt.2016.01.017

Chevalier, J., 2006. What future for zirconia as a biomaterial? Biomaterials 27, 535–543. https://doi.org/10.1016/j.biomaterials.2005.07.034

Chevalier, J., Cales, B., Drouin, J., 1999. Low-Temperature Aging of Y-TZP Ceramics. J. Am. Ceram. Soc. 54, 2150–2154. https://doi.org/10.1111/j.1151-2916.1999.tb02055.x

Chevalier, J., Gremillard, L., Virkar, A. V., Clarke, D.R., 2009. The tetragonal-monoclinic transformation in zirconia: Lessons learned and future trends. J. Am. Ceram. Soc. 92, 1901–1920. https://doi.org/10.1111/j.1551-2916.2009.03278.x

Cullity, B.D., 1956. Powder photographs, in: Elements of X-Ray Diffraction. pp. 149–173. https://doi.org/10.1017/CBO9781107415324.004

Dorozhkin, S. V., 2018. Current state of bioceramics. J. Ceram. Sci. Technol. 9, 353–370. https://doi.org/10.4416/JCST2018-00026

Duh, J.G., Dai, H.T., Hsu, W.Y., 1988. Synthesis and sintering behaviour in CeO_2 -ZrO_2 ceramics. J. Mater. Sci. 23, 2786–2791. https://doi.org/10.1007/BF00547451

Duwez, P.O.L., Odell, F., Brown Jr., F.H., 1952. Stabilization of Zirconia with Calcia and Magnesia. J. Am. Ceram. Soc. 35, 107–113. https://doi.org/10.1111/j.1151-2916.1952.tb13081.x

Fabris, S., Paxton, A.T., Finnis, M.W., 2002. A stabilization mechanism of zirconia based on oxygen vacancies only. Acta Mater. 50, 5171–5178. https://doi.org/10.1016/S1359-6454(02)00385-3

Fadli, A., Alfarisi, C.D., 2015. Recent Research and Development in Porous Alumina Ceramics for Biomedical Applications.

Ferraris, M., Verné, E., Appendino, P., Moisescu, C., Krajewski, A., Ravaglioli, A., Piancastelli, A., 2000. Coatings on zirconia for medical applications. Biomaterials 21, 765–773. https://doi.org/10.1016/S0142-9612(99)00209-4

Ferreira, G.B.P., Silva, J.F. da, Nascimento, R.M. do, Gomes, U.U., Martinelli, A.E., 2012. Two-Step Sintering Applied to Ceramics. Sinter. Ceram. – New Emerg. Tech. 423–437.

Garvie, R.C., Hannink, R.H., Pascoe, R.T., 1975. Ceramic steel? Nature 258, 703–704. https://doi.org/10.1038/258703a0

Garvie, R.C., Nicholson, P.S., 1972. Phase Analysis in Zirconia Systems. J. Am. Ceram. Soc. 55, 303–305. https://doi.org/10.1111/j.1151-2916.1972.tb11290.x

Gremillard, L., Chevalier, J., Epicier, T., Deville, S., Fantozzi, G., 2004. Modeling the aging kinetics of zirconia ceramics. J. Eur. Ceram. Soc. 24, 3483–3489. https://doi.org/10.1016/j.jeurceramsoc.2003.11.025

Guo, F., Xiao, P., 2012. Effect of Fe_2O_3 doping on sintering of yttria-stabilized zirconia. J. Eur. Ceram. Soc. 32, 4157–4164. https://doi.org/10.1016/j.jeurceramsoc.2012.07.035

Gurushantha, K., Anantharaju, K.S., Sharma, S.C., Nagaswarupa, H.P., Prashantha, S.C., Mahesh, K.R.V., Renuka, L., Vidya, Y.S., Nagabhushana, H., 2016. Bio-mediated Sm doped nano cubic zirconia: Photoluminescent, Judd–Ofelt analysis, electrochemical impedance spectroscopy and photocatalytic performance. J. Alloys Compd. 685, 761–773. https://doi.org/10.1016/j.jallcom.2016.06.105

Hamadouche, M., Sedel, L., 2000. Ceramics in orthopaedics. J. Bone Jt. Surg. - Ser. B 82, 1095–1099. https://doi.org/10.1302/0301-620X.82B8.11744

Hannink, R.H.J., Kelly, P.M., Muddle, B.C., 2004. Transformation Toughening in Zirconia-Containing Ceramics. J. Am. Ceram. Soc. 83, 461–487. https://doi.org/10.1111/j.1151-2916.2000.tb01221.x

Haraguchi, K., Sugano, N., Nishii, T., Miki, H., Oka, K., Yoshikawa, H., 2001. Phase transformation of a zirconia ceramic head after total hip arthroplasty. J. Bone Jt. Surg. - Ser. B 83, 996–1000. https://doi.org/10.1302/0301-620X.83B7.12122

Hartmanová, M., Kubel, F., Buršková, V., Jergel, M., Navrátil, V., Lomonova, E.E., Navratil, K.,

Kundracik, F., Kosti, I., 2007. Effect of composition changes on properties and defect structure of crystalline Sm-doped ZrO_2. Russ. J. Electrochem. 43, 381–389. https://doi.org/10.1134/S1023193507040040

Hassan, A.M., Naga, S.M., Awaad, M., 2015. Toughening and strengthening of Nb_2O_5 doped zirconia/alumina (ZTA) composites. Int. J. Refract. Met. Hard Mater. 48, 338–345. https://doi.org/10.1016/j.ijrmhm.2014.10.006

Herath, H.M.T.U., Di Silvio, L., Evans, J.R.G., 2015. Osteoblast response to zirconia surfaces with different topographies. Mater. Sci. Eng. C 57, 363–370. https://doi.org/10.1016/j.msec.2015.07.052

Hernigou, P., Bahrami, T., 2003. Zirconia and alumina ceramics in comparison with stainless-steel heads. J. Bone Jt. Surg. - Ser. B 85, 504–509. https://doi.org/10.1302/0301-620X.85B4.13397

Heussner, K.H., Claussen, N., 1989. Strengthening of Ceria-Doped Tetragonal Zirconia Polycrystals by Reduction-Induced Phase Transformation. J. Am. Ceram. Soc. 72, 1044–1046. https://doi.org/10.1111/j.1151-2916.1989.tb06267.x

Higuchi, F., Shiba, N., Inoue, A., Wakebe, I., 1995. Fracture of an alumina ceramic head in total hip arthroplasty. J. Arthroplasty 10, 851–854. https://doi.org/10.1016/S0883-5403(05)80086-5

Hsu, Y.F., 2005. Influence of Nb_2O_5 additive on the densification and microstructural evolution of fine alumina powders. Mater. Sci. Eng. A 399, 232–237. https://doi.org/10.1016/j.msea.2005.03.101

Hwang, S.L., Chen, I.W., 1990. Grain Size Control of Tetragonal Zirconia Polycrystals Using the Space Charge Concept. J. Am. Ceram. Soc. 73, 3269–3277. https://doi.org/10.1111/j.1151-2916.1990.tb06449.x

Ishiyama, M., Tominaga, H., Shiga, M., Sasamoto, K., Ohkura, Y., Ueno, K., 1996. A Combined Assay of Cell Viability and in Vitro Cytotoxicity with a Highly Water-Soluble Tetrazolium Salt, Neutral Red and Crystal Violet. Biol. Pharm. Bull. 19, 1518–1520. https://doi.org/10.1248/bpb.19.1518

ISO, 2015. ISO 13356:2015(E) Implants for surgery — Ceramic materials based on yttria-stabilized tetragonal zirconia (Y-TZP). Int. Organ. Stand.

ISO, 2009. ISO 10993-5 Biological Evaluation of Medical devices-Part 5: Test for in vitro Cytotoxicity. Int. Stand. Organ. 2007, 1–11.

Jansen, S.R., Winnubst, A.J.A., He, Y.J., Verweij, H., Van Der Varst, P.G.T., De With, G., 1998. Effects of Grain Size and Ceria Addition on Ageing Behaviour and Tribological Properties

of Y-TZP Ceramics. J. Eur. Ceram. Soc. 18, 557–563. https://doi.org/10.1016/S0955-2219(97)00153-2

Ke, J., Ye, J., He, F., 2017. Enhancing the Bioactivity of Yttria-Stabilized Tetragonal Zirconia Ceramics via Grain Boundary Activation Enhancing the Bioactivity of Yttria-Stabilized Tetragonal Zirconia Ceramics via. https://doi.org/10.1021/acsami.7b03405

Kim, D.J., 1990. Effect of Ta_2O_5, Nb_2O_5, and HfO_2 Alloying on the Transformability of Y_2O_3-Stabilized Tetragonal ZrO2. J. Am. Ceram. Soc. 73, 115–120. https://doi.org/10.1111/j.1151-2916.1990.tb05100.x

Kim, D.J., Jung, H.J., Jang, J.W., Lee, H.L., 2005. Fracture Toughness, Ionic Conductivity, and Low-Temperature Phase Stability of Tetragonal Zirconia Codoped with Yttria and Niobium Oxide. J. Am. Ceram. Soc. 81, 2309–2314. https://doi.org/10.1111/j.1151-2916.1998.tb02626.x

Ko, H.C., Han, J.S., Bächle, M., Jang, J.H., Shin, S.W., Kim, D.J., 2007. Initial osteoblast-like cell response to pure titanium and zirconia/alumina ceramics. Dent. Mater. 23, 1349–1355. https://doi.org/10.1016/j.dental.2006.11.023

Kobayashi, K., Kuwajima, H., Masaki, T., 1981. Phase change and mechanical properties of ZrO_2-Y_2O_3 solid electrolyte after ageing. Solid State Ionics 3–4, 489–493. https://doi.org/10.1016/0167-2738(81)90138-7

Kohorst, P., Borchers, L., Strempel, J., Stiesch, M., Hassel, T., Bach, F.W., Hübsch, C., 2012. Low-temperature degradation of different zirconia ceramics for dental applications. Acta Biomater. 8, 1213–1220. https://doi.org/10.1016/j.actbio.2011.11.016

Kokubo, T., Takadama, H., 2006. How useful is SBF in predicting in vivo bone bioactivity? Biomaterials 27, 2907–2915. https://doi.org/10.1016/j.biomaterials.2006.01.017

Kopeliovich, D., 2000. General classification of ceramics [WWW Document]. URL https://www.substech.com/dokuwiki/doku.php?id=general_classification_of_ceramics

Kuete, V., Karaosmanoğlu, O., Sivas, H., 2017. Anticancer Activities of African Medicinal Spices and Vegetables, in: Medicinal Spices and Vegetables from Africa Drugs. Academic Press, pp. 271–297. https://doi.org/10.1016/B978-0-12-809286-6.00010-8

Kurtz, S.M., Kocagöz, S., Arnholt, C., Huet, R., Ueno, M., Walter, W.L., 2014. Advances in zirconia toughened alumina biomaterials for total joint replacement. J. Mech. Behav. Biomed. Mater. 31, 107–116. https://doi.org/10.1016/j.jmbbm.2013.03.022

Lakusta, M., Danilenko, I., Volkova, G., Loladze, L., Burchovetskiy, V., Konstantinova, T., 2018. Comparative analyses of the IV group oxides additives influence on the sintering kinetics of zirconia nanopowders. PLoS One 13, 1–17.

https://doi.org/10.1371/journal.pone.0200869

Lange, F.F., 1982. Transformation toughening - Part 1 Size effects associated with the thermodynamics of constrained transformations. J. Mater. Sci. 17, 225–234. https://doi.org/10.1007/BF00809057

Lange, F.F., Dunlop, G.L., Davis, B.I., 1986. Degradation During Aging of Transformation-Toughened Materials at 250 ° C. J. Am. Ceram. Soc. 40, 237–240.

Lee, D.Y., Kim, D.J., Cho, D.H., Lee, M.H., 1998. Effect of Nb_2O_5 and Y_2O_3 alloying on the mechanical properties of TZP ceramics. Ceram. Int. 24, 461–465. https://doi.org/10.1016/S0272-8842(97)00036-9

Lee, J.H., Lee, Y.K., Kim, J.Y., Kim, K.H., Her, S., Kim, Y.G., Park, J.W., Suh, J.Y., 2016. Cytocompatibility Evaluation of Etched Zirconia Ceramics Using Human Osteoblast-Like MG 63 Cells. Korean J. Dent. Mater. 43, 331–341. https://doi.org/10.14815/kjdm.2016.43.4.331

Li, P., Chen, I. -W, Penner-Hahn, J.E., 1994a. Effect of Dopants on Zirconia Stabilization—An X-ray Absorption Study: III, Charge-Compensating Dopants. J. Am. Ceram. Soc. 77, 1289–1295. https://doi.org/10.1111/j.1151-2916.1994.tb05404.x

Li, P., Chen, I.W., Penner Hahn, J.E., 1994b. Effect of dopants on zirconia stabilization - an X-ray absorption study: II, Tetravalent Dopants. J. Am. Ceram. Soc. 77, 1289–1295. https://doi.org/10.1111/j.1151-2916.1994.tb05404.x

Lóh, N.J., Simao, L., Faller, C.A., De Noni, A., Montedo, O.R.K., 2016. A review of two-step sintering for ceramics. Ceram. Int. 42, 12556–12572. https://doi.org/10.1016/j.ceramint.2016.05.065

Masonis, J.L., Bourne, R.B., Ries, M.D., McCalden, R.W., Salehi, A., Kelman, D.C., 2004. Zirconia femoral head fractures: A clinical and retrieval analysis. J. Arthroplasty 19, 898–905. https://doi.org/10.1016/j.arth.2004.02.045

Matsumoto, R.L.K., 1988. Aging Behavior of Ceria-Stabilized Tetragonal Zirconia Polycrystals. J. Am. Ceram. Soc. 71, C-128-C-129. https://doi.org/10.1111/j.1151-2916.1988.tb05031.x

Mosmann, T., 1983. Rapid colorimetric assay for cellular growth and survival: Application to proliferation and cytotoxicity assays. J. Immunol. Methods 65, 55–63. https://doi.org/10.1016/0022-1759(83)90303-4

Naga, S.M., Hassan, A.M., Awaad, M., 2015. Physical and mechanical properties of Ta_2O_5 doped zirconia-toughened alumina (ZTA) composites. Ceram. Int. 41, 6248–6255. https://doi.org/10.1016/j.ceramint.2015.01.039

Nakamura, M., Inuzuka, M., 2011. Improving bioactivity and durability of yttria-stabilized zirconia 7335–7343. https://doi.org/10.1007/s10853-011-5695-1

Navrotsky, A., 2005. Thermochemical insights into refractory ceramic materials based on oxides with large tetravalent cations. J. Mater. Chem. 15, 1883–1890. https://doi.org/10.1039/b417143h

Ouyang, J., Yang, H., Tang, A., 2016. Phase and optical properties of solvothermal prepared Sm_2O_3 doped ZrO_2 nanoparticles: The effect of oxygen vacancy. J. Alloys Compd. 682, 654–662. https://doi.org/10.1016/j.jallcom.2016.05.060

Pandey, A.K., Biswas, K., 2014. In vitro cytocompatibility, ageing and wear behavior of ceria stabilized zirconia bioceramic. Ceram. Int. 40, 15889–15895. https://doi.org/10.1016/j.ceramint.2014.07.117

Pandey, A.K., Biswas, K., 2011. Influence of sintering parameters on tribological properties of ceria stabilized zirconia bio-ceramics. Ceram. Int. 37, 257–264. https://doi.org/10.1016/j.ceramint.2010.08.041

Pandey, A.K., Pati, F., Mandal, D., Dhara, S., Biswas, K., 2013. In vitro evaluation of osteoconductivity and cellular response of zirconia and alumina based ceramics. Mater. Sci. Eng. C 33, 3923–3930. https://doi.org/10.1016/j.msec.2013.05.032

Park, J.H., Moon, S.W., 1992. Stability and sinterability of tetragonal zirconia polycrystals costabilized by CeO_2 and various oxides. J. Mater. Sci. Lett. 11, 1046–1048. https://doi.org/10.1007/BF00729756

Pereira, G.K.R., Venturini, A.B., Silvestri, T., Dapieve, K.S., Montagner, A.F., Soares, F.Z.M., Valandro, L.F., 2015. Low-temperature degradation of Y-TZP ceramics: A systematic review and meta-analysis. J. Mech. Behav. Biomed. Mater. 55, 151–163. https://doi.org/10.1016/j.jmbbm.2015.10.017

Piconi, C., Burger, W., Richter, H.G., Cittadini, A., Maccauro, G., Covacci, V., Bruzzese, N., Ricci, G.A., Marmo, E., 1998. Y-TZP. Biomaterials 19, 1489–1494. https://doi.org/10.1140/epja/i2018-12457-x

Piconi, C., Maccauro, G., 1999. Zirconia as a ceramic biomaterial. Biomaterials 20, 1–25. https://doi.org/10.1016/S0142-9612(98)00010-6

Piconi, C., Maccauro, G., Muratori, F., Brach Del Prever, E., 2003. Alumina and zirconia ceramics in joint replacements. J. Appl. Biomater. Biomech. 1, 19–32. https://doi.org/10.1177/228080000300100103

Piconi, C., Maccauro, G., Pilloni, L., Burger, W., Muratori, F., Richter, H.G., 2006. On the fracture of a zirconia ball head. J. Mater. Sci. Mater. Med. 17, 289–300.

https://doi.org/10.1007/s10856-006-7316-0

Powers, J.D., Glaeser, A.M., 1998. Grain Boundary Migration in Ceramics. Interface Sci. 6, 23–39. https://doi.org/10.1023/A:1008656302007

Pyda, W., Haberko, K., 1987. CaO-containing tetragonal ZrO_2 polycrystals (Ca-TZP). Ceram. Int. 13, 113–118. https://doi.org/10.1016/0272-8842(87)90048-4

Ragnhild E . Aune, D.S. and S.S., 1997. Phase Relationships in the System Mn-Co-C. Netsu Sokutei 24, 171–178.

Rahaman, M.N.., 2007. Solid state and viscous sintering, in: Sintering of Ceramics. CRC Press, Boca Raton, pp. 45–104. https://doi.org/10.1201/b15869

Rainforth, W.M., 2004. The wear behaviour of oxide ceramics-A review. J. Mater. Sci. 39, 6705–6721. https://doi.org/10.1023/B:JMSC.0000045601.49480.79

Ramabulana, K., Tambani, M., Machio, C., Makhatha, M.E., 2019. Effect of particle size distribution on green properties and sintering of Ti-6Al-4V. IOP Conf. Ser. Mater. Sci. Eng. 655. https://doi.org/10.1088/1757-899X/655/1/012020

Ramesh, T.R., Gangaiah, M., Harish, P.V., Krishnakumar, U., Nandakishore, B., 2012. Zirconia ceramics as a dental biomaterial - An overview. Trends Biomater. Artif. Organs 26, 154–160.

Richter, H.G., Willmann, G., 1999. Reliability of ceramic components for total hip endoprostheses. Br. Ceram. Trans. 98, 29–34. https://doi.org/10.1179/bct.1999.98.1.29

Sabu, T., Preetha, B., Sreekala, M.S., 2018. Fundamental Biomaterials: Ceramics, Fundamental Biomaterials: Polymers. Woodhead publishing limited, Cambridge. https://doi.org/10.1016/c2016-0-03544-1

Sato, T., Ohtaki, S., Endo, T., Shimada, M., 1986. Improvement of thermal stability of Yttria-doped tetragonal zirconia polycrystals by alloying with various oxides. Int. J. High Technol. Ceram. 2, 167–177. https://doi.org/10.1016/0267-3762(86)90048-2

Sato, T., Shimada, M., 1985. Transformation of ceria-doped tetragonal zirconia polycrystals by annealing in water.

Shon, I.J., Jeong, I.K., Park, J.H., Kim, B.R., Lee, K.T., 2009. Effect of Fe_2O_3 addition on consolidation and properties of 8 mol% yttria-stabilized zirconia by high-frequency induction heated sintering (HFIHS). Ceram. Int. 35, 363–368. https://doi.org/10.1016/j.ceramint.2007.11.006

Stockert, J.C., Horobin, R.W., Colombo, L.L., Blázquez-Castro, A., 2018. Tetrazolium salts and

formazan products in Cell Biology: Viability assessment, fluorescence imaging, and labeling perspectives. Acta Histochem. 120, 159–167. https://doi.org/10.1016/j.acthis.2018.02.005

Subbarao, E.C., Maiti, H.S., Srivastava, K.K., 1974. Martensitic transformation in zirconia. Phys. Status Solidi 21, 9–40. https://doi.org/10.1002/pssa.2210210102

Teufer, G., 1962. The crystal structure of tetragonal ZrO2. Acta Crystallogr. 15, 1187. https://doi.org/10.1107/S0365110X62003114

Theunissen, G.S.A.M., Winnubst, A.J.A., Burggraaf, A.J., 1989. Segregation aspects in the ZrO_2-Y_20_3 ceramic system. J. Mater. Sci. Lett. 8, 55–57.

Tsukuma, K., 1986. Mechanical properties and thermal stability of CeO_2 containing tetragonal zirconia polycrystals. Am. Ceram. Soc. Bull. 65, 1386–1389.

Tsukuma, K., Kubota, Y., Tsukidate, T., 1983. Thermal and mechanical properties of Y_2O_3-stabilized tetragonal zirconia polycrystals. American Ceramic Society, Inc, United States.

Tsukuma, K., Shimada, M., 1985. Strength , fracture toughness and Vickers hardness of CeO_2-stabilized tetragonal. J. Mater. Sci. 20, 1178–1184.

Turon-Vinas, M., Zhang, F., Vleugels, J., Anglada, M., 2018. Effect of calcia co-doping on ceria-stabilized zirconia. J. Eur. Ceram. Soc. 38, 2621–2631. https://doi.org/10.1016/j.jeurceramsoc.2017.12.053

Uchida, M., Kim, H.M., Kokubo, T., Miyaji, F., Nakamura, T., 2001. Bonelike Apatite Formation Induced on Zirconia Gel in a Simulated Body Fluid and Its Modified Solutions. J. Am. Ceram. Soc. 84, 2041–2044. https://doi.org/10.1111/j.1151-2916.2001.tb00955.x

Uchida, M., Kim, H.M., Kokubo, T., Nawa, M., Asano, T., Tanaka, K., Nakamura, T., 2002a. Apatite-forming ability of a zirconia/alumina nano-composite induced by chemical treatment. J. Biomed. Mater. Res. 60, 277–282. https://doi.org/10.1002/jbm.10071

Uchida, M., Kim, H.M., Miyaji, F., Kokubo, T., Nakamura, T., 2002b. Apatite formation on zirconium metal treated with aqueous NaOH. Biomaterials 23, 313–317. https://doi.org/10.1016/S0142-9612(01)00110-7

University of cambridge, 2005. The fundamental properties of the most common materials used as electrolytes in SOFCs [WWW Document]. URL https://www.doitpoms.ac.uk/tlplib/fuel-cells/sofc_electrolyte.php?printable=1

Vleugels, J., Zhao, C., Van Der Biest, O., 2004. Toughness enhancement of Ce-TZP by annealing in argon. Scr. Mater. 50, 679–683. https://doi.org/10.1016/j.scriptamat.2003.11.017

Watanabe, W., Iiu, S., Fukuura, I., 1983. Aging behavior of Y-TZP. American Ceramic Society, Inc, United States.

Williams, D., 1987. Definitions in biomaterials. Prog. Biomed. Eng. 26, 414. https://doi.org/10.1002/pol.1988.140260910

Yang, S.Y., Lee, J.H., Kim, J.J., Lee, J.S., 2004. Sintering behavior of Y-doped ZrO_2 ceramics: the effect of Al_2O_3 and Nb_2O_5 addition. Solid State Ionics 172, 413–416. https://doi.org/10.1016/j.ssi.2004.03.026

Yoshimura, M., Noma, T., Kawabata, K., Somiya, S., 1987. Role of H_2O on the degradation process of Y-TZP. J. Mater. Sci. Lett. 6, 465–467. https://doi.org/10.1007/BF01756800

Zhang, W., Bao, J., Jia, G., Guo, W., Song, X., An, S., 2017. The effect of microstructure control on mechanical properties of 12Ce-TZP via two-step sintering method. J. Alloys Compd. 711, 686–692. https://doi.org/10.1016/j.jallcom.2017.04.059

Zhang, W., Bao, J., Song, X., An, S., 2018a. The effect of La_2O_3 on the microstructure and mechanical properties of 12Ce-TZP. Ceram. Int. 44, 6713–6718. https://doi.org/10.1016/j.jre.2017.04.007

Zhao, C., Vleugels, J., Basu, B., Van Der Biest, O., 2000. High toughness Ce-TZP by sintering in an inert atmosphere. Scr. Mater. 43, 1015–1020. https://doi.org/10.1016/S1359-6462(00)00529-7

Zhou, M., Huang, Z., Qi, J., Wei, N., Wu, D., Zhang, Q., Wang, S., Feng, Z., Lu, T., 2017. Densification and grain growth of $Gd_2Zr_2O_7$ nanoceramics during pressureless sintering. J. Eur. Ceram. Soc. 37, 1059–1065. https://doi.org/10.1016/j.jeurceramsoc.2016.09.019

Publications from the Present Work

Journal papers published:

1. **Shiva Bejugama**, Ajoy Kumar Pandey, "*Effect of Nb_2O_5 on sintering and mechanical properties of ceria stabilized zirconia*", J. Alloys Compd. 765 (2018) 1049–1054. (SCI, Impact factor: 4.65)

2. **Shiva Bejugama**, Narendra Kumar Gadwal, Ajoy Kumar Pandey, "*Two-step sintering of Sm_2O_3 doped ceria stabilized zirconia*", Ceram. Int. 45 (2019) 10348–10355. (SCI, Impact factor: 3.83)

3. **Shiva Bejugama**, Shibu Chameettachal, Falguni Pati, Ajoy KumarPandey, "*In vitro cellular response and hydrothermal aging of two-step sintered Nb_2O_5 doped ceria stabilized zirconia ceramics*", Ceram. Int 47 (2020)1594-1601. (SCI, Impact factor: 3.83)

4. **Shiva Bejugama**, Shibu Chameettachal, Falguni Pati, Ajoy KumarPandey, "*Tribology and in-vitro biological characterization of samaria doped ceria stabilized zirconia ceramics*", Ceram. Int. (In press, accepted on March 9, 2021). (SCI, Impact factor: 3.83)

International conferences:

1. **Shiva Bejugama**, Ajoy Kumar Pandey "*Development and characterization of Samarium oxide doped zirconia*", at Indian Institute of Metals, NMD-ATM 2017,71st annual meeting, BITS Goa.

2. **Shiva Bejugama**, Ajoy Kumar Pandey "*Effect of two-step sintering on properties of Nb_2O_5 doped ceria stabilized zirconia*", at Indian Institute of Metals, NMD-ATM 2018,72st annual meeting, Kolkata.

3. **Shiva Bejugama**, Ajoy Kumar Pandey"*Influence of Nb_2O_5 and Sm_2O_3 Co-doping on sintering and mechanical properties of 12Ce-TZP*",at Indian Institute of Metals, NMD-ATM 2019,73rd annual meeting, Trivandram.

About the author

The author was born in Siddipet, a town in Telangana State, India on 25th July 1992. After completion of his B. Tech in Mechanical engineering in the year 2013 from KasireddyNarayan reddyCollege of Engineering and Research (KNRCER), Hyderabad, Telangana;he joined for his M.Tech in Metallurgy discipline at Jawaharlal Nehru Technological University, Hyderabad (JNTUH), Telangana, India in the year 2013. After successful completion of his M.Tech in the year 2015, the author joined National Institute of Technology Warangal, Telangana, India to pursue his doctoral program. The author published several papers in international journals and presented his research work in international conferences.